Universidad
Rey Juan Carlos

Tesis Doctoral

Robust Elasticity and Damping Models for High-Fidelity Textile Simulation

Autor: **Rosa María Sánchez Banderas**

Director: **Miguel Ángel Otaduy**

Programa de Doctorado en Tecnologías de la Información y las Comunicaciones

Escuela Internacional de Doctorado

Madrid, 2021

Acknowledgements

To *Miguel Ángel*. I will always be grateful for giving me the opportunity to work with you and learn countless new things every day. I consider myself really fortunate to have you as my advisor and to have had the chance of embarking on this adventure under your supervision. Thank you for everything, but especially for your endless patience with me.

To the members of my PhD. committee, thank you for evaluating this thesis. To the reviewers, thank you for providing feedback for our publications.

To the organizations and institutions that have supported this thesis. This work was funded in part by the Spanish Ministry of Science (FPI fellowship of grant TIN2015-70799-R Simverso, Torres Quevedo fellowship PTQ-17-09154, and grant RTI2018-098694-B-I00 VizLearning) and the European Research Council (ERC Proof-of-Concept grant 713742 FabricMetrics and ERC Consolidator Grant 772738 TouchDesign).

To *Ignacio* and *Miguel* from University of Valencia. You introduced me to the fascinating world of physically-based simulation and taught me to appreciate what has now become my profession. I consider myself really fortunate to have met you, and without any doubt, I would not be here today if it hadn't been for your invaluable support.

To *Álex* and *Gabriel*, thank you very much for lending me your help with the yarn-level code base and multiple technical aspects of this thesis. To all the people on MSLab and SEDDI. Thank you for accompanying me on this journey and assisting me when I needed it most. You have made my deadlines more bearable. It has been a lot of fun working with you.

To *Tuur* and all the people I met during my internship at Facebook Reality Labs. Thank you very much for giving me the opportunity to work with you. It was a pleasure to met you. I enjoyed a lot my time there and I learned a lot from you.

To *Carol*, thank you very much for helping me all this time, you have been a great support for me.

To those in Madrid who were colleagues and today are close friends. I arrived here knowing no one and filled with doubts and fears. The beginnings were rough, but you made the road easier for me. Thank you for accompanying and supporting me in this journey, and I hope in many more in the future. I love you guys!

To my friends in Valencia. Regardless of the distance, you have always been there. Thank you for supporting me when I most needed it. You encouraged me when I was down and, most of all, you endured me for more than ten years, which is quite a huge feat!. I have no words to describe how lucky I am to have you. I'm looking forward to living and sharing new experiences along with you all. You are my family. I love you very much.

To my family and everyone I consider my family. I love you. Thank you for being there. To Dad and Laura, for having put up with me with endless patience and, in spite of the distance, for having supported me during all these years. I consider myself extremely lucky to have the family that I do. I love you very much. Thank you for everything.

To Hector, because when I deposit this thesis, it will mark the 10^{th} anniversary since we started a new adventure together. I love you very much, you are my biggest support, my other half. Thank you for your infinite help all this time, for the great patience you had with me and, above all, for always being you. This thesis would not have been possible without you. I love you infinitely.

To everyone I have met here and there throughout my life. Thank you because I am sure you have been important or still are. I don't want to leave anyone out, so if you don't identify with any of the above, this is your group!

To *Centefico*, thank you for teaching me a valuable lesson that has helped me throughout this thesis: "La cencia no se ace sola ahi que acerla".

To you, who are reading this dull thesis. I hope you can learn something by reading it. If not, I'm sure it will work great for your wobbly table.

To you, Mom, because I'm sure that if you were here you'd be super proud of me and of all that I have accomplished. I miss you, and any dedication will always fall short of expressing how much I love you and how much I miss you. This thesis is especially dedicated to you.

Abstract

Textiles are ubiquitous in our daily lives, being the fashion and textile industry one of the main drivers of the global economy. Despite technological advances, the fashion industry resists the irruption of digital design processes. The reason lies in the fact that existing computational models found in engineering, albeit accurate, do not satisfy the performance requirements compatible with industrial processes. Recently, advances in computer graphics simulation methods have resulted in the development of high-performance solutions for the simulation of fabrics at the yarn level that narrow the accuracy gap with engineering approaches. Although current trends point towards the emergence in the near future of high-fidelity models that will satisfy the requirements for predictive digital prototyping, today there remain open challenges that limit the achievement of this objective. In this thesis, we address some of these challenges and contribute towards the creation of high fidelity simulation models.

To this end, we approach two relevant aspects for the characterization and behavior of cloth. First, we address the modeling of dissipative behavior in cloth. We propose a framework for the design of damping forces based on dissipation potentials formulated as functions of strain rate. We study its application to continuum and discrete deformation models, its practical implications, and advantages over commonly adopted dissipation models. We demonstrate its applicability to two highly different deformation models, Saint Venant-Kirchhoff (StVK) hyperlasticity and yarn-level cloth with sliding persistent contacts. Then, we address the challenge of simulating multilayered clothing. We introduce a robust method for the simulation of complex rod assemblies and stacked layers with implicit contact handling. Previous methods fail to robustly handle such complex situations due to ubiquitous and intrinsic degeneracies. Our novel discretization supports accurate and efficient contact while remaining insensitive to such degeneracies. Our solution is simple and elegant, producing robust simulations even on large-scale scenarios with pervasive degeneracies.

Contents

List of Figures

List of Tables

Chapter 1

Introduction

Textiles play a significant role in our daily lives. Beyond their biological utility in protecting us from environmental hazards, they serve an important cultural function. Status, personality, history, values or convictions: clothing and ornamental textiles serve as a medium for humans to establish their individual and collective identities. It is not surprising, then, that they have aroused so much interest throughout history.

Over the last few centuries, the fashion and textile industries have become one of the main drivers of the global economy [Karthik and Gopalakrishnan, 2014]. The industrial revolution brought with it the appearance of machinery capable of manufacturing fabrics on a large scale, leading to a dramatic leap in terms of cost reduction and, therefore, in the accessibility of these essential goods to the population.

Since then, the growing consumption of manufactured goods and the demand for sustainable fabrics that meet increasing criteria of quality and variety, among other technical requirements, have led to an intense revision of the industry. In recent decades, this has materialized in the adoption of automation and digitalization techniques in order to optimize the production process.

However, despite technological advances, the fashion industry continues to resist the irruption of digital design processes [Arribas and Alfaro, 2018]. While digital prototyping and evaluation are well established in other industries such as the automotive or aeronautics industries, the fashion industry essentially maintains a development model based on physical prototypes. This iterative process is slow and costly, both from the environmental and business perspectives.

The primary reason behind this lies in the state of the existing computational models. Although the industry has developed tools that allow pattern digitization, the

mechanical models that reflect fabric behavior are still far from the required levels of accuracy and performance to be compatible with industrial processes. This is not surprising, given that the phenomena behind fabric behavior is inherently chaotic.

The study of cloth and its simulation began in the 1930s, when the engineering community developed textile mechanics to support the textile industry [Peirce, 1937]. Since then, advances in computing and computational methods have resulted in the creation of highly accurate models capable of predicting textile behavior even at mesoscopic levels, down to individual fibers [Durville, 2009]. Although these models have been applied to a variety of engineering problems [Long et al., 2011], including the analysis of mechanical properties and damage, the study of draping behavior and the development of functional materials for specialized equipment, their use has been limited to small sections of fabric (on the millimeter scale) due to the computational challenges they entail.

Parallel to the engineering industry, the rapid evolution of computer-generated imagery and computer animation in the 1980s ignited an interest in the virtual representation of fabrics among the computer graphics community. Its focus, however, was markedly different from that of the textile community: instead of focusing on high-accuracy solutions, computer graphics is concerned with generating visually plausible representations within a reasonable amount of computational time.

Today, both fields are converging. Advances in computing capability (backed by the vast parallelism offered by modern graphics hardware), along with a deeper understanding of the problem and the numerical tools involved, have led to the development of high-accuracy, high-performance solutions for yarn-level fabric simulation [Kaldor et al., 2008, Yuksel et al., 2012, Cirio et al., 2017]. Although these technologies are not yet accurate enough for engineering applications, current trends indicate that the gap between engineering and computer graphics will progressively become narrower.

As a result, we expect to see the advent of what we refer to as *high-fidelity fabric simulation models* in the near future: methods that achieve accuracy comparable to engineering approaches while maintaining the high performance of graphics methods. These methods will hold the key to revolutionizing the fashion industry by finally meeting the productivity constraints of accuracy and efficiency needed for digital predictive prototyping and, as a result, significantly accelerate, improve, and lower the environmental, social, economic, and cultural costs associated with design processes in the fashion supply chain.

In this thesis, we take steps towards the creation of such high fidelity models. To this end, we focus on two interesting aspects of cloth simulation that are crucial for fabric characterization: the study of the dissipative properties and their impact on the behavior of the cloth, and the representation of complex yarn assemblies and stacked layers of fabric in persistent contact.

1.1 Cloth Simulation in Computer Graphics

The creation of high fidelity simulation models capable of accurately reproducing the complex mechanical properties of fabrics, remains the core pillar of cloth simulation. However, graphics applications require a delicate balance between computational cost and accuracy to make these approaches practical.

The numerous and complex challenges that arise in cloth simulation make it a difficult task. As a result, it has sparked research efforts for many decades. On one hand, the mechanical representation of the fabric must be precise enough to capture the nonlinearities and large deformations inherent in the cloth, whether they are wrinkles, waves, or different types of folds. On the other hand, interactions between fabrics and rigid and deformable materials, as well as self-collisions, must be treated efficiently and precisely to prevent simulation artifacts. This requires advanced collision detection and resolution methods.

The first approaches to fabric modeling leveraged on geometrical formulations [Weil, 1986]. These models employed simple geometrical descriptions of the fabric without its physical and mechanical properties, primarily focusing on its appearance, especially its folds and wrinkles. However, many authors date the beginning of cloth simulation in computer graphics to 1987, with the work of [Terzopoulos et al., 1987], who pioneered the first physics-based approach (Fig. 1.1).

Although limited to simple scenes, these early models opened up cloth research to the graphics community. By the 90s, a large body of literature began to emerge, simulating complete garments while taking into account a variety of other phenomena such as body modeling and animation, as well as collision detection and response. Since then, most developments were devoted to produce higher accuracy simulations while maintaining or improving their efficiency.

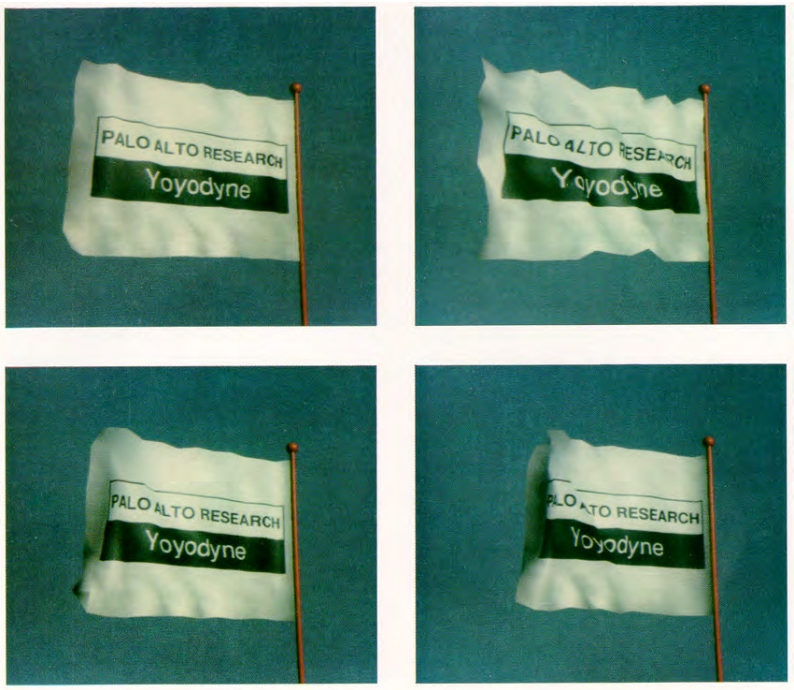

Figure 1.1: [Terzopoulos et al., 1987] introduced a deformable model intended for generalized flexible objects. Their finite element simulations demonstrated 3-D cloth-like structures that bend, fold, wrinkle and interact with solid geometry.

For decades, the outstanding approach to cloth simulation in computer graphics has been the use of thin-shell models. From simple mass-spring systems to more sophisticated finite element methods, the efforts of graphics researchers led to a substantial leap in accuracy of cloth behavior modeling. However, these models have difficulties capturing macroscopic effects that arise from subtle interactions occurring at the yarn-level (under the millimeter scale) and those are critical for high-fidelity characterization.

[Kaldor et al., 2008] pioneered the simulation of large pieces of cloth at yarn-level in computer graphics. They captured the mechanics of individual yarns through an inextensible rod model and explicitly modeled inter-yarn frictional contact to mimic the behavior of real clothing. Nevertheless, the sheer amount of yarns present on a real garment makes contact-related computation impractical, being the primary bottleneck of the model. Few years later, [Cirio et al., 2014], improved the efficiency of yarn-level cloth models by considering persistent contact between yarns, thus avoiding contact management altogether at the expense of limiting the range of possible yarn structures that the model is able to represent.

Both works suppose a milestone towards the development of high fidelity cloth simulation. By modeling the dynamics of cloth at yarn-level, macroscopic non-linear and anisotropic behavior that is otherwise difficult to capture with triangles, emerges naturally. Moreover, thanks to their computational efficiency, real-size garments can be simulated at the yarn scale within reasonable times. However, despite these outstanding advances, these methods are still far from the levels of accuracy and efficiency to which high-fidelity simulation methods aspire, leaving many challenges yet to be addressed.

1.2 Dissipative Phenomena

Among the challenges that remain in the characterization of real fabrics, we found that the modeling of dissipative properties has often been one of the most overlooked in computer graphics works. The energy accumulated in oscillating mechanical systems may be dissipated for a variety of purposes, including collisions, friction, or ultimately due to the resistance of matter to change its current shape or structure. In the field of mechanics, many of these dissipative effects are referred to as damping.

Many interesting materials exhibit highly varying damping behaviors, from the inviscid behavior of water to the highly damped behavior of flesh. Nevertheless, and despite the large amount of literature on the subject, neither the mechanisms nor the relevant state variables that give rise to it are still well understood. As such, many works in the computer graphics literature simply rely on linear damping models or focus on mitigating the dissipation induced by numerical integration [Barbič and James, 2005, Gast et al., 2015, Cirio et al., 2014].

However, dissipation is a central component in fabric characterization. Cloth tends to exhibit highly damped motion across different deformation modes. As such, accurate modeling of dissipative properties that enables a controllable description of dissipative behavior (i.e. decoupled across the different modes) is critical for achieving accurate simulations.

In Chapter 3 we propose a framework for the design of damping forces based on strain rate dissipation potentials. Our method guarantees the controllability criterion by design, enabling its application to a wide range of simulation problems, including high fidelity cloth. Furthermore, we develop diverse applied examples that prompt the

considerations to be addressed for practical implementations. On one hand, we show the application of the proposed formulation to the Saint-Venant Kirchhoff (StVK) hyperelasticity model. In this setting, we study the design of continuum dissipation models and their discretization, possibilities for parameterization under multi-dimensional strain metrics, as well as the implications of implicit integration. On the other hand, we apply it to yarn-level cloth simulation with sliding persistent contacts [Cirio et al., 2014]. This model allows us to analyze the application to discretizations that combine Lagrangian and Eulerian coordinates.

1.3 Multilayered and Stacked Clothes

Daily-life garments are usually composed of multiple layers of cloth in contact: the flounces of a dress, the pockets of jeans or the embroidery on jackets, are all examples of how different patches of cloth can be stacked or sewn together to attain a desired look or behavior. It is not surprising that these composite structures have attracted the interest of researchers, both from a graphics and engineering point of view, as they exhibit highly distinctive visual and mechanical properties that make them desirable for a variety of applications, ranging from fashion to the creation of functional garments and fabrics. Therefore, a high fidelity cloth simulation method must pay close attention to how these contacts between the different layers are resolved and be able to robustly and reliably replicate their behavior.

However, contact handling still remains as another significant unsolved problem. While detection and resolution algorithms have evolved to a point in which they offer reliable solutions to the intricate configurations that usually appear in cloth simulation, they are often complex and computationally challenging, particularly when considering the sheer amount of degrees of freedom required for the simulation of a full-scale garment.

Nonetheless, it is possible to identify partial solutions that enjoy higher computational efficiency if their scope is limited to specific problems under certain assumptions. Such is the case of the work by [Cirio et al., 2014], who followed this strategy and employed a special discretization to reduce the computational cost associated with inter-yarn contact handling by assuming persistent contact. However, while their method enables the representation of yarns sliding at contact points up to a certain degree, their discretization precludes the application of the same concept to problems

involving multiple layers sliding against each other due to the vulnerability of this discretization to degenerate configurations.

In Chapter 4 we propose a highly efficient approach for the simulation of complex rod assemblies and stacked layers that overcomes these limitations. We accomplish this by extending the persistent contact assumption to multiple layers, developing a novel mixed discretization that supports accurate and efficient contact while being transparent to internal rod forces and hence insensitive to degeneracies. By combining our novel discretization with the one employed by [Cirio et al., 2014] as appropriate, we enable free sliding motion between different cloth layers, thus extending the capabilities of the method to the simulation of multilayered structures such as pockets, labels, tablecloths and certain complex knitting patterns (all of which present complex rod arrangements and pervasive degeneracies) at a comparable computational cost.

1.4 Overview and Contributions

The main contributions of this thesis can be summarized as follows:

- In Chapter 3 we introduce a framework for the design of damping using dissipation potentials formulated as functions of strain rate. Our damping model is built on top of the concept of dissipation potentials from classical mechanics. This approach parallels the design of elastic deformation models based on energy formulations and simplifies the enforcement of what we refer to *good damping* conditions. This framework also helps us demonstrate why the popular Rayleigh damping model fails for nonlinear deformation models.

- In Chapter 3 we also analyze in detail the application of strain rate dissipation potentials to two highly different deformation models, StVK hyperelasticity and yarn-level cloth with sliding persistent contacts. These deformation models are representative of the range of applicability of the damping model.

- Chapter 4 introduces a method to simulate complex rod assemblies and stacked layers of cloth with implicit contact handling, through Eulerian-on-Lagrangian (EoL) discretizations. Previous EoL methods fail to handle such complex situations, due to ubiquitous and intrinsic degeneracies in the contact geometry, which prevent the use of remeshing and make simulations unstable. We propose

a novel mixed Eulerian-Lagrangian discretization that supports accurate and efficient contact as in EoL methods, but is transparent to internal rod forces, and hence insensitive to degeneracies.

- In Chapter 4 we also combine standard and novel EoL discretizations as appropriate, deriving mixed statics-dynamics equations of motion that can be solved in a unified manner with standard solvers. Our solution is simple and elegant in practice, and produces robust simulations on large-scale scenarios with complex rod arrangements and pervasive degeneracies. In our results, we show the application of our solution to challenging simulations of yarn-level cloth. We extend the power of EoL methods to stacked layers of fabrics, by handling implicitly both intra-fabric as well as inter-fabric contacts.

1.5 Publications

The following chapters are based on the following publications

- Chapter 3: "Dissipation Potentials for Yarn-Level Cloth" - Rosa M. Sánchez-Banderas and Miguel A. Otaduy - *CEIG, 11-18* [Sánchez-Banderas and Otaduy, 2017]. This paper, presented at the Spanish Conference of Computer Graphics (CEIG), establishes the foundations of the design of damping forces based on dissipation potentials and presents its application to yarn-level formulations.

- Chapter 3: "Strain Rate Dissipation for Elastic Deformations" - Rosa M. Sánchez-Banderas and Miguel A. Otaduy - *Computer Graphics Forum 37 (8), 161-170.* [Sánchez-Banderas and Otaduy, 2018]. This paper extends the previous one by applying dissipation potentials to other domains such as thin-shell formulations, further formalizing the concept of *good damping*. For simplicity, both works are presented under the same chapter.

- Chapter 4: "Robust eulerian-on-lagrangian rods" - Rosa M. Sánchez-Banderas, Alejandro Rodríguez, Héctor Barreiro and Miguel A. Otaduy - *ACM Transactions on Graphics (TOG) 39 (4), 59: 1-59: 10.* [Sánchez-Banderas et al., 2020]. This paper introduces an efficient and robust method to simulate complex rod assemblies and stacked layers in sliding motion.

1.6 Outline

This thesis is organized as follows

- **Background**. Chapter 2 summarizes the major works that influenced this thesis, highlighting their advantages and disadvantages and demonstrating why further analysis in those areas was essential. We have grouped the literature into a general section about cloth simulation and two main topics: dissipative phenomena and multilayer and stacked clothes.

- **Strain Rate Dissipation for Elastic Deformations**. Chapter 3 describes and analyzes in detail our proposed damping model based on strain rate dissipation potentials. We start by defining the desired properties of a good damping model. Then, we introduce strain rate dissipation potentials and the generic derivation of damping forces. Finally, we compare our method to the Rayleigh damping model, a simple method commonly used in the computer animation literature.

- **Robust Eulerian-On-Lagrangian Rods**. Chapter 4 introduces a method to simulate complex rod assemblies and stacked layers with implicit contact handling, through Eulerian-on-Lagrangian(EoL) discretizations. We start with a recap of the regular EoL discretizations and its application to yarn-level cloth simulation. Then, we discuss the sources of degenerate discretizations and their devastating effects, to conclude with our new discretization solution.

- **Conclusions**. Chapter 5 contains discussions about the methods developed in this thesis, along with an analysis of the limitations of the proposed models, possible applications and potential future work.

Chapter 2
Background

The simulation of cloth has been a widely studied topic in the field of computer graphics and it covers a large number of research areas. In this section we outline the works that have inspired the development of this thesis. First, we will summarize the most important works in cloth simulation, reviewing the literature in continuum descriptions of cloth as well as those based on discrete elements such as yarns. Second, we will talk about the previous works in dissipative phenomena, and finally we will overview related work on multilayered and stacked cloth.

2.1 Cloth Simulation

For many years, cloth simulation has been an extensive field of research. The representation of virtual cloth can be categorized into two main groups. The first one, oriented to the textile industry, tries to understand the cloth from a mechanical engineering perspective to develop an accurate representation for predicting the cloth properties. The second group is the computer graphics industry, whose main objective is to obtain plausible behavior and visualization of cloth at minimal computational cost. Our research is more tightly connected to this last group.

The animation and simulation of cloth in computer graphics is full of technical challenges: creating realistic results of complex garments at faster run-times is one of the largest drives of research in this area. Around the 1980s, researchers became interested in more physically based techniques to model clothing behavior. Since then, cloth simulation has driven most of the notable breakthroughs in the field: mechanical modeling, contact handling, friction or numerical integration, among others. The

broad range of potential applications and run-time constraints has led to the development of different techniques that describe the behavior of cloth with different degrees of accuracy.

We group cloth simulation methods into two main categories. On one hand, thin-shell models describe fabrics as a continuous surface, therefore disregarding the underlying yarn structure. On the other hand, rod-based models treat the problem of simulating each independent yarn present in the fabric. Following that, we will go over some of the key literature in both categories.

2.1.1 Thin-Shell Models

A wide range of simulation models used in Computer Graphics considers the fabric as a continuous thin-shell. Such models enable simple treatment of cloth kinematics, providing a tradeoff between performance and accuracy. The work by [Terzopoulos et al., 1987] pioneered this way of approaching cloth simulation using continuum mechanics. This work inspired later researchers to explore different methods while maintaining this thin-shell assumption.

Some of the earliest approaches discretized the fabric surface into sets of mass-spring networks to model the elasticity of cloth. The seminal work of [Provot et al., 1995] introduced ensembles of spring networks with different topologies for modeling resistance to different deformation modes, the so-called structural, shear and flexion springs. While simple and highly performant, these formulations often come across several limitations: their accuracy is low, and due to their ad-hoc nature, parameterization of their elastic properties is often artist-driven. Moreover, they are limited in their ability to model relevant phenomena present in real-world textiles such as anisotropy or non-linear material response. Provot noted this last limitation and introduced a local strain limiting procedure to prevent unrealistically large elongations. Later works [Bridson et al., 2002, Bridson et al., 2003, Thomaszewski et al., 2009] would adopt this strategy to overcome the limitations of linear elasticity, even enabling anisotropy [Hernandez et al., 2013].

The use of high stiffnesses can alleviate the problems associated with linear elasticity models. However, this involves considerations of numerical stability or computational cost. One such problem is buckling instability. When subjected to compression, forces applied at the extremes of a thin material reach critical levels, the structure

reaches unstable equilibrium which leads to sudden changes in its shape (i.e. the structure buckles). This manifests in the simulation as numerical instabilities and ill-conditioned system matrices in implicit integration schemes, proving to be problematic in applications where robustness is key. Previous works solve this problem by introducing large dissipative forces on out-of-plane motions [Baraff and Witkin, 1998, Volino and Magnenat-Thalmann, 2000]. However, this diminishes the realism of naturally-emerging wrinkles in cloth, sometimes even removing them altogether. [Choi and Ko, 2005] circumvent this problem by handling buckling explicitly through an approximation of the post-buckling state, thus increasing both robustness and performance.

Alternatively to these, several works explored methods derived from continuum mechanics foundations, employing different discretization approaches. Out of these, the finite element method (FEM) is perhaps the most well-known, often based on the geometrically exact thin-shell formulation by [Simo and Fox, 1989]. Thanks to its continuum foundations, cloths modelled using this method enjoy several advantages over discrete approaches. On one hand, they enable the use of a large number of possible constitutive models with different degrees of geometrical and material nonlinearity [Müller et al., 2002, Grinspun et al., 2003, Volino et al., 2009] while providing resolution-independence, a quality that has been successfully exploited by adaptive schemes to bring detail only to certain regions of interest. In this regard, the seminal work of [Narain et al., 2012], dynamically refines and coarsens triangle meshes to introduce detail in some areas while preserving the curvature and wrinkles of the cloth (Fig. 2.1). On the other hand, material characterization is well understood and can be obtained through standard engineering measurement [Penava et al., 2014], leading to plausible matches to real-world fabrics.

While a clear improvement over mass-spring networks, these models are not free of limitations: continuum mechanics primarily address membrane elasticity (i.e. stretching, shearing and area preservation), requiring explicit formulation that model resistance to out-of-plane (i.e. bending) deformations. [Grinspun et al., 2003] formulate a discrete flexural energy through the discrete approximation of continuous curvature measurements. A similar formulation was proposed by [Bridson et al., 2003], who identified an independent bending mode that does not affect rigid body transformations nor in-plane deformations. [Thomaszewski et al., 2005] designed a subdivision-

Figure 2.1: [Narain et al., 2012] proposed a technique to dynamically refine and coarsen a finite element mesh used for cloth simulation. To this end, they create anisotropic elements that follow the curvature of wrinkles and creases in the cloth.

based finite element based in the Kirchhoff-Love shell theory that models both membrane and bending energy in a consistent way.

Moreover, capturing interesting yarn-scale subtleties such as anisotropic and plastic behavior is very challenging under these formulations, often requiring very complex constitutive models. Researchers leveraged on data-driven models for capturing such phenomena using real-world data [Wang et al., 2011, Miguel et al., 2012, Miguel et al., 2016].

2.1.2 Rod-Based Models

The simulation of rods, strands, or deformable curves in general, has attracted the attention of Computer Graphics researchers for many years. Earlier approaches in the literature relied on networks of masses connected by springs to simulate hair and fur [Rosenblum et al., 1991]. Not long ago, these mass-spring methods were modified to meet the needs of production animations [Selle et al., 2008, Iben et al., 2013]. However, although simple and robust, these methods were problematic when trying to capture twisting behavior. Following the mass-spring idea, other approaches model rods as a serial chain of rigid bodies connected by joints [Choe et al., 2005, Hadap, 2006].

[Pai, 2002] introduced the Cosserat theory of elastic rod simulation to the computer graphics community. In his work, rods are represented by using curvature as minimal coordinates. Although efficient, the centerline is only represented implicitly by the rod's curvature and has to be recovered through integration, thus making contact handling difficult. [Bertails et al., 2006] extended this approach to the super-helix

Figure 2.2: The discrete elastic rod model proposed by [Bergou et al., 2008] uses a curve-angle parameterization to guarantee that the orientation frame naturally remains adapted to the centerline.

model, specially designed to simulate the dynamics of helical elastic rods such as curly hair.

Other alternative approaches represent rods using an explicit representation of the centerline. [Spillmann and Teschner, 2007] simulate the dynamics of rods by applying the finite element method to continuous deformation energies from Cosserat theory. Thanks to the explicit representation of the centerline, collisions can be handled efficiently, which allows them to simulate knots at interactive rates [Spillmann and Teschner, 2008].

[Bergou et al., 2008] introduced the discrete elastic rod model (Fig. 2.2), where an oriented frame automatically follows the deformation of the rod center line thanks to a curve-angle parameterization. This work was later extended to simulate discrete viscous threads [Bergou et al., 2010a].

Most of these previous works rely on implicit integration schemes for solving the rod's stiff equations of motion. However, such integration schemes are often not suitable for applications where real-time rates are required. To overcome this, some recent works have focused on developing models based on constrained dynamics solvers such as position-based dynamics (PBD) [Müller et al., 2007] to simulate rods [Umetani et al., 2014].

Rod-based models have been successfully applied for modeling cloth at yarn level. The first incursion arguably began with [Peirce, 1937] who derived in a set of parameters and equations for modeling the crossing of yarns as inextensible curves in woven fabric. Since then, textile research has dedicated a lot of attention to yarn-level models to better understand the behavior of cloth.

Several methods have been developed for predicting the mechanical behavior of yarns [Kawabata et al., 1973, Hearle et al., 1969], as well as to alleviate the large

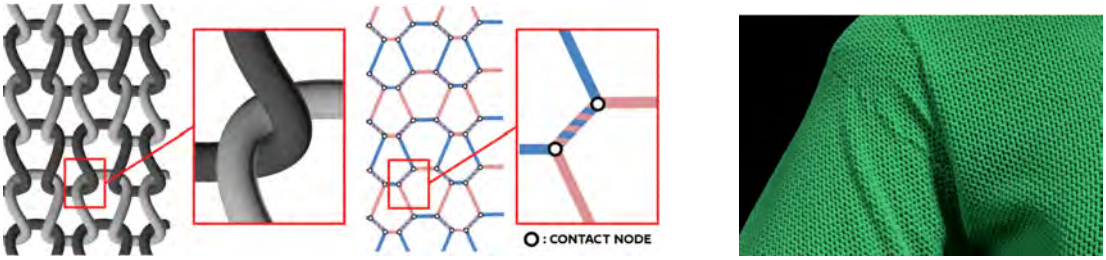

Figure 2.3: Cirio et al. proposed a yarn-level cloth model that managed intra-fabric contacts implicitly. This work was applied for the simulation of woven [Cirio et al., 2014] and knitted garments [Cirio et al., 2017].

computational cost of yarn-level models [Nadler et al., 2006, Reese, 2003, McGlockton et al., 2003]. However, all these works focused on studying the mechanics from an engineering point of view, often paying attention to very small patches of fabric in controlled conditions, ignoring the computational complexity of full-size garments.

In computer graphics, the seminal work of [Kaldor et al., 2008] was the first able to simulate entire knitted garments at the yarn level. In their method, yarns were modeled as inextensible rods, and inter-yarn contacts were explicitily computed through stiff penalty forces and velocity-filter friction. Their work was later extended to accelerate contact handling through the use of local rotated linearizations of penalty forces [Kaldor et al., 2010]. However, despite the improvements introduced in the method, the sheer number of contacts present in knitted garments led to important time step constraints in order to guarantee robust and accurate contact handling.

To avoid explicit inter-yarn contact handling, [Cirio et al., 2014] introduced an alternative yarn-level model based in the discretization proposed by [Sueda et al., 2011], assuming that yarns are in persistent contact (Fig. 2.3). This way, yarns were modeled as flexible rods with additional sliding degrees of freedom to allow them to slide along each other. Thanks to this discretization they were able to represent complex plastic effects such as snags or pulls. Their innovative method for woven fabrics was later extended to support some types of knits [Cirio et al., 2017]. However, the method was limited to some specific knit patterns, as yarns are not allowed to cross each other while sliding. Recently, [Pizana et al., 2020] improved the model proposed by [Cirio et al., 2014] by introducing a robust and controllable bending model for yarn-level cloth simulation with nodal discretizations.

Yarn-level cloth models are also used in computer graphics for the design of fabrics and fabrication processes, in particular for knits. In 2018, [Leaf et al., 2018] extended the model of [Kaldor et al., 2008] for the authoring and editing of small periodic knit patches. Thanks to the efficient GPU implementation of the method and the formulation of periodic boundary conditions, they were able to simulate a multitude of stitches and patterns at interactive rates.

[Yuksel et al., 2012], on the other hand, created a stitch mesh data structure to define the construction of knit garments as a tiling procedure. This work was later extended to fulfill fabrication constraints [Wu et al., 2019], to represent crochet patterns [Guo et al., 2020] and to use it in the context of fabrication-oriented editing [Narayanan et al., 2019].

Recent approaches have focused on improving the yarn-level simulation models by pursuing a good trade-off between efficiency and realism. In this context, [Casafranca et al., 2020] developed a method that enriches triangle-based representations with yarn-level details at regions of interest, solving both in a seamless and robust manner. On the other hand, [Sperl et al., 2020] introduced a homogenization method that estimates thin-shell deformations from yarn-scale simulations. The use of the Material Point Method [Jiang et al., 2017] has also shown success to track yarn-level details while allowing robust treatment of collisions, thus achieving cost-effective simulations.

2.2 Dissipative Phenomena

Computer animation has addressed the simulation of materials and effects with very diverse damping behaviors, from the highly damped behavior of flesh to the inviscid behavior of water. The relevant works in the literature usually distinguish three distinct types of damping, depending on their nature and purpose. **(i)** Damping that is deliberately formulated in order to simulate the nature of the given material is often referred to as material-intrinsic damping [Choi and Ko, 2005]. **(ii)** Damping produced by implicit formulations of the system dynamics is referred to as artificial or numerical damping. **(iii)** Damping added to enhance stability is usually referred to as fictitious damping [Yu et al., 2000].

In this section we will focus on describing some material-intrinsic damping approaches, as the purpose of our work is particularly related to this type of damping. We separate the literature into two groups, depending on the relevant state variables that determine energy dissipation. On one hand, the most common approach is to assume that dissipation is only determined by instantaneous velocities, which gives rise to velocity-dependent damping forces. This type of damping is usually so-called *Viscous damping*. On the other hand, some recent works have explored different approaches to define the dissipative behavior of materials. We have grouped them into *Other damping approaches*.

2.2.1 Viscous Damping

Characterization of damping mechanisms in dynamics simulation is an active area of research to achieve realistic behavior of real-world materials and to improve the stability of the simulated systems. However, in spite of a large amount of literature, understanding of damping mechanisms is still quite primitive. A major reason for this is that, in contrast with inertia and stiffness forces, it is not clear which state variables are relevant to determine the damping forces. By far, the most common approach in computer graphics is to use the so-called *linear viscous damping*, in which the damping force linearly depends on the instantaneous velocities. This is commonly formulated as:

$$\mathbf{f}_d = -\mathbf{D}\mathbf{v}, \tag{2.1}$$

where $\mathbf{D}$ is a positive semi-definite damping matrix, $\mathbf{v}$ is the linear velocity of all the degrees of freedom in the simulated system, and $\mathbf{f}_d$ is the resulting damping force.

In cloth simulation, one of the first works that recognized the need of damping forces was developed by [Terzopoulos et al., 1987]. In their work, the cloth was discretized as a rectangular mesh, and energy functions were derived using a continuum formulation. In terms of damping, they only implemented a simple viscous drag force.

Following Terzopoulos et al.'s treatment of deformable surfaces, [Carignan et al., 1992] described a cloth simulation system using a rectangular discretization. They recognized the need of damping functions that do not penalize rigid-body motions of the cloth (unlike simple viscous damping), hence they added a force which damps

cloth stretch and shear (but not bending). Nevertheless, their damping function —a linear function of velocity— does not match the quartic energy functions of their continuum formulation.

Among all the works that make use of linear viscous damping, Rayleigh damping [Rayleigh, 1896] is probably the oldest but still the most widely used one. Rayleigh damping is a linear approximation of Caughey damping [Caughey and O'Kelly, 1965], a method designed for regulating the strength of damping for different spectral components. In this model, the damping force is formulated as the linear combination of the mass and stiffness matrices. This way, the damping force can be defined as $\mathbf{f} = \mathbf{C}\mathbf{v}(t)$, where $\mathbf{C}$ is usually formulated as:

$$\mathbf{C} = \alpha\mathbf{M} + \beta\mathbf{K}, \tag{2.2}$$

being $\mathbf{M}, \mathbf{K}$ the mass and stiffness matrices respectively and α, β are constants of proportionality. One advantage of this method is that it enables a straightforward reuse of the mass and stiffness matrices when using implicit integration schemes, thus avoiding explicit formulation of damping forces. However, for systems with many degrees of freedom, it is difficult to guess meaningful values of α and β. Moreover, such damping approach affects the global object dynamics, often producing an overly damped system, which turns out in an undesirable loss of kinetic energy and therefore unrealistic behavior. A detailed analysis of this problem is presented in Section 3.2.5 of Chapter 3.

Finer control over the damping behavior can be achieved by splitting the stiffness-proportional term and assigning a different one to each deformation mode (i.e. $\mathbf{C} = \alpha\mathbf{M} + \beta_a\mathbf{K}_a + \beta_b\mathbf{K}_b + \beta_c\mathbf{K}_c + ...$). However, while more controllable, the problem of excessive kinetic loss still remains.

In computer animation several works implement linear damping models that follow Rayleigh's approach. [Grinspun et al., 2003] used Rayleigh damping for the simulation of thin flexible structures with a Newmark ODE integration scheme. [Cirio et al., 2014] employed this same scheme in the context of yarn-level cloth simulation using a backward Euler implicit integrator, and [Gast et al., 2015] used a "lagged version" of Rayleigh damping to define a damping energy function for optimization-based integration.

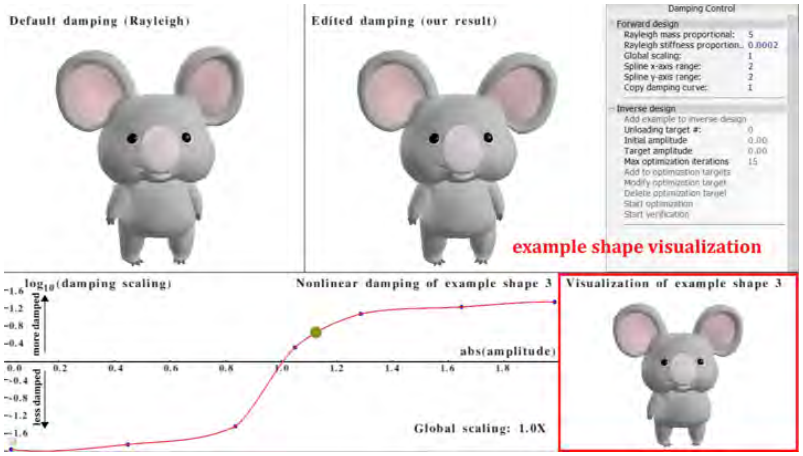

Figure 2.4: [Xu and Barbič, 2017] proposed an example-based method for the design of nonlinear anisotropic damping in an artist-friendly fashion, enabling independent damping design for each example deformation.

Recent works take inspiration from Rayleigh damping to design different dissipation approaches. [Xu and Barbič, 2017] introduced a method to design damping behaviors in an artist-friendly manner. Starting from a regular Rayleigh damping model, they developed a framework to modify the damping behavior for arbitrary deformation directions as illustrated in Fig. 2.4. [Li et al., 2018] introduced a new type of damping model specifically designed for Projective Dynamics. Through the use of the Laplacian matrix of Projective Dynamics, they can approximate Rayleigh's stiffness matrix and remove high-frequency vibrations.

Nevertheless, as mentioned before, Rayleigh damping tends to overdamp high frequency responses, usually leading to an underwhelming loss of kinetic energy, which is very problematic when fine control is necessary. To avoid this loss of kinetic energy, other works proposed alternative dissipation strategies. [Baraff and Witkin, 1998] described a general treatment for damping that was independent of the specific energy function being damped. They defined damping forces aligned with soft-constraint elastic forces, but proportional to constraint velocities instead. Inadvertently, Baraff and Witkin designed a damping model that constitutes a particular case of dissipation potential [Goldstein et al., 2002], with the benefit of avoiding unnecessary dissipation of the system's total kinetic energy. Our work on this topic, further described in section 3.2, draws inspiration from the damping approach proposed by Baraff and Witkin and proposes a formalization of the requirements for designing a good damp-

ing model. [Bender and Deul, 2013] also used this type of damping for adaptive cloth simulation with corotational finite elements and [Oh et al., 2006] further improved it with an implicit integration technique that is able to reproduce stable cloth without introducing excessive damping forces.

Other works, such as that by [Volino and Magnenat-Thalmann, 2000, Volino and Magnenat-Thalmann, 2001] found that inappropriate damping forces may prevent wrinkles from forming or disappearing correctly, or may prevent fabrics even from falling under their own weight. Later, [Choi and Ko, 2005] proposed a method that includes artificial damping and material-intrinsic damping, but avoids fictitious damping through the use of a predicted static post-buckling response, effectively handling the instabilities associated with post-buckling situations.

2.2.2 Other Damping Sources

Some causes of dissipation may not be directly related to velocities. One example is the numerical dissipation that appears as a result of the dynamics integration process. Implicit solvers are a prime example of this: although highly stable, these methods trade off stability at the cost of high kinetic energy damping. As a result, researchers have explored different approaches to mitigate such dissipation. Variational methods formulate integration preserving dynamic invariants accurately, minimizing numerical damping [Kharevych et al., 2006, Gast et al., 2015]. Other approaches find success in mitigating this problem by tracking undesired dissipation and injecting it back into the system as a post-process. These strategies are common practice in the context of fluid simulation. In such context, [Fedkiw et al., 2001] introduced vorticity confinement forces to computer graphics for restoring kinetic energy at vortices and eddies, counteracting dissipation produced by semi-Lagrangian advection schemes. In the context of deformable bodies, [Su et al., 2013] devised momentum-conserving correction forces to preserves the system's global energy.

2.3 Multilayered and Stacked Clothes

Daily-life garments are usually composed of multiple layers of cloth, either sewn or stacked, whose appearance and behavior is greatly influenced by the contacts occurring between them. Consequently, if we want to reproduce the behavior of such gar-

ments, we must pay special attention to how such contacts between these different layers are handled.

Unfortunately, this is still an open challenge in the cloth simulation literature: because of the thin-shell nature of cloth, contact detection algorithms require a high degree of accuracy (both spatial and temporal) to prevent tunneling effects. Moreover, even if detected, solving robustly the actual contacts poses a very challenging problem, specially due to the sheer amount of contact arrangements that arise in common situations. Both facts make the whole procedure very costly in terms of performance, usually becoming one of the bottlenecks in a simulation pipeline.

In this section, we will review the different works in the literature that have approached the problem of modeling multi-layered cloth or stacked garments. We will classify the different approaches in two main categories, according to the way in which contact is handled: on one hand, explicit methods, which make use of collision detection and resolution mechanisms to manage the contact between the different layers. On the other hand, implicit methods, which manage contact indirectly through the preservation of certain mesh attributes or as a consequence of the discretization.

2.3.1 Explicit Contact Handling

Explicit methods constitute the most prominent approach in the contact handling literature. The earliest works in the field primarily addressed contact detection and handling of rigid bodies, drawing inspiration from the well-established methods in the Computer-Assisted Design (CAD) and robotics fields. However, deformable bodies introduce additional challenging problems, especially for two-dimensional manifolds such as cloth.

The traditional explicit contact handling pipeline usually consists of two steps: a collision detection, and a contact resolution step. Formally, detection of inter-object collisions and self collisions involves testing all potential pairs of geometric features (e.g. triangles, tetrahedra) for intersection. However, while rigid body simulations often produce relatively few contacts per object, deformable bodies naturally give rise to large numbers of them. Therefore, this task usually becomes the most expensive part of a collision handling pipeline.

Over the years, researchers have proposed different schemes to accelerate this process by exploiting spatial relationships in order to cull large sets of potential contacts. The use of bounding volume hierarchies (BVH) is arguably the most prominent strategy used in the deformable bodies literature [Bergen, 1997]. Given a set of geometric features (e.g. primitives), BVH-based methods construct a tree structure by recursively partitioning the space surrounding the geometry, forming a hierarchical structure and wrapping each level using a bounding volume. This way, contact detection becomes a tree-traversal problem which enables the pruning of large potential contact sets.

The performance of BVH trees is largely affected by the bounding volume and partitioning heuristic of choice. Deformable objects and self-collision in general also impose additional complexities. The spatial relationship between primitives changes in every simulation step as objects deform. Moreover, in the case of self-collisions, geodesically nearby surface primitives cannot be easily pruned away. As such, large efforts have been put in different aspects of their design: use of different bounding volumes, good split heuristics, accelerated parallel traversal, fast construction and updating. A comprehensive summary covering such approaches can be found in [Ericson, 2004].

Other acceleration schemes have been successfully applied for collision and self-collision detection. Some examples are spatial hashing [Teschner et al., 2003], the use of representative primitives [Curtis et al., 2008] or visibility-based culling [Govindaraju et al., 2003] at different hierarchical levels [Johnson and Cohen, 2001].

While physical integrators evaluate the new states of the deformable objects at distinct intervals only, collisions can occur at any instant in between such intervals. Failing to detect such events can create entangled states from which it is hard to recover later, specially due to the thin nature of structures such as cloth and hair. Algorithms based on continuous collision detection (CCD) can handle these cases in a robust way [Provot, 1997, Bridson et al., 2002, Bridson et al., 2003], but special consideration needs to be taken to ensure that the detection procedures are fail-proof against numerical and rounding error [Wang, 2014].

Once the contacting manifolds have been determined, an appropriate response has to be computed in order to resolve the contact. Collision response algorithms can be classified into three categories on a general basis[Baraff and Witkin, 1997]: constraint-based methods, penalty-based methods and impulse-based methods.

Constraint-based methods [Pauly et al., 2004, Otaduy et al., 2009] model contact response by the introduction of non-penetration constraints, usually formulated and solved within linear complementarity problem (LCP) or non-linear programming frameworks. While these are observed to produce the highest quality results, their resolution is computationally challenging, therefore relegating their use to rigid body simulations due to the scarce number of potential contacts. Penalty-based and impulse-based methods offer a more computationally amenable alternative to constraints.

Penalty-based approaches aim to transform the constrained dynamics problem into an unconstrained one by formulating a conservative force field (i.e. "soft-constraint") that attempts to restore the non penetrating state [Terzopoulos et al., 1987]. While simple, these approaches suffer from many robustness and stability issues. Inappropriate choices of penetration metrics yielding force discontinuities or poorly estimated magnitudes can lead to problems such as jittery behavior, instabilities or constraint violation altogether in the form of over-penetration or even pop-through. [Harmon et al., 2009] mitigated this problem by introducing a barrier formulation instead of stiff springs. [Tang et al., 2012] employ time-continuous force computation to determine a well-behaved collision response, significantly improving the stability and robustness in contrast with previous penalty approaches. Despite these limitations, penalty methods have been widely used for complex applications such as cloth [Baraff and Witkin, 1998, Choi and Ko, 2005].

First introduced by [Mirtich and Canny, 1995], impulse-based methods sit on a middle ground between constraint and penalty-based methods. Instead of introducing forces or accelerations, contacts are resolved by introducing a series of instantaneous changes in velocities (i.e. impulses) between colliding objects. These methods enjoy relatively good stability and performance, although special attention must be paid to ensure energy conservation [Tang et al., 2013]. Nonetheless, they have found success in the simulation of complex contact arrangements. [Bridson et al., 2002, Bridson et al., 2003] leveraged on a hybrid strategy combining penalty for near-penetration scenarios and impulse methods with rigid impact areas for penetrating features.

2.3.2 Implicit Contact Handling

Beyond the use of explicit methods for the detection and resolution of contacts between different layers of cloth, other approaches proposed implicit or indirect strategies.

Some works handle contact indirectly by posing the problem as the preservation of some mesh or field attributes. [Sifakis et al., 2008] proposed a method motivated by the response of an incompressible fluid inserted between the colliding surfaces. Instead of explicitly modeling this fluid, they approximate it by using the tetrahedra defined by colliding point-triangle or edge-edge pairs. This idea was further extended by [Müller et al., 2015]. They proposed an efficient unified approach to dynamically handle collision detection and contact modeling without the requirement of testing pairs of geometric elements. They accomplish this by meshing empty regions between objects (i.e. generating an *air mesh*). This way, inter-object intersections manifest as element inversions in the air mesh, which are solved by the introduction of unilateral volume constraints to each element. Although these approaches are able to efficiently handle multiple layers of cloth, they require an initial collision-free state as input. Moreover, a mesh optimization procedure is required to ensure that the meshes satisfy the Delaunay condition, which is computationally challenging on tetrahedral meshes.

Other approaches take advantage of the discretization of cloth to efficiently manage contact. Classical methods usually rely on Lagrangian schemes to represent the cloth behavior, which are closely related to explicit contact handling methods. In Lagrangian discretizations, each individual node of the computational mesh follows the associated material particle during motion. This allows easy tracking of free surfaces and facilitates the treatment of materials with history-dependent constitutive relations. However, it is not possible to follow large distortions of the computational domain without resorting to frequent remeshing operations [Narain et al., 2012].

In contrast, Eulerian discretizations track the evolution of the continuum at fixed points in space. This allows handling large distortions in the continuum motion with relative ease, at the expense of precise free surface tracking and level of detail. Although this representation has been more commonly used in the fluid mechanics literature, recent works have successfully applied it for the simulation of deformable objects [Levin et al., 2011]. Because Eulerian simulations represent multiple objects un-

Figure 2.5: Anisotropic Elastoplasticity for Cloth, Knit and Hair Frictional Contact [Jiang et al., 2017]

der the same spatial discretization, contact detection and resolution naturally emerge without the need for any explicit mechanism.

The benefits of Eulerian discretizations in contact resolution have attracted the interest of computer graphics researchers, who explored hybrid discretization schemes. [McAdams et al., 2009] combined features of Eulerian and Lagrangian discretization to simulate hair. In particular, they take advantage of Eulerian representations to manage bulk hair interactions and Lagrangian schemes for detailed contact. [Faure et al., 2007] mapped the geometry of the bodies to a regular Eulerian grid at each timestep, which acts as a common mechanical layer where detection and resolution of collisions take place. [Li et al., 2013] proposed an Eulerian discretization of hyperelastic membranes moving on a triangulated surface to simulate skin. This way, the skin is automatically constrained to move on the body and not separate from it, avoiding the need of contact processing.

Recently, combined Eulerian-Lagrangian methods have also shown success for the robust simulation of stacks of cloth within the Material Point Method. These methods enable accurate Lagrangian tracking of cloth surfaces, plus efficient Eulerian contact handling using a constitutive model of frictional contact [Jiang et al., 2017] (Fig. 2.5). Later methods have been extended to handle rich bending models [Guo et al., 2018].

[Fan et al., 2013] coined the term *Eulerian-on-Lagrangian* (EoL) to denote simulations that use both Eulerian and Lagrangian coordinates to define aggregate kinematics. They used their method to combine large rigid or modal motion with robust deformation on Eulerian grids. In their setting, the combined Eulerian and Lagrangian

kinematics yield an ambiguous representation, which is resolved by minimizing the Eulerian contribution.

Earlier, however, [Sueda et al., 2011] had introduced an EoL method for the simulation of rods in contact with other objects. Their method places nodes with both Eulerian and Lagrangian coordinates at contact locations, and ensures that rod bending is accurately and efficiently resolved even when contacts slide. [Cirio et al., 2014] leveraged on this method for the simulation of cloth at the yarn level. [Weidner et al., 2018] extended Sueda's rod discretization to cloth modeled as a thin shell. By setting discretization nodes at sharp contacts, simulations avoid locking and spurious energy artifacts. In their work, conformal remeshing is used to maintain good mesh quality while contact nodes slide in the material domain. However, in the examples shown by the authors, contact nodes are sparse, and there are no sandwiched contacts or multiple stacked cloth layers, hence contact nodes never approach and cross each other.

Our work, further described in Chapter 4, is based in the *Eulerian-on-Lagrangian* assumption to allow the simulation of multiple stacked cloth layers and complex knit patterns. Contrary to the method of [Weidner et al., 2018], our model is able to represent sandwiched contacts crossing each other in the material domain without the use of remeshing techniques. Detailed information can be found in Chapter 4.

Chapter 3

Strain Rate Dissipation for Elastic Deformations

3.1 Introduction

Damping is a defining characteristic of real-world deformable objects. It determines the duration of oscillations, and hence the perception of dynamics and sound. Due to this relevance, it becomes a basic ingredient of physics-based computer animated deformations.

However, despite the omnipresence of damping, its study has received far less attention than its companion elasticity. Few works have been explicitly dedicated to the problem, with notable exceptions to avoid spurious damping [Su et al., 2013], estimate model parameters [Bhat et al., 2003], or design damping behaviors in an artist-friendly manner [Xu and Barbič, 2017]. Perhaps due to the limited attention, many computer animation works have used simplistic damping models, such as Rayleigh damping [Rayleigh, 1896].

In our experience, Rayleigh damping, although simple, turns problematic when fine control is necessary, either for artistic design or to match real-world behaviors. This fact has motivated us to study the design of simple damping models that satisfy important conditions by construction. In particular, we seek forces that damp only the change of deformation, and leave other dynamics unaffected. Although such conditions have been advocated before [Baraff and Witkin, 1998, Bridson et al., 2003], we formalize the requirements for *good damping* and establish a framework for the design of simple damping models.

Figure 3.1: With strain rate dissipation potentials, we ensure by construction that damping forces affect only motions that produce a change of deformation. The damping model is simple yet rich and versatile, as demonstrated by the examples. We have tested strain rate dissipation potentials on cloth simulations modeled with StVK elasticity and with yarns with sliding persistent contacts. The snapshots show a yarn-level shirt with over one million nodes.

We build our damping model on top of the concept of dissipation potential from classical mechanics [Goldstein et al., 2014]. This approach parallels the design of elastic deformation models based on energy formulations [Xu et al., 2015, Miguel et al., 2016], simplifying the process of designing damping forces that satisfy the good damping condition. As described in Section 3.2, we propose a framework for damping

models with dissipation potentials based on strain rate. This framework also helps us demonstrate why the popular Rayleigh damping model fails for nonlinear deformation models.

Furthermore, we develop diverse applied examples that prompt the considerations to be addressed for practical implementations. In Section 3.3, we discuss the application of strain rate dissipation potentials to the Saint-Venant Kirchhoff (StVK) hyperelasticity model [Sifakis and Barbic, 2012]. In this setting, we study the design of continuum dissipation models and their discretization, possibilities for parameterization under multi-dimensional strain metrics, and implications of implicit integration. In Section 3.4, we discuss the application of strain rate dissipation potentials to yarn-level cloth simulation with sliding persistent contacts [Cirio et al., 2014]. This model allows us to analyze the application to discretizations that combine Lagrangian and Eulerian coordinates. In addition, damping of yarn bending gives rise to challenges in the design of strain metrics, which are not present in elastic deformations alone.

We have evaluated the implementation of strain rate dissipation potentials on StVK elasticity for cloth simulation as well as yarn-level cloth (Fig. 3.1). Thanks to their diversity, these two examples cover many aspects of elastic deformation models, namely, nonlinear, multidimensional, and/or angular deformation metrics, as well as Lagrangian and mixed Lagrangian-Eulerian discretizations.

3.2 Dissipation Potentials for Good Damping

In this section, we describe and analyze the damping model based on strain rate dissipation potentials. We start by defining the desired properties of a good damping model. Then, we introduce strain rate dissipation potentials and the generic derivation of damping forces. We follow with practical considerations for the implementation of strain rate dissipation potentials on continuum and discrete elastic deformation models. And we discuss the computation of force Jacobians for implicit integration.

To conclude the section, we compare strain rate dissipation potentials to other simple damping models used in computer animation. In particular, for the Rayleigh damping model, we provide theoretical and experimental analysis.

3.2.1 Good Damping

Let us assume that deformation is measured through some generic strain metric ε. We define that a certain velocity $\mathbf{v}$ is decoupled from deformation if it produces no strain rate, or change of deformation, i.e., $\dot{\varepsilon} = \nabla_{\mathbf{x}}\varepsilon^T \mathbf{v} = 0$. In other words, a velocity that is decoupled from deformation lies on the null-space of the strain gradient $\nabla_{\mathbf{x}}\varepsilon$.

We define *good damping* as the dissipative forces $\mathbf{f}_d$ that produce no effect on velocities that are decoupled from deformation. Even though real-world dissipative forces may also act on velocities that are decoupled from deformation, such relationship is complex and generally unknown. Then, our strategy is to model coupled and decoupled damping separately, as also advocated by others before [Baraff and Witkin, 1998, Bridson et al., 2003].

From the definition of velocities that are decoupled from deformation, good damping implies that dissipative forces have a null projection onto the null-space of the strain gradient, i.e.,

$$\left(\mathbf{I} - \nabla_{\mathbf{x}}\varepsilon \left(\nabla_{\mathbf{x}}\varepsilon^T \nabla_{\mathbf{x}}\varepsilon\right)^{-1} \nabla_{\mathbf{x}}\varepsilon^T\right) \mathbf{f}_d = 0. \tag{3.1}$$

3.2.2 Strain Rate Dissipation Potential

We model dissipation using the concept of dissipation potential from classical mechanics [Goldstein et al., 2014]. Given a dissipation potential V_d, dissipative forces are obtained as the negative velocity-gradient of the dissipation potential. These forces can be added to the regular Euler-Lagrange equations.

For a system with kinetic energy $T = \frac{1}{2}\mathbf{v}^T \mathbf{M}\,\mathbf{v}$, conservative potential V_e, and dissipation potential V_d, the Euler-Lagrange equations on reduced coordinates $\mathbf{x}$, with velocities $\mathbf{v} = \dot{\mathbf{x}}$, are:

$$\mathbf{M}\,\dot{\mathbf{v}} = \nabla_{\mathbf{x}} T - \nabla_{\mathbf{x}} V_e - \nabla_{\mathbf{v}} V_d - \dot{\mathbf{M}}\,\mathbf{v}. \tag{3.2}$$

We propose to define the dissipation potential in terms of the strain rate metric $\dot{\varepsilon}$, i.e., $V_d(\dot{\varepsilon})$. Then, the dissipative forces $\mathbf{f}_d$ can be expressed as

$$\mathbf{f}_d = -\nabla_{\mathbf{v}} V_d = -\nabla_{\mathbf{x}}\varepsilon\, \nabla_{\dot{\varepsilon}} V_d. \tag{3.3}$$

The term $\nabla_{\dot{\varepsilon}} V_d$ can be regarded as an (integrated) dissipative stress. Then, we observe that strain rate dissipation potentials produce dissipative forces that can be obtained by projecting a dissipative stress onto the space of motions defined by the strain gradient. And it follows that these dissipative forces have a null projection onto the null-space of the strain gradient. We can confirm this by plugging the dissipative forces (3.3) into (3.1), and we conclude that strain rate dissipation potentials satisfy the good damping condition by construction.

3.2.3 Integration of Potential Densities

Furthermore, we consider a particular type of potential, obtained by integrating potential densities. We start from an elastic potential, defined in terms of some multi-dimensional strain metric ε, i.e.,

$$V_e = \sum_i w_i \, \Psi_{e,i}(\varepsilon), \tag{3.4}$$

where $\Psi_{e,i}(\varepsilon)$ is a strain energy density evaluated on some integration point, and w_i is the corresponding weight. Such integrated models are ubiquitous, and they encompass both discrete elastic models, as well as FEM models where energies are evaluated using quadrature formulations. Note that, for example, the simple FEM model with linear basis functions on simplicial meshes corresponds to the case where the strain energy density is evaluated once per mesh element, and the integration weight is the volume of the element.

From the elastic potential above, we may derive elastic forces $\mathbf{f}_e$. For Lagrangian discretizations, where integration weights w_i are constant, the elastic forces can be obtained as

$$\mathbf{f}_e = -\nabla_{\mathbf{x}} V_e = -\sum_i w_i \, \nabla_{\mathbf{x}} \varepsilon \, \mathbf{S}_{e,i}. \tag{3.5}$$

Here, the term $\mathbf{S}_{e,i} = \nabla_{\varepsilon} \Psi_{e,i}$ is, by definition, the *elastic stress*. We define similarly a dissipation potential, by integrating dissipation potential densities that depend on the strain rate $\dot{\varepsilon}$:

$$V_d = \sum_i w_i \, \Psi_{d,i}(\dot{\varepsilon}). \tag{3.6}$$

And we derive the corresponding dissipative forces:

$$\mathbf{f}_d = -\nabla_{\mathbf{v}} V_d = -\sum_i w_i \, \nabla_{\mathbf{x}} \varepsilon \, \mathbf{S}_{d,i}. \tag{3.7}$$

Here, $\mathbf{S}_{d,i} = \nabla_{\dot{\varepsilon}} \Psi_{d,i}$ is the *dissipative stress*. By contrasting (3.7) and (3.5), we can conclude that, for purely Lagrangian discretizations, elastic and dissipative forces can be obtained by following a similar procedure. In both cases, they can be obtained as weighted sums of the respective stress values multiplied by the strain gradient.

In Section 3.4 we visit the case of recently popular mixed Lagrangian-Eulerian discretizations, which do not follow the same pattern.

3.2.4 Force Jacobians

Implicit integration methods require the computation of force Jacobians for the linearization of accelerations. Damping forces (3.7) depend on both positions and velocities, hence we need both Jacobians.

The Jacobian w.r.t. velocities is:

$$\frac{\partial \mathbf{f}_d}{\partial \mathbf{v}} = -\sum_i w_i \, \nabla_{\mathbf{x}} \varepsilon \, \frac{\partial \mathbf{S}_{d,i}}{\partial \dot{\varepsilon}} \, \nabla_{\mathbf{x}} \varepsilon^T. \tag{3.8}$$

This Jacobian is typically not problematic. The term $\frac{\partial \mathbf{S}_{d,i}}{\partial \dot{\varepsilon}}$ is symmetric and, for the case of quadratic dissipation potentials, constant. In that case, positive definiteness can easily be enforced.

The Jacobian w.r.t. positions is:

$$\frac{\partial \mathbf{f}_d}{\partial \mathbf{x}} = -\sum_i w_i \left(\frac{\partial^2 \varepsilon}{\partial \mathbf{x}^2} \, \mathbf{S}_{d,i} + \nabla_{\mathbf{x}} \varepsilon \, \frac{\partial \mathbf{S}_{d,i}}{\partial \dot{\varepsilon}} \, \nabla_{\mathbf{x}} \dot{\varepsilon}^T \right). \tag{3.9}$$

This Jacobian may be problematic for two reasons. The second term is not symmetric, and we choose to discard it. The first term, on the other hand, may not be positive definite. To enforce positive definiteness, we propose to clamp the negative eigenvalues of the stress $\mathbf{S}_{d,i}$. Note that a similar term $\frac{\partial^2 \varepsilon}{\partial \mathbf{x}^2} \mathbf{S}_{e,i}$ arises in the Jacobian $\frac{\partial \mathbf{f}_e}{\partial \mathbf{x}}$ of elastic forces (3.5); therefore, implicit integration of damping forces based on strain rate dissipation potentials does not add notable complexity or cost.

We have validated that the two modifications to the Jacobian are beneficial in practice. We have tested them on implicit integration with Newmark and backward Euler methods with full Newton solves, and in the backward Euler case also with just one Newton iteration. The modifications to the Jacobian provide faster convergence of the Newton solves, as they enable the use of fast solvers for symmetric positive-definite matrices. Under just one Newton iteration, we have observed a slight difference in kinetic energy (less than 2% in our tests), which is far less than the error introduced by exiting the solve early.

3.2.5 Damping Models in Computer Animation

[Baraff and Witkin, 1998] designed dissipative forces for soft constraints, where their constraints can be paralleled to strain metrics. Their formulation enforces that dissipative forces are aligned with constraint gradients, hence they satisfy the good damping condition by construction.

Our strain rate dissipation potentials can be regarded as a generalization of their dissipative forces. By working with dissipation potentials, and not directly with forces as they do, our formulation supports arbitrary nonlinearity, anisotropy, etc., while theirs is limited to quadratic dissipation potentials. Furthermore, by integrating potential densities as described in Section 3.2.3, our formulation enables a discretization-independent parameterization.

A very common damping model in computer animation is the Rayleigh dissipation function [Rayleigh, 1896], which defines a generic dissipation potential that is quadratic on the velocities, i.e., $V_d = \frac{1}{2}\mathbf{v}^T\mathbf{D}\mathbf{v}$. Unfortunately, there is no guarantee that the resulting forces satisfy the good damping condition.

As a particular case of Rayleigh dissipation function, the Rayleigh damping model chooses $\mathbf{D} = \alpha\mathbf{M} + \beta\frac{\partial^2 V_e}{\partial \mathbf{x}^2}$. The scalar values α and β weight, respectively, the mass matrix and the Hessian of the elastic energy (or tangent stiffness matrix). These two terms are supposed to provide damping of absolute motion and change of deformation respectively, hence $\alpha = 0$ is a trivial requirement for our condition of good damping. From (3.5), and assuming a purely Lagrangian discretization, we conclude that the tangent stiffness matrix can be expressed in terms of the strain gradient as

$$\frac{\partial^2 V_e}{\partial \mathbf{x}^2} = \frac{\partial^2 \varepsilon}{\partial \mathbf{x}^2}\nabla_\varepsilon V_e + \nabla_{\mathbf{x}}\varepsilon\frac{\partial^2 V_e}{\partial \varepsilon^2}\nabla_{\mathbf{x}}\varepsilon^T. \tag{3.10}$$

With $\alpha = 0$, the resulting Rayleigh damping force is

$$\mathbf{f}_R = -\beta \left(\frac{\partial^2 \varepsilon}{\partial \mathbf{x}^2} \nabla_\varepsilon V_e + \nabla_\mathbf{x} \varepsilon \, \frac{\partial^2 V_e}{\partial \varepsilon^2} \nabla_\mathbf{x} \varepsilon^T \right) \mathbf{v}. \tag{3.11}$$

By plugging this force in the good damping condition (3.1), we conclude that Rayleigh damping is *good* damping only if the strain metric is linear, i.e., $\frac{\partial^2 \varepsilon}{\partial \mathbf{x}^2} = 0$.

Unfortunately, linear strain metrics fail for large deformations. In the next section, we analyze the effect of Rayleigh damping on a simple experiment.

Another corollary is that, by dropping the offending term of the stiffness matrix, we can obtain good Rayleigh damping which is equivalent to the following strain rate dissipation potential:

$$V_d = \frac{1}{2} \beta \, \dot{\varepsilon}^T \frac{\partial^2 V_e}{\partial \varepsilon^2} \dot{\varepsilon}. \tag{3.12}$$

3.2.6 Experimental Analysis: Damping a Linear Spring

Let us consider a linear spring on a horizontal plane, with one moving end-point $\mathbf{x}$ and the other end-point fixed at the origin, as shown in Fig. 3.2. With rest-length L, the strain of the spring is $\varepsilon = \frac{\|\mathbf{x}\|}{L} - 1$. It follows that the strain gradient is $\nabla_\mathbf{x} \varepsilon = \frac{1}{L} \cdot \frac{\mathbf{x}}{\|\mathbf{x}\|}$, the strain Hessian is $\frac{\partial^2 \varepsilon}{\partial \mathbf{x}^2} = \frac{1}{L} \left(\mathbf{I} - \frac{\mathbf{x}}{\|\mathbf{x}\|} \frac{\mathbf{x}^T}{\|\mathbf{x}\|} \right)$, and the strain rate is $\dot{\varepsilon} = \frac{1}{L} \cdot \frac{\mathbf{x}^T}{\|\mathbf{x}\|} \dot{\mathbf{x}}$. We design a quadratic elastic energy of the form $V_e = \frac{1}{2} L \, k_e \, \varepsilon^2$, Rayleigh damping with $\alpha = 0$, and an *equivalent* strain rate dissipation potential $V_d = \frac{1}{2} \beta \, L \, k_e \, \dot{\varepsilon}^2$.

In Fig. 3.2 we plot kinetic energy profiles for several animations where we compare Rayleigh damping and strain rate dissipation potentials. In all the animations, the moving end-point is initialized with a velocity of 20 tangent to the spring, with the spring undeformed. The simulation parameters were: rest-length $L = 2$, elastic stiffness $k_e = 100$, mass $m = 1$.

Fig. 3.2 compares the behavior for several values of β. With strain rate dissipation potentials, damping affects only the oscillation of the spring length, and the system reaches a uniform circular motion where the elastic force acts as centripetal force. With Rayleigh damping, the system slows down toward a full stop.

The results were obtained with a time step of 0.01, and are practically identical for symplectic Euler and implicit Newmark, hence we can rule out effects due to the

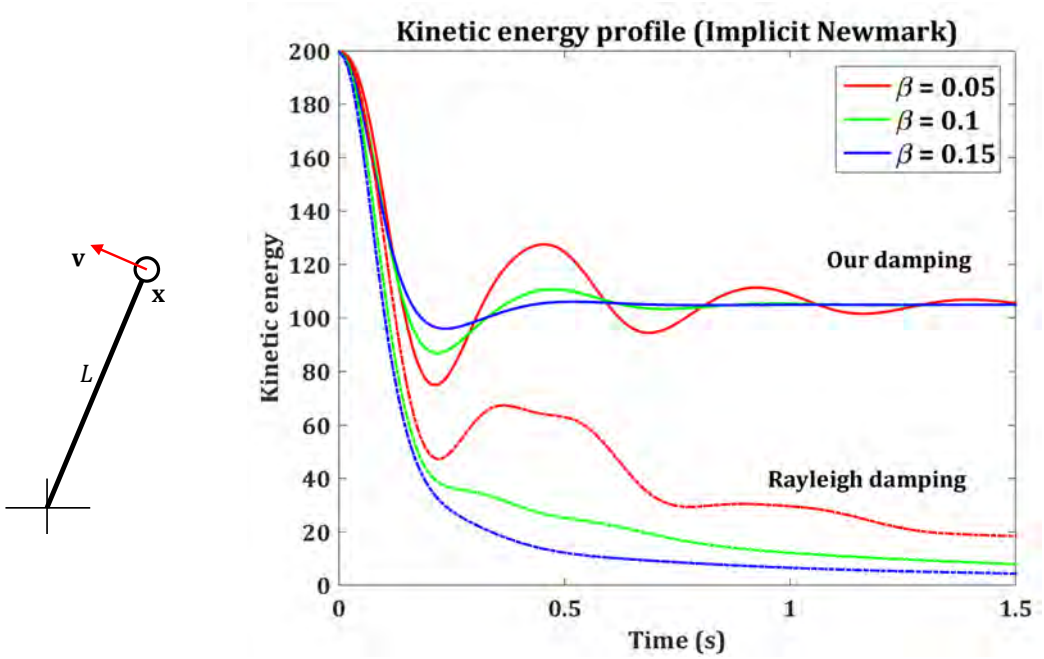

Figure 3.2: We simulate a spring rotating on a horizontal plane under different damping models. Left: Initial conditions, with mass at position $\mathbf{x}$ and velocity $\mathbf{v}$ tangent to the spring, of rest-length L. Right: Evolution of the kinetic energy with our strain rate dissipation potential *vs.* Rayleigh damping, for three different values of damping coefficient β. The dissipation potential is modeled according to (3.12) in this experiment.

integration method. Backward Euler, on the other hand, suffers noticeable numerical damping, however far less than the one introduced by Rayleigh damping. With implicit Newmark and a time step of 0.1, the damping behavior is still well preserved under a full Newton solve, while exiting the Newton solve after one iteration introduces some error, again far less than the error introduced by Rayleigh damping.

3.3 Application to StVK Hyperelastic Model

We choose the StVK elastic material model as an example of hyperelasticity. In this section, we study the application of strain rate dissipation potentials to this deformation model, and we propose a parameterization that produces a linear isotropic dissipative stress.

Given deformed and undeformed positions $\mathbf{x}$ and $\bar{\mathbf{x}}$ respectively, the deformation gradient is defined as $\mathbf{F} = \frac{\partial \mathbf{x}}{\partial \bar{\mathbf{x}}}$. Then, the Green strain tensor is defined as $\varepsilon = \frac{1}{2}\left(\mathbf{F}^T\mathbf{F} - \mathbf{I}\right)$, and the StVK elastic material model defines a strain energy density

$$\Psi_e = \frac{\lambda}{2}\operatorname{tr}(\varepsilon)^2 + \mu \operatorname{tr}\left(\varepsilon^2\right), \tag{3.13}$$

with λ and μ the Lamé constants.

This energy definition yields the second Piola-Kirchhoff stress

$$\mathbf{S}_e = \nabla_\varepsilon \Psi_e = \lambda \operatorname{tr}(\varepsilon)\,\mathbf{I} + 2\mu\varepsilon. \tag{3.14}$$

The use of a nonlinear strain metric turns the complete model nonlinear, yet the stress-strain relationship is linear and isotropic.

Based on the integral formulation (3.4) of the StVK strain energy density (3.13), we could define a dissipation potential for StVK by following the Rayleigh damping analogy (3.12). However, strain rate dissipation potentials allow much more versatile formulations.

Here, we explore one example, using a parameterization anologous to the StVK strain energy density (3.13). We formulate an analogous dissipation potential, substituting the strain with the strain rate:

$$\Psi_d = \frac{\lambda_d}{2}\operatorname{tr}(\dot{\varepsilon})^2 + \mu_d \operatorname{tr}\left(\dot{\varepsilon}^2\right), \tag{3.15}$$

We consider two independent material parameters λ_d and μ_d, analogous to the Lamé parameters for the elastic case. Interestingly, isotropic Newtonian fluids are also parameterized by two parameters, typically the dynamic viscosity and the bulk viscosity. However, the mapping to these two parameters is unclear, as they are defined for a different strain rate tensor.

Our proposed dissipation potential definition yields the following linear isotropic dissipative stress:

$$\mathbf{S}_d = \nabla_{\dot{\varepsilon}} \Psi_d = \lambda_d \operatorname{tr}(\dot{\varepsilon})\,\mathbf{I} + 2\mu_d\dot{\varepsilon}. \tag{3.16}$$

This formulation enables very simple implementation in practice, as discussed in Section 3.2.3. At each integration point, the dissipative stress is evaluated and added

to the second Piola-Kirchhoff stress, and the rest of the force computation follows as usual. The evaluation of the dissipative stress requires the strain rate, which is obtained by differentiating the Green strain tensor, and yields:

$$\dot{\varepsilon} = \frac{1}{2}\left(\mathbf{F}^T \dot{\mathbf{F}} + \dot{\mathbf{F}}^T \mathbf{F}\right). \tag{3.17}$$

The time derivative of the deformation gradient is nothing else but the gradient of the velocity w.r.t. undeformed coordinates, i.e., $\dot{\mathbf{F}} = \frac{\partial \mathbf{v}}{\partial \bar{\mathbf{x}}}$. For linear shape functions, the deformation gradient is obtained per element as $\mathbf{F} = \mathbf{X} \cdot \bar{\mathbf{X}}^{-1}$, where $\mathbf{X}$ is a matrix built with element node positions as columns, and $\bar{\mathbf{X}}$ is a constant matrix that depends on undeformed node positions [Sifakis and Barbic, 2012]. The time derivative of the deformation gradient can be obtained similarly as $\dot{\mathbf{F}} = \mathbf{V} \cdot \bar{\mathbf{X}}^{-1}$, where $\mathbf{V}$ is a matrix built with element node velocities as columns.

The dissipative stress (3.16) could be applied also to other deformation models. One example is corotational elasticity, with strain $\varepsilon = \mathbf{R}^{-1}\mathbf{F} - \mathbf{I}$, and $\mathbf{R}$ a rotation matrix obtained through polar decomposition of the deformation gradient $\mathbf{F}$. The implementation would differ in the computation of the gradient and the time derivative of the strain, and we leave the test of such extensions for future work.

As discussed in Section 3.2.4, the application of the model with implicit integration requires the computation of force Jacobians. With our stress definition (3.16), ensuring well-behaved Jacobians is simple. In the Jacobian w.r.t. velocities (3.8), the term $\frac{\partial \mathbf{S}_{d,i}}{\partial \dot{\varepsilon}}$ is constant, symmetric, and also positive definite for the right values of λ_d and μ_d. In the Jacobian w.r.t. positions (3.9), we do as proposed in Section 3.2.4, and clamp the negative eigenvalues of the stress $\mathbf{S}_{d,i}$ for each mesh element.

3.4 Application to Yarn-Level Cloth

[Cirio et al., 2014, Cirio et al., 2017] designed a yarn-level cloth model that represents yarns as flexible rods in persistent contact, but with the option to slide with respect to each other. Their reduced-coordinate representation combines Lagrangian coordinates for the 3D position of yarn crossings, with Eulerian coordinates for the sliding arc-length positions of such yarn crossings. Thanks to the sliding arc-length coordinates, their method avoids altogether the computation of collision detection and

collision response between yarns that are permanently in contact, and handles such inter-yarn contact implicitly as discussed in Section 2.3.2 of Chapter 2.

The model of yarns with sliding persistent contacts poses two interesting questions for the design of good damping. First, due to the existence of Eulerian coordinates, the analysis of elastic and damping forces in Section 3.2.3 does not hold. Second, the straightforward design of strain rate dissipation potentials for rod bending suffers robustness problems due to indeterminacy of the strain gradient.

In this section, we address these two questions, demonstrating the application of strain rate dissipation to yarn-level cloth simulation.

3.4.1 Forces and Their Jacobians

Yarns with sliding persistent contacts constitute a case of mixed Lagrangian-Eulerian discretization [Sueda et al., 2011, Fan et al., 2013]. In such models, the integration weights of elastic energies formulated as (3.4) are not constant, as they depend on the Eulerian coordinates. Revisiting the derivation of elastic forces, we obtain the following expression:

$$\mathbf{f}_e = -\nabla_{\mathbf{x}} V_e = -\sum_i w_i \, \nabla_{\mathbf{x}} \varepsilon \, \nabla_{\varepsilon} \Psi_{e,i} - \sum_i \nabla_{\mathbf{x}} w_i \, \Psi_{e,i}. \tag{3.18}$$

Unlike the elastic force (3.5) for purely Lagrangian discretizations, in this case the elastic force does not point in the direction of the strain gradient $\nabla_{\mathbf{x}}\varepsilon$. It exhibits a term that minimizes elastic energy simply by smearing it out by changing the Eulerian discretization. This term points in the direction $\nabla_{\mathbf{x}} w_i$.

The damping force (3.7) for Lagrangian discretizations is valid for the mixed Lagrangian-Eulerian case, as the integration weights depend on positions, not velocities. Several authors in the past, notably [Baraff and Witkin, 1998], have argued for damping forces that are aligned with elastic forces. As shown here, this should not be the case for mixed Lagrangian-Eulerian discretizations.

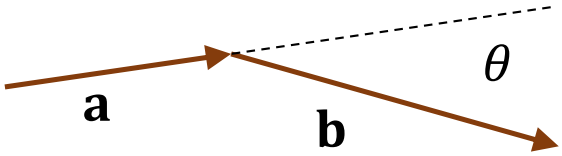

Figure 3.3: Computation of bending strain angle of two consecutive segments **a** and **b**. The strain gradient vanishes when the bending angle approaches $\theta = 0$, which is not problematic for elastic forces but leads to an undefined force direction for damping forces.

In the computation of force Jacobians, the Jacobian w.r.t. positions (3.9) also needs to be revisited. For mixed Lagrangian-Eulerian discretizations, it turns:

$$\frac{\partial \mathbf{f}_d}{\partial \mathbf{x}} = -\sum_i w_i \left(\frac{\partial^2 \varepsilon}{\partial \mathbf{x}^2} \mathbf{S}_{d,i} + \nabla_{\mathbf{x}} \varepsilon \frac{\partial \mathbf{S}_{d,i}}{\partial \dot{\varepsilon}} \nabla_{\mathbf{x}} \dot{\varepsilon}^T \right) + \nabla_{\mathbf{x}} \varepsilon \, \mathbf{S}_{d,i} \, \nabla_{\mathbf{x}} w_i^T . \tag{3.19}$$

The added term, due to the gradient of the integration weight $\nabla_{\mathbf{x}} w_i$, is not symmetric. Following the same recommendations discussed in Section 3.2.4, we choose to discard this term.

3.4.2 Damping for Rod Bending

[Cirio et al., 2014] model individual yarns as twist-free isotropic elastic rods. They are discretized into linear segments, with stretch and bending elastic energies that capture their internal resistance to deformation. Unfortunately, the bending deformation model is problematic for the formulation of strain rate dissipation potentials, due to indeterminacies at small angles. This problematic behavior is independent of the Eulerian discretization; therefore, we limit our discussion to a purely Lagrangian discretization.

Given two consecutive rod segments as shown in Fig. 3.3, with segment vectors **a** and **b**, and added rest-length L, bending strain ε_θ can be defined as

$$\varepsilon_\theta = \frac{\theta}{L}, \quad \text{with } \tan\theta = \frac{|\mathbf{a} \times \mathbf{b}|}{\mathbf{a}^T \mathbf{b}}. \tag{3.20}$$

Others have proposed similar bending strain formulations, using, e.g., $\tan\frac{\theta}{2}$ [Bergou et al., 2008] or $\sin\frac{\theta}{2}$ [Bridson et al., 2003] instead of the angle θ. However, they are

not well behaved for the large bending angles suffered by cloth yarns. $\tan\frac{\theta}{2} \to \infty$ for $\theta \to \pi$, and $\sin\frac{\theta}{2}$ yields a nonconvex energy for $\theta > \frac{\pi}{2}$.

From the strain expression (3.20), bending strain rate can be derived as $\dot{\varepsilon}_\theta = \frac{\dot{\theta}}{L}$, with angular velocity

$$\dot{\theta} = \frac{\cos^2\theta}{\mathbf{a}^T\mathbf{b}}\left(\left(\mathbf{a}^T\dot{\mathbf{b}} + \mathbf{b}^T\dot{\mathbf{a}}\right)\tan\theta + \frac{(\mathbf{a}\times\mathbf{b})^T}{|\mathbf{a}\times\mathbf{b}|}\left(\mathbf{a}\times\dot{\mathbf{b}} - \mathbf{b}\times\dot{\mathbf{a}}\right)\right). \tag{3.21}$$

The strain gradient is not defined when the bending angle is $\theta = 0$. This is not a problem for elastic forces (3.5) as long as the stress cancels out, which is the case, for example, for typical quadratic energies. However, in damping forces (3.7), the stress at $\theta = 0$ may be arbitrary, leading to an undefined force direction.

The indeterminacy problem at vanishing angles can be circumvented thanks to a small-angle approximation of the bending strain. In particular, and based on the small-angle approximation of the tangent, i.e., $\lim_{\theta\to 0}\frac{\tan\theta}{\theta} = 1$, we propose the following vector strain metric for small bending angles:

$$\varepsilon_{\mathbf{k}} = \frac{\mathbf{k}}{L}, \qquad \text{with } \mathbf{k} = \frac{\mathbf{a}\times\mathbf{b}}{\mathbf{a}^T\mathbf{b}}. \tag{3.22}$$

For quadratic energies, the energy for the large-angle bending strain (3.20) and the small-angle bending strain (3.22) are equivalent under small angles, as demonstrated through

$$\lim_{\theta\to 0}\frac{\varepsilon_\theta^2}{\varepsilon_{\mathbf{k}}^T\varepsilon_{\mathbf{k}}} = \lim_{\theta\to 0}\frac{\theta^2}{\|\mathbf{k}\|} = \lim_{\theta\to 0}\frac{\theta^2}{\tan^2\theta} = 1. \tag{3.23}$$

From the small-angle strain expression (3.22), bending strain rate can be derived as

$$\dot{\varepsilon}_{\mathbf{k}} = \frac{1}{L}\cdot\frac{1}{\mathbf{a}^T\mathbf{b}}\left(\left(\mathbf{a}^T\dot{\mathbf{b}} + \mathbf{b}^T\dot{\mathbf{a}}\right)\mathbf{k} + \mathbf{a}\times\dot{\mathbf{b}} - \mathbf{b}\times\dot{\mathbf{a}}\right). \tag{3.24}$$

The small-angle bending strain (3.22) has a well-defined gradient for vanishing angles; therefore, it enables robust computation of damping forces. For angles larger than a threshold, we switch back to the regular bending strain (3.20), as the small-angle bending strain tends to infinity for large angles.

3.5 Results

We have tested the practical implementation of strain rate dissipation potentials on the two deformation models described in Section 3.3 and Section 3.4, both applied to cloth simulation. For StVK cloth, we have used the implementation with remeshing available in ARCSim [Narain et al., 2012]. The simulator uses backward Euler integration with one Newton iteration per time step, and this integration method introduces numerical damping. For yarn-level cloth, we have used the woven cloth simulation method with sliding persistent contacts [Cirio et al., 2014], with repulsive forces for collision handling. We use backward Euler numerical integration with adaptive time stepping, with a full Newton solve per time step. Again, the integration method introduces numerical damping. The code is implemented fully on the GPU. The StVK and yarn-level cloth models are not supposed to be compared to each other, as the examples use models of very different resolution, and the parameters do not necessarily produce best-match behaviors.

In Fig. 3.4 we demonstrate the ability of strain rate dissipation potentials to control damping behavior on specific deformation modes, while leaving other motions unaffected. We have executed two different experiments.

Using the StVK cloth model on a square patch with $1,089$ vertices (with remeshing disabled), we compare the behavior with no damping, Rayleigh damping with $\beta = 0.15$, and our damping tuned to match Rayleigh damping as in (3.12). Damping is applied only to membrane deformation, not to bending. The two left plots in Fig. 3.4 show the evolution of kinetic energy for two different motions ('hanging' and 'swinging'), shown beneath. In the 'hanging' motion, our damping and Rayleigh damping produce almost equivalent overdamped motion. In the 'swinging' motion, on the other hand, our model produces a result close to the no-damping case, while Rayleigh suffers high damping.

Using the yarn-level cloth model on a square patch with $20,402$ nodes, we compare the behavior for different values of stretch damping (β_s) and bending damping (β_b). In both cases, we parameterize the dissipation potential following the analogy to Rayleigh damping (3.12).

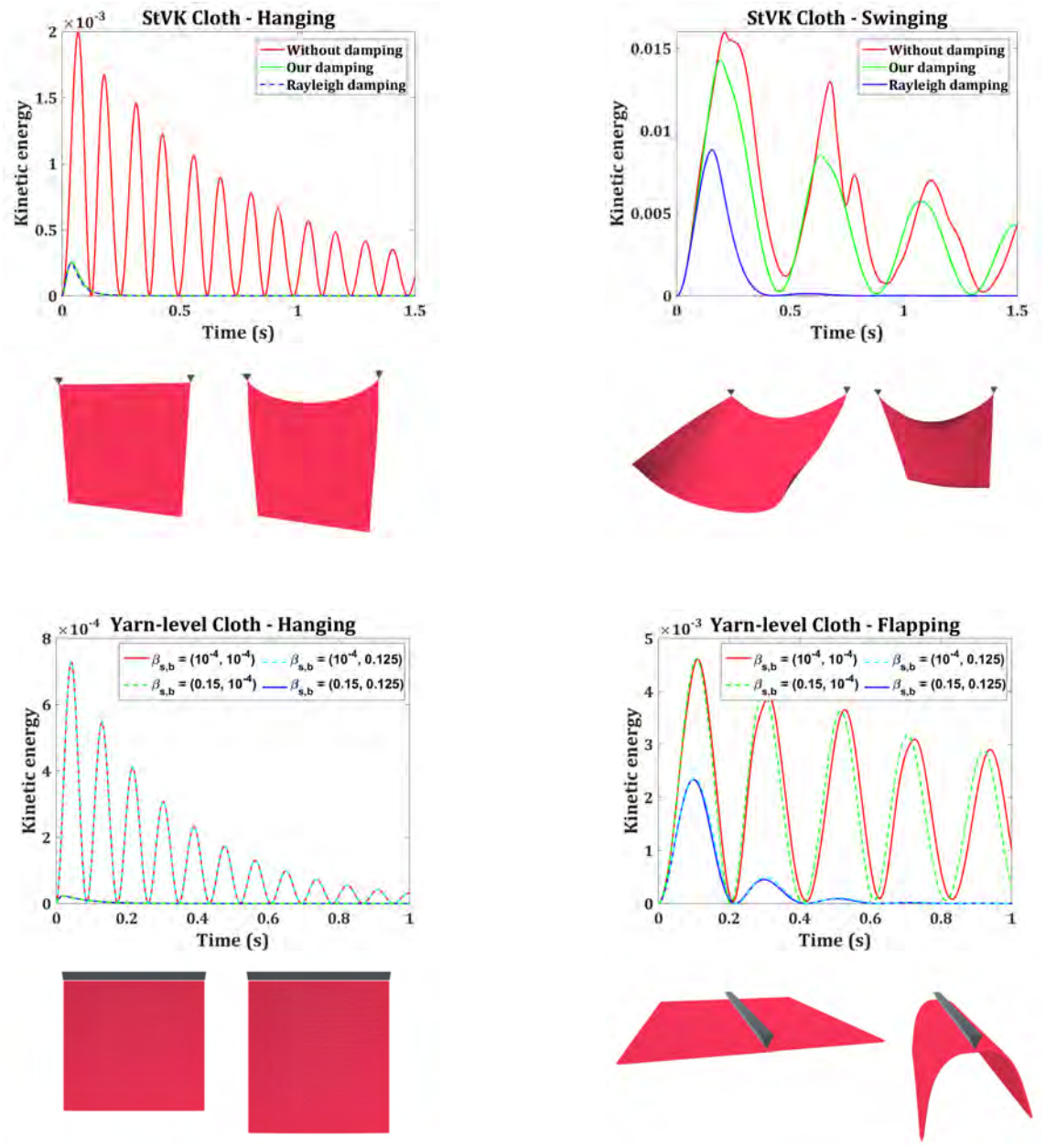

Figure 3.4: The plots demonstrate the ability of strain rate dissipation potentials to correctly damp target deformations, leaving others unaffected. All plots show the evolution of kinetic energy under various settings, for the motions depicted beneath. The two plots on the left correspond to the StVK cloth model with no damping, Rayleigh damping with $\beta = 0.15$, and our damping tuned to match Rayleigh damping as in (3.12). Damping is applied only to the membrane StVK model, not to bending. In the 'hanging' motion, our damping and Rayleigh damping produce almost equivalent overdamped motion. In the 'swinging' motion, on the other hand, our model produces a result close to the no-damping case, while Rayleigh suffers high damping. The two plots on the right correspond to the yarn-level cloth model using our damping model, comparing two combinations of stretch damping β_s and two combinations of bending damping β_b. As desired, the stretch damping coefficient determines the behavior in the 'hanging' motion, while the bending damping coefficient determines the behavior in the 'flapping' motion.

The two right plots in Fig. 3.4 show the evolution of kinetic energy for two different motions ('hanging' and 'flapping'), shown beneath. As desired, the stretch damping coefficient determines the behavior in the 'hanging' motion, while the bending damping coefficient determines the behavior in the 'flapping' motion.

We have also tested the strain rate dissipation potentials on larger animations. We have dressed a character model with a shirt, and we have simulated the motion of the shirt using both the StVK and yarn-level cloth models, with two different sets of damping parameters each (medium damping and low damping). The character is animated using publicly available data [Pons-Moll et al., 2015]. Figs. 3.5, 3.6, 3.7, 3.8 shows several snapshots of the animation for each cloth model and choice of damping parameters. In the snapshots, the examples with less damping exhibit more folds.

For the StVK simulation, we have followed the parameterization of dissipation potentials in (3.15), with the following parameter values: in the medium damping case, $\lambda_d = 30$ and $\mu_d = 20$ (Fig. 3.7); in the low damping case, $\lambda_d = 1.5$ and $\mu_d = 1$ (Fig. 3.8). With remeshing, the number of vertices in the simulation ranges from $3,300$ to $5,976$ in the medium damping case, and from $3,386$ to $6,926$ in the low damping case. Performance varies as the mesh resolution changes, which in turn depends on the amount of dynamics and fine wrinkles. To calibrate performance, we have used a fixed mesh with $10,437$ vertices. With a time step of 1.6 ms, the simulation took roughly 1.45 seconds per time step. We have also compared performance w.r.t. the Rayleigh damping model, and dissipation potentials add an overhead of just 2%, due to a slight increase in the cost of collision processing under more vivid dynamics, not due to force computation or solver convergence.

For the yarn-level simulation, we have followed the parameterization of dissipation potentials with the Rayleigh damping analogy described in (3.12), with the following parameter values: in the medium damping case, stretch damping with $\beta_s = 0.03$ and bending damping with $\beta_b = 0.16$ (Fig. 3.5); in the low damping case, stretch damping with $\beta_s = 3 \times 10^{-4}$ and bending damping with $\beta_b = 0.016$ (Fig. 3.6). With a shirt with $136,741$ nodes and an average time step of 1 ms, the simulation took roughly 9.85 seconds per time step. We have also simulated a higher resolution shirt, shown in Fig. 3.1, with $1,053,175$ nodes and intermediate damping values of $\beta_s = 3 \times 10^{-3}$ and $\beta_b = 0.1$. With an average time step of 1 ms, the simulation took roughly 86 seconds per time step.

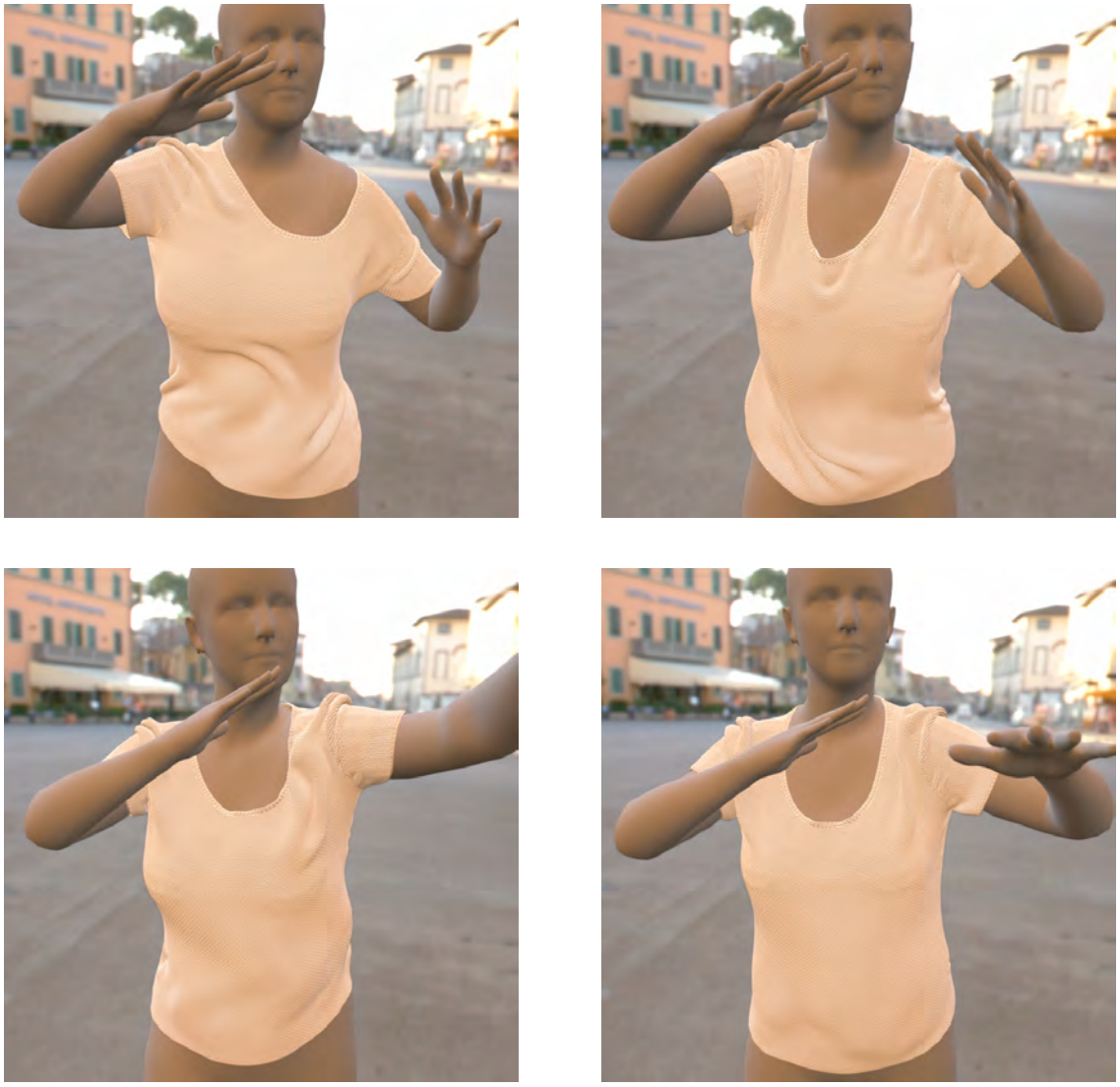

Figure 3.5: We compare a simulation of a shirt with two different deformation models and different settings of the strain rate dissipation potentials. These four pictures illustrate the yarn-level cloth simulation example with medium damping ($\beta_s = 0.03$ and $\beta_b = 0.16$)

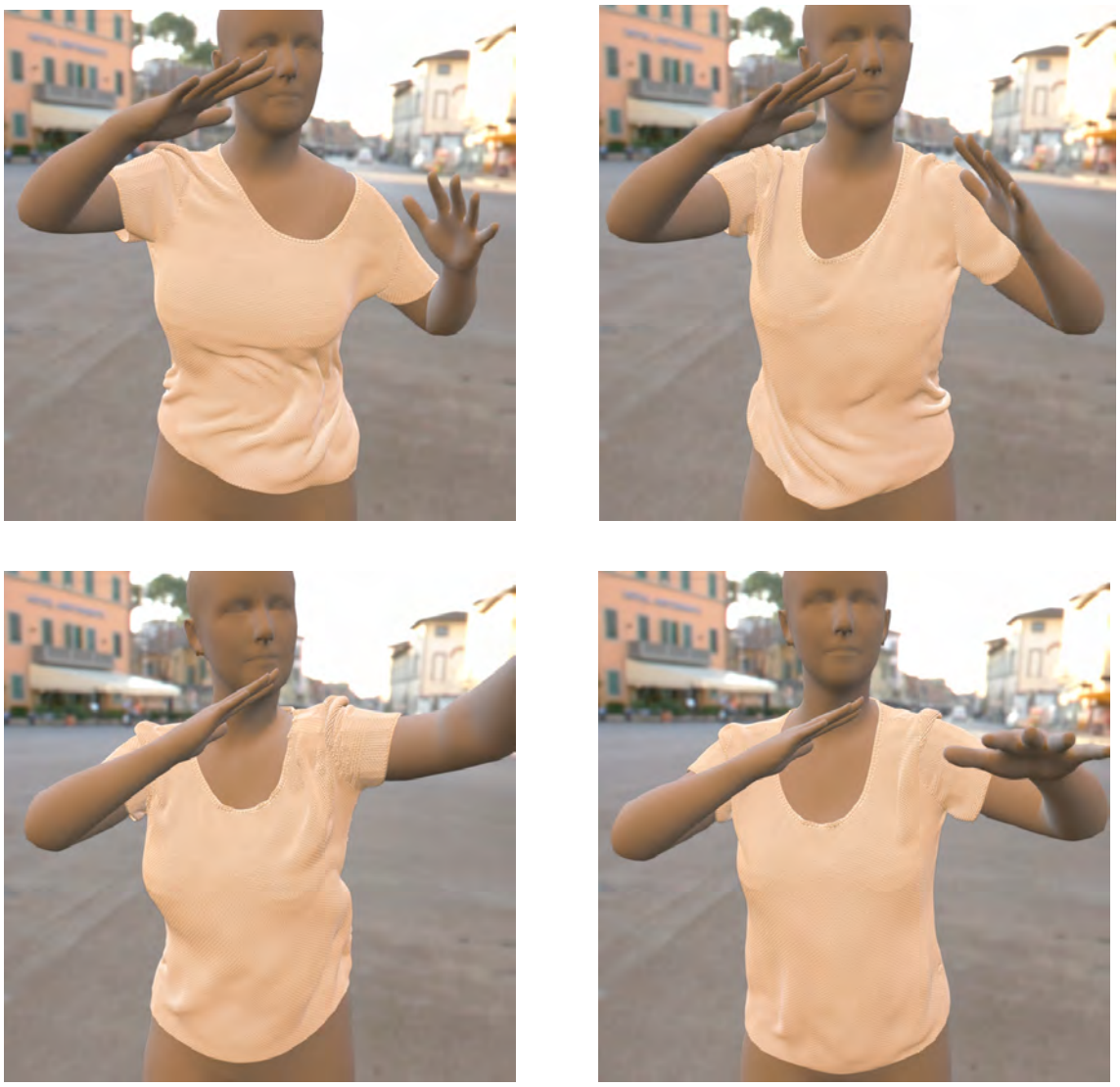

Figure 3.6: We compare a simulation of a shirt with two different deformation models and different settings of the strain rate dissipation potentials. These four pictures illustrate the yarn-level cloth simulation example with low damping ($\beta_s = 3 \times 10^{-4}$ and $\beta_b = 0.016$)

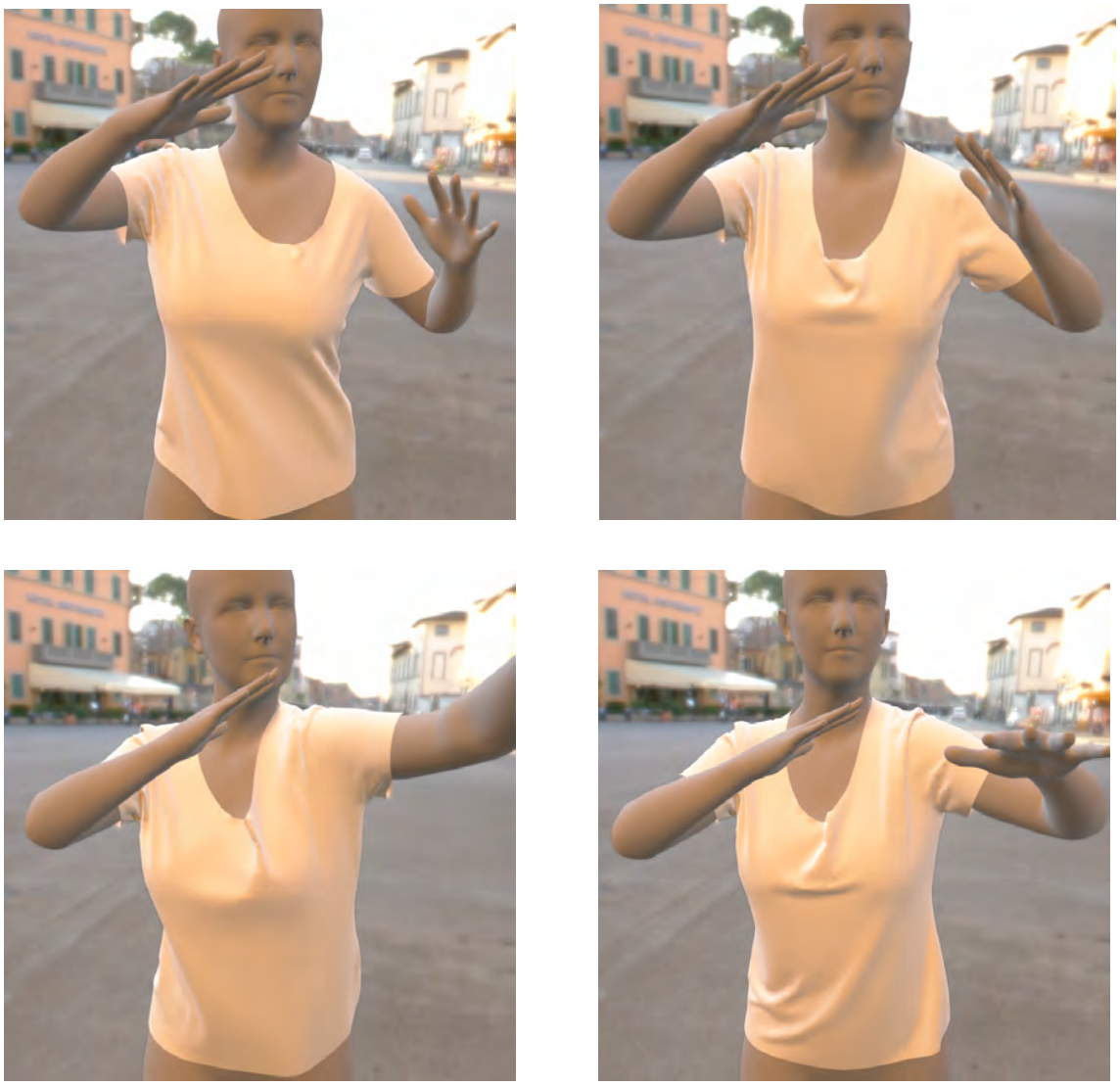

Figure 3.7: We compare a simulation of a shirt with two different deformation models and different settings of the strain rate dissipation potentials. These four pictures illustrate the StVK cloth simulation with medium damping ($\lambda_d = 30$ and $\mu_d = 20$).

Figure 3.8: We compare a simulation of a shirt with two different deformation models and different settings of the strain rate dissipation potentials. These four pictures illustrate the StVK cloth simulation with low damping ($\lambda_d = 1.5$ and $\mu_d = 1$).

3.6 Discussion and Future Work

We have presented a framework for the design of damping models, building on the concept of dissipation potentials. We show that a formulation based on strain rate achieves controllable damping for deformation modes, leaving other motions unaffected. We discuss parameterization and implementation aspects, and demonstrate the method on diverse deformation models.

Our approach also suffers some limitations. Since the strain rate is tightly coupled to the choice of strain, the damping model may inherit some limitations of the elastic deformation model. In addition, constraining damping forces to the direction of the strain gradient is the major strength of the model, but it also constitutes a limitation. Our model is not capable of modeling dissipative effects in the null-space of the strain gradient at all, hence it needs to be complemented with other damping forces to achieve such effects. Note, however, that the constitutive model that maps strain rate to dissipation potential may be arbitrarily nonlinear, anisotropic, or heterogeneous, not limited to the characteristics of the elastic constitutive model.

Our work opens interesting avenues for future work. Same as energy-based elastic models set a solid framework for the design of elastic behavior, damping models based on strain rate dissipation potentials set a solid framework for the design of dissipative behavior. The model could be used as an integral building block of measurement-based damping estimation or artist-driven damping design. To this end, it is important to identify artist-friendly parameterizations.

Chapter 4

Robust Eulerian-On-Lagrangian Rods

4.1 Introduction

The simulation of rods has been extensively studied in computer graphics. This is not surprising, as many daily-life objects are composed of rod-like structures, such as ropes [Pai, 2002, Bergou et al., 2008], chains, belts, cloth [Kaldor et al., 2008], cables [Servin et al., 2010], hair [Selle et al., 2008], tendons [Sachdeva et al., 2015], spaghetti, or even fluid filaments [Bergou et al., 2010b].

Rod simulations become particularly challenging under complex contact arrangements, as their small cross-section makes them vulnerable to collision handling errors. But when contacts persist over time, with rods sliding with respect to each other, Eulerian-on-Lagrangian (EoL) discretizations [Sueda et al., 2011] offer an attractive approach to gain robustness in contact handling, at the expense of a slightly more complex derivation of the equations of motion. EoL methods augment the classic Lagrangian discretization of deformable solids with Eulerian coordinates that allow nodes to move in the material domain. The power of EoL methods is the ability to track explicitly contact points both in the spatial and material domains, simply by placing nodes at contact locations, and thus reduce the complexity and increase the accuracy of contact handling.

However, we have observed that existing EoL works exploit only moderately this power. To the best of our knowledge, none of them shows multiple stacked layers of rods or shells sliding with respect to each other. As we discuss in detail later in Section 4.2, there is a fundamental reason for this. With sliding contacts, EoL discretizations easily become degenerate. To avoid simulation instabilities, previous EoL

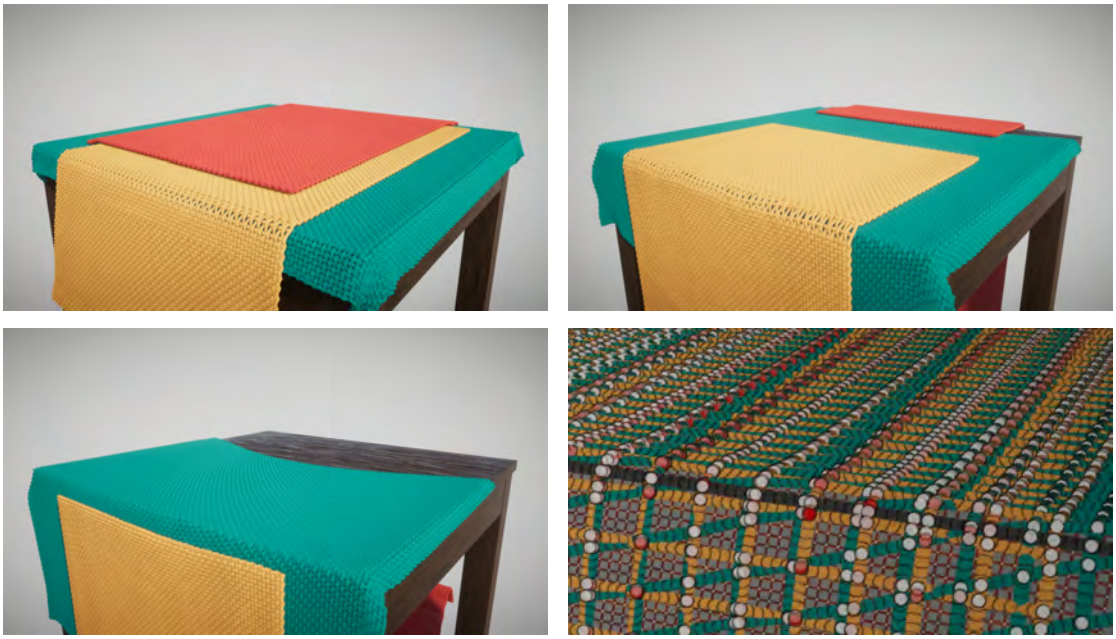

Figure 4.1: Simulation of three yarn-level tablecloths stacked on top of each other. We handle both intra-fabric and inter-fabric contacts implicitly with our novel Eulerian-on-Lagrangian (EoL) simulation. Frictional contact is correctly handled, even under extreme sliding and crossing of yarns. We introduce novel EIL nodes to handle robustly pervasive degeneracies in the discretization. The rightmost image shows the soup of nodes around the edge of the table. White dots represent contacts between standard EoL nodes, red dots contacts between our novel EIL nodes, and pink dots contacts between EoL and EIL nodes.

works use remeshing, but this strategy cannot be used under multiple stacked layers, when the geometry of the contact configuration is intrinsically degenerate, with contacts crossing each other.

We propose a simulation method that handles robustly degenerate discretizations in EoL rods. Our method does not use remeshing; it relies instead on a formulation of equations of motion that is insensitive to degenerate elements. As a result, we can simulate stacks of rods sandwiched between sliding contacts, with nodes constantly crossing each other in the material domain, all with implicit contact handling enabled by the EoL approach.

The key to our solution is a type of mixed Eulerian-Lagrangian discretization node, carefully designed to support accurate and efficient modeling of contact interactions as in EoL methods, but transparent to the modeling of internal rod forces, and hence insensitive to degeneracies in the discretization. In Section 4.2 we describe this type

of node, which we call *Eulerian with Interpolated Lagrangian* (EIL in short), and we discuss its beneficial properties.

Based on a combination of the new EIL and regular EoL discretizations, we have designed a simple and elegant algorithm to derive robust equations of motion at runtime. The strategy is to replace offending EoL nodes with EIL nodes, and skip EIL nodes in the definition of internal forces. Our algorithm, described in Section 4.3, yields a combination of dynamics and statics equations, which can be solved in a unified manner with standard solvers.

In our results, we show the application of our solution to challenging simulations of yarn-level cloth. Beyond single woven or knit fabrics [Cirio et al., 2014, Cirio et al., 2017], we extend the power of EoL methods to stacked layers of fabrics, by handling implicitly both intra-fabric as well as inter-fabric contacts. We demonstrate results on several familiar settings: tablecloth layers, pant pockets, and shirt tags. We also show that our method enables scalable EoL-based simulation of complex knit fabrics where multiple yarns slide and cross each other. To date, these fabrics could be handled only through traditional Lagrangian methods with explicit contact handling [Kaldor et al., 2008], assuming periodicity to predict the relaxed pattern shapes [Leaf et al., 2018].

The combined simplicity and effectiveness of our solution leads to an elegant implementation and robust results, despite ubiquitous discretization degeneracies as shown in Fig. 4.1. While we only demonstrate our ideas on rods, we believe that the core concepts can also be extended to other EoL domains such as thin shells [Weidner et al., 2018].

4.2 Eulerian-Lagrangian Rods

In this section, we present a novel mixed Eulerian-Lagrangian discretization of rods. We start with a recap of the regular EoL discretization [Sueda et al., 2011], and its application to yarn-level cloth simulation [Cirio et al., 2014]. Then we discuss the sources of degenerate discretizations and their devastating effects. We conclude with the introduction of our new discretization.

All our exposition refers to the representation of the center line of a rod. The representation of twist is complementary. In our implementation, we use twist-free

rods and we assume a homogeneous cross-section, but our approach can be extended to rod representations with twist.

4.2.1 Eulerian on Lagrangian Discretization

When rods are in contact with other objects, contact points tend to concentrate large local bending, due to the low bending stiffness of the rod and the action of localized external forces. Then, it appears particularly interesting to introduce discretization nodes at contact points, and thus represent efficiently and accurately rod bending. Moreover, if contacts are persistent, using these points in the discretization may simplify overall computations, by avoiding explicit detection and resolution of contacts.

However, contact points may not be stationary in the material domain, due to sliding. To account for the motion of discretization nodes within the material domain, [Sueda et al., 2011] introduced the EoL discretization of constrained rods. As shown in Fig. 4.2-a, a rod node is placed at the contact point between the rod and an arbitrary object O, and its coordinates $(u, \mathbf{x})$ store both Lagrangian (spatial) coordinates $\mathbf{x}$ and Eulerian (material) coordinates u. We use as Eulerian coordinate the undeformed arc length of the rod. With both Eulerian and Lagrangian coordinates, the kinematics of the rod can suffer ambiguities. However, by forcing the rod node to remain at the contact point, its Lagrangian coordinates are constrained, and the ambiguity is resolved. We denote the contact point on the other object O as $\mathbf{x}_o$, and then, without loss of generality, the constraint on the rod node can be expressed as

$$\mathbf{x} - \mathbf{x}_o = 0. \tag{4.1}$$

Later, [Cirio et al., 2014] considered the particular case of rod-rod contact. Then, the contact point on object O is also an EoL rod node, with Eulerian coordinate v. Moreover, in rod-rod contact, the contact constraint (4.1) can be enforced implicitly, by making both EoL nodes share their Lagrangian coordinates. In other words, the two EoL nodes have coordinates $(u, \mathbf{x})$ and $(v, \mathbf{x})$, as shown in Fig. 4.2-b. Another way of looking at the EoL discretization of rod-rod contact is as a 5-dimensional reduced-coordinate formulation.

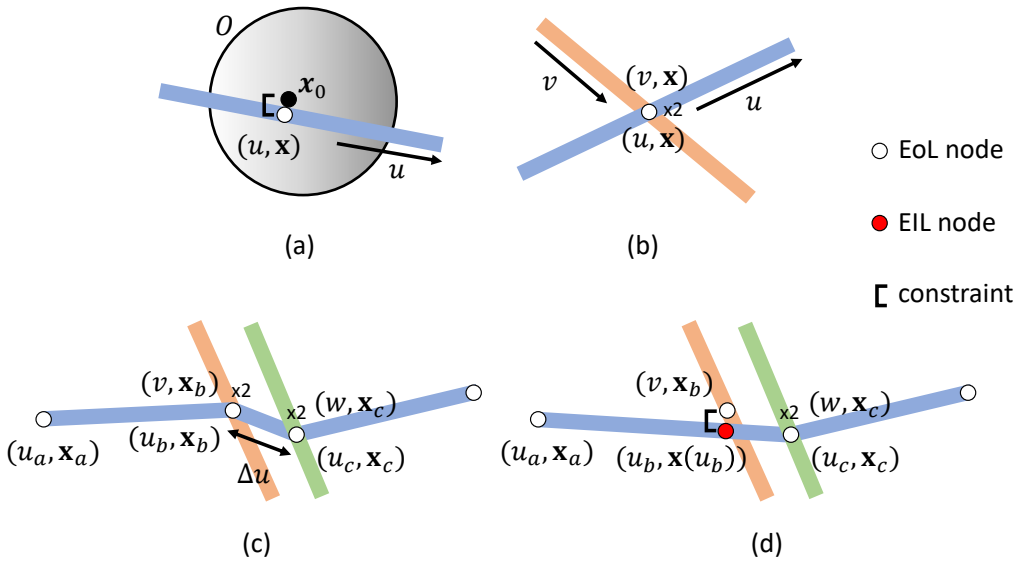

Figure 4.2: Examples of mixed Eulerian-Lagrangian discretization of rods. (a) EoL discretization of a rod in sliding contact with an arbitrary object O, proposed by [Sueda et al., 2011]. (b) Application of the EoL discretization to sliding rod-rod contact, proposed by [Cirio et al., 2014]. (c) Two rods (orange and green) slide on another rod (blue). As the material distance Δu between the contact points gets smaller, forces become infinitely stiff, even in the undeformed case. The degeneracy in the discretization makes the simulation unstable. (d) We propose a novel discretization of sliding rod contacts. When a rod segment is close to degenerate, we replace one EoL node with an EIL node (in red). In this node, the Eulerian coordinate is free, while the Lagrangian coordinates are linearly interpolated. The material distance of the degenerate segment does not participate in the discrete elastic energy of the rod, which results in robust equations.

4.2.2 Degeneracies and Instabilities

While EoL rod discretizations are beneficial for the efficient and accurate simulation of rods in contact, they are not free of difficulties. Elastic forces become infinitely stiff when two sliding rod nodes get arbitrarily close to each other. Consider the situation shown in Fig. 4.2-c. The orange and green rods in the figure slide on the blue rod, and approach each other. Their contact points define a blue rod segment with material length $\Delta u = u_c - u_b$ and spatial length $\Delta \mathbf{x} = \|\mathbf{x}_c - \mathbf{x}_b\|$. The stretch energy V_s of a

rod segment can be expressed as a function of the ratio between the Lagrangian and Eulerian lengths [Cirio et al., 2014], i.e.,

$$V_s = \frac{1}{2} k_s \Delta u \left(\frac{\|\Delta \mathbf{x}\|}{\Delta u} - 1 \right)^2, \tag{4.2}$$

where k_s is the material stiffness.

In the undeformed case, i.e., $\|\Delta \mathbf{x}\| = \Delta u$, the effective stiffness of the stretch energy with respect to either the Lagrangian or Eulerian length is $\frac{\partial^2 V_s}{\partial \|\Delta \mathbf{x}\|^2} = \frac{\partial^2 V_s}{\partial \Delta u^2} = \frac{k_s}{\Delta u}$. It is evident that as the nodes slide and get closer in the material domain, the stiffness tends to infinity, making simulations unstable.

The problem at hand boils down to a degeneracy in the discretization. The classic approach to avoid degenerate discretizations is to remesh the geometry, as done as well in other EoL methods [Weidner et al., 2018]. In the case of rods, the trivial approach to remeshing is to collapse both adjacent nodes into one. However, this approach is not viable when the nodes represent two sliding contacts. It is paramount to retain the Eulerian coordinates of both nodes in order to determine how the contacts continue sliding. To the best of our knowledge, no prior work on EoL rods shows situations where sliding contacts get arbitrarily close and cross each other. [Sueda et al., 2011] showed sliding contact of rods with fixed or rigid bodies; [Cirio et al., 2014, Cirio et al., 2017] considered rod-rod contact in woven and knitted cloth, but they applied a repulsive force when two contacts were in close proximity; remeshing due to degeneracies was used in EoL cloth [Weidner et al., 2018], but the examples did not exhibit arbitrarily close sliding contacts either. Challenging situations may appear when rods are sandwiched and the contacts cross each other, and this situation cannot be handled by simply collapsing nearby nodes.

4.2.3 Eulerian with Interpolated Lagrangian Discretization

To robustly handle degenerate discretizations under sliding contact, we introduce another type of mixed Eulerian-Lagrangian node. This node has only a free Eulerian coordinate, as this property is key to correctly capture sliding. Its Lagrangian coordinates, on the other hand, are interpolated between adjacent nodes. We call this node an *Eulerian with Interpolated Lagrangian* node (EIL).

Looking again at Fig. 4.2-c, we take the node with Eulerian coordinate u_b, and we transform into an EIL node, as shown in Fig. 4.2-d, with the node highlighted in red. Then, its Lagrangian coordinates are computed through linear interpolation of its adjacent EoL nodes as:

$$\mathbf{x}(u_b) = \frac{u_c - u_b}{u_c - u_a}\,\mathbf{x}_a + \frac{u_b - u_a}{u_c - u_a}\,\mathbf{x}_c. \tag{4.3}$$

Linear interpolation of the Lagrangian coordinates produces geometric properties that make the EIL node transparent to internal rod forces. There is no bending, hence the node does not participate in any bending energy computation. Stretch is the same on the two adjacent segments, hence stretch energy can be measured between the two adjacent nodes, bypassing the EIL node. As a result, even if the Eulerian distance between the EIL node and its adjacent nodes becomes arbitrarily short, there is no pernicious effect on the numerical stiffness, and the degenerate discretization becomes harmless. Later in Section 4.3.2, we provide more details about the definition of elastic energy terms.

At an EIL node, the contact constraint (4.1) can not be enforced trivially, as the Lagrangian coordinates are not free coordinates. Therefore, this constraint must be handled explicitly. In the rod-rod contact shown in Fig. 4.2-d, this translates into an explicit constraint between $\mathbf{x}(u_b)$, the interpolated position of the EIL node, and $\mathbf{x}_b$, the position of the corresponding EoL node along the orange rod. Through the interpolation (4.3) of the Lagrangian coordinate on the EIL node, the constraint affects its Eulerian coordinate, and thus it induces sliding despite the degeneracy, as desired. It also affects the motion of the adjacent nodes, and thus it satisfies two-way coupling at the contact. To compute the effect of the constraint on the various free coordinates, we make use of the Jacobian of the linear interpolation (4.3).

4.3 Robust Discrete Mechanics

In this section, we describe our runtime algorithm to robustly simulate the dynamics of complex arrangements of rods in sliding contact. Our central strategy to avoid instabilities under degenerate discretizations is to replace offending EoL nodes with the novel EIL nodes described in the previous section, and formulate internal rod forces that ignore the EIL nodes. We start the section with a description of the dynamic node

assignment, we continue with the formulation of internal and external force terms, and we conclude with the derivation of the equations of motion.

4.3.1 Node Assignments

On each simulation step, we start by identifying EoL and EIL nodes for all rods in the simulation scene. To do this, we check the material distance between pairs of consecutive nodes along each rod, and we ensure that an EIL node is introduced every time that the distance is below a safety threshold. We do this efficiently through simple list sorting and traversal operations.

For each step and each rod, let us consider as input a set of nodes defined by their current Eulerian and Lagrangian coordinates $(u, \mathbf{x})$. These nodes may be sliding contacts inherited from the previous step, new contacts detected through collision detection, discretization points with fixed Eulerian coordinates (e.g., end points), or persistent contacts in the woven or knitted structure of a yarn-level fabric which can be defined at preprocessing.

We initialize all nodes as EoL. Then, we sort the nodes according to their Eulerian coordinates, which yields a sorted sequence $\{(u_i, \mathbf{x}_i)\}, u_i > u_{i-1}$. Next, we traverse the sequence in order. Whenever we find that a node is closer than a safety threshold distance d from the previous node, we tag it as EIL node (In our implementation, the safety distance is $0.1\times$ the length of rest-shape rod segments). In a special case, when the current node has a fixed Eulerian coordinate (e.g., it is an end node), we leave it as EoL node, and we tag as EIL the last EoL node instead. Thanks to this simple node assignment strategy, we ensure that the material distance between any pair of consecutive EoL nodes is above the safety threshold. As EIL nodes are determined based on sorting, they switch when two adjacent nodes actually cross each other. However, this has little effect on the simulation, as the nodes are co-located when they cross. We have not observed noticeable effects due to the EIL selection policy.

We revise the assignment of nodes on every simulation step. More specifically, in our implementation we revise them before the first Newton step of a full nonlinear solve. Switching node assignments to and from EoL and EIL introduces discontinuities in energy and momentum. These discontinuities could be reduced by locally optimizing the Lagrangian and Eulerian coordinates of the nodes in contact.

Consider a node with Eulerian coordinate u_b, which transitions from EoL (as in Fig. 4.2-c) to EIL (as in Fig. 4.2-d) and vice versa. This transition produces a discontinuity in the local energy. Under certain assumptions, the discontinuity can be minimized through a closed-form optimization of the Eulerian coordinate u_b. In this optimization, we assume that the matching node $(v, \mathbf{x}_b)$ remains fixed, and we consider only stretch energies.

In the transition from EIL to EoL, the Lagrangian coordinate moves from $\mathbf{x}(u_b)$ to $\mathbf{x}_b$, to join the matching node. This jump introduces stretch energy, which can be minimized by making stretch uniform across the new EoL node. Then, the optimal Eulerian coordinate can be computed as

$$u_b \leftarrow \frac{\|\mathbf{x}_b - \mathbf{x}_c\| u_a + \|\mathbf{x}_a - \mathbf{x}_b\| u_c}{\|\mathbf{x}_a - \mathbf{x}_b\| + \|\mathbf{x}_b - \mathbf{x}_c\|}. \tag{4.4}$$

In the transition from EoL to EIL, the Lagrangian coordinate is now interpolated from $\mathbf{x}_a$ and $\mathbf{x}_c$. This jump introduces a non-zero energy in the newly created soft-constraint with $\mathbf{x}_b$. This energy can be minimized by placing $\mathbf{x}(u_b)$ on the closest point to $\mathbf{x}_b$ along the segment between $\mathbf{x}_a$ and $\mathbf{x}_c$. Then, the optimal Eulerian coordinate can be computed as

$$u_b \leftarrow \max\left(\frac{(\mathbf{x}_a - \mathbf{x}_c)^T (\mathbf{x}_b - \mathbf{x}_c) u_a + (\mathbf{x}_a - \mathbf{x}_c)^T (\mathbf{x}_a - \mathbf{x}_b) u_c}{(\mathbf{x}_a - \mathbf{x}_c)^T (\mathbf{x}_a - \mathbf{x}_c)}, u_c\right). \tag{4.5}$$

This result can also be expressed as a function of the angle θ between the rod segments $(\mathbf{x}_a - \mathbf{x}_b)$ and $(\mathbf{x}_b - \mathbf{x}_c)$:

$$\begin{aligned} &u_b \leftarrow \max\left(\frac{w_a u_a + w_c u_c}{w_a + w_c}, u_c\right), \\ &\text{with } w_a = \|\mathbf{x}_b - \mathbf{x}_c\|^2 + \|\mathbf{x}_a - \mathbf{x}_b\| \|\mathbf{x}_b - \mathbf{x}_c\| \cos\theta, \\ &\text{and } w_c = \|\mathbf{x}_a - \mathbf{x}_b\|^2 + \|\mathbf{x}_a - \mathbf{x}_b\| \|\mathbf{x}_b - \mathbf{x}_c\| \cos\theta. \end{aligned} \tag{4.6}$$

Furthermore, with uniform stretch in both segments, the result can be expressed as a function of the Eulerian coordinates alone:

$$\begin{aligned} w_a &= (u_b - u_c)^2 + (u_a - u_b)(u_b - u_c) \cos\theta, \\ w_c &= (u_a - u_b)^2 + (u_a - u_b)(u_b - u_c) \cos\theta. \end{aligned} \tag{4.7}$$

Then, it is easy to see that, as the segments become collinear, i.e., $\theta \to 0$, the optimal result is to simply leave the Eulerian coordinate u_b of the EIL node unchanged. We have opted for this simple solution in practice. Furthermore, whenever a node changes its status between two steps from EIL to EoL, we initialize its Lagrangian coordinates according to the contact constraint (4.1). Energy and momentum discontinuities could also be smoothed by making the transitions progressive within an interval of material distance, but we found that this was not necessary in practice. All our simulations were executed with no smoothing, yet there are no artifacts, despite the ubiquitous node transitions.

4.3.2 Definition of Force Terms

In our simulations of rods, we consider internal forces that model the resistance of rods to deformation, inter-rod forces that account for yarn-yarn contacts in yarn-level cloth simulation, other external forces due to rod-rod contact between different layers of cloth, or due to additional contacts, plus gravity and damping effects. We focus the attention on internal forces and yarn-yarn contacts. Gravity, damping, and external collisions are unaffected by our proposed discretization. In all cases, we follow the definitions of force terms in previous yarn-level cloth models [Cirio et al., 2014, Cirio et al., 2017].

Stretch and bending are defined using discrete strains, which yield strain energy densities that are then integrated along yarn segments. The stretch energy is defined in (4.2), and the bending energy is rewritten from [Cirio et al., 2014] as

$$V_b = k_b \frac{\theta^2}{\Delta u_1 + \Delta u_2}, \tag{4.8}$$

where k_b is the bending stiffness, θ is the angle between two segments, and Δ_1 and Δ_2 are the material lengths of the two segments.

As introduced in Section 4.2.3, the key to a robust formulation under degeneracies is to avoid EIL nodes in the definition of stretch and bending energy terms. Then, on each simulation step, and for each rod, we traverse the sequence of sorted nodes $\{(u_i, \mathbf{x}_i)\}$, and we define a stretch (resp. bending) energy term for every pair (resp. triple) of consecutive EoL nodes.

The inclusion of EIL nodes also requires the explicit addition of the constraint (4.1). We enforce this constraint using a soft constraint with large stiffness (In our implementation, 1000× larger than the effective stretch stiffness $\frac{k_s}{\Delta u}$ of rest-shape rod segments). Note that the constraint may be acting between two EIL nodes (one on each rod, if both rods suffer a degeneracy close to their contact), or between an EIL node and an EoL node. For EIL nodes, the force on the interpolated Lagrangian coordinates is mapped to the actual free coordinates through the Jacobian of linear interpolation, as discussed in Section 4.2.3. We have opted for stiff soft constraints because, in our experience, stiff zero-rest-length springs are comparatively less problematic than other elastic terms. Note that the alternative of hard constraints would yield a complex system of equations, combining Lagrange multipliers with implicit integration of stiff stretch forces. Our constraints are similar to the soft bindings of [Sifakis et al., 2007], but we set springs with EIL nodes, which are not fixed in the material domain, while soft bindings set springs between particles and fixed points on a meshed object.

[Cirio et al., 2014] proposed to model friction for rod-rod contacts as a trivial anchored spring on Eulerian coordinates. In our case, this force model can be adopted with no changes, as both EoL and EIL nodes retain free Eulerian coordinates. The joint effect of the contact constraint (4.1) and the friction force is actually the main reason for sliding of contact points, and therefore for the change of the Eulerian coordinates of rod nodes. Thanks to our proposed discretization, with free Eulerian coordinates at EIL nodes, the dynamics of rods are correctly and robustly represented when sliding contacts cross each other. Remeshing through naïve node collapse misses the required free Eulerian coordinates, and does not allow correct sliding. Fig. 4.3 demonstrates the validity of our friction model.

The simulation of cloth with yarn-level persistent contacts requires special force terms that resist the deformation modes of yarn-yarn contact. These are, for example, shear forces [Cirio et al., 2014] and, in the case of knits, wrapping forces [Cirio et al., 2017]. These forces are defined on Lagrangian coordinates only, with no effect on the material length of yarn segments; therefore, they do not induce robustness problems under degenerate discretizations. For EIL nodes, the force is mapped to the free coordinates in the same way as for the contact constraint discussed above.

The last relevant force is the parallel-yarn contact force, designed by [Cirio et al., 2014] to model the inability of some yarns to cross each other within fabric patterns. In our setting, some rod nodes should receive parallel-yarn contact forces as well, but

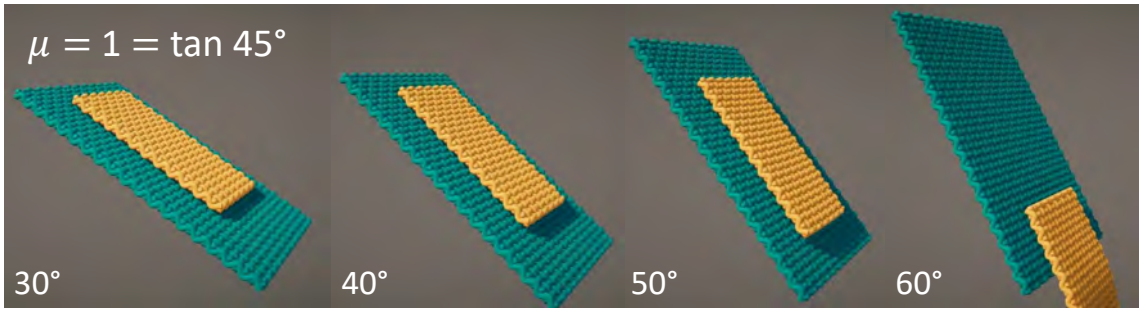

Figure 4.3: Validation of the friction model and sliding of two patches of cloth. All contacts are handled implicitly using EoL and EIL nodes. The green patch is fixed, and the friction coefficient with the yellow patch is $\mu = 1$. The yellow patch remains still at inclines below 45 degrees, and slides at steeper inclines, as expected with Coulomb's model.

others should not, to allow them to cross each other. We disable parallel-yarn contact forces between a pair of nodes if (a) one of the nodes represents an external contact (e.g., with another fabric), or (b) the two colliding yarns lie on different sides of the rod and they do not bend around the rod. To test if a colliding yarn bends around the rod, we compute a bending vector by averaging the direction vectors of the two incident yarn segments, and we check if the dot product of this bending vector and the contact normal is above a threshold (0.25 in our implementation).

4.3.3 Mixed Statics-Dynamics

Once that force terms are defined, we can also define inertial terms and derive the equations of motion using the general Euler-Lagrange equations [Goldstein et al., 2002], as done by [Sueda et al., 2011] for the original formulation of EoL rods. Lagrangian velocities along a rod are obtained by interpolating Lagrangian velocities of EoL nodes, while EIL nodes are irrelevant in this regard. Since EIL nodes do not affect Lagrangian velocities, they do not affect kinetic energy either. As a corollary, EIL nodes do not carry inertial terms, i.e., they can be considered massless, and then their coordinates are defined through static equilibrium. Therefore, to obtain the kinetic energy of each rod, we traverse the sequence of sorted points $\{(u_i, \mathbf{x}_i)\}$, and we sum a kinetic energy term for each pair of consecutive EoL nodes. For details on the computation of the kinetic energy term of a rod segment and the associated mass submatrix, we refer the reader to [Cirio et al., 2014].

The combined Lagrangian and Eulerian coordinates of the simulation scene form a set of reduced coordinates. We split this set into two: $\mathbf{q}$ are the coordinates of EoL nodes, and $\mathbf{q}_{\text{eil}}$ are the (Eulerian only) coordinates of EIL nodes. We denote as V the total potential energy of the simulation scene, and as $\mathbf{M}$ the mass matrix of EoL nodes. Note that all mass terms of EIL coordinates $\mathbf{q}_{\text{eil}}$ are null. Despite these null terms, the equations of motion can be derived using the general Euler-Lagrange equations. They result in:

$$\mathbf{M}\,\dot{\mathbf{q}} + \nabla_{\mathbf{q}} V = \mathbf{M}\,\dot{\mathbf{q}} + \mathbf{f}(\mathbf{q}, \mathbf{q}_{\text{eil}}) = 0; \quad \text{dynamic} \tag{4.9}$$

$$\nabla_{\mathbf{q}_{\text{eil}}} V = \mathbf{f}_{\text{eil}}(\mathbf{q}, \mathbf{q}_{\text{eil}}) = 0; \quad \text{static} \tag{4.10}$$

The vector $\mathbf{f}$ (resp. $\mathbf{f}_{\text{eil}}$) represents the forces on EoL nodes (resp. EIL nodes). As denoted in the equations, there are two distinct sets. EoL nodes are governed by dynamics, while EIL nodes are governed by static equilibrium. Despite this apparent difference, we can safely solve all equations together. We apply implicit Euler integration to the dynamics equations on EoL nodes, and we solve the combined system of equations using Newton's method. We do not resize the system matrix when nodes transition to/from EIL. Instead, we just cancel the matrix rows and columns of the Lagrangian coordinates of EIL nodes.

4.4 Results

Implementation Details

We have applied our rod simulation method to yarn-level cloth. To this end, we have adapted the GPU solver proposed by [Cirio et al., 2014] to handle dynamic rod discretizations. On every simulation step, we first execute the node sorting and assignment operations of Section 4.3.1, in parallel over all rods. These operations have negligible cost compared to the actual solver. Next, we execute force computations and Jacobian evaluations, parallelized at node level. Note that forces can be referenced to nodes thanks to the linear structure of rods, hence force stencils can be defined implicitly from the node ordering and rod-rod contacts.

Case	Lagrangian	EoL Intra-Fabric	EoL Inter-Fabric (max)	EIL (max)	Default step	Sim cost (secs/step)
Tablecloth (Figs. 4.1 and 4.8)	1 576	96 290	132 200	79 019	1 ms	15.9
Pocket (Fig. 4.6)	2 484	398 782	245 024	45 742	1 ms	93.9
Tag (Fig. 4.7)	1 010	68 810	18 356	4 563	2 ms	18.18
Knit 1 (Fig. 4.5-left)	184	75 096	—	671	0.5 ms	17.33
Knit 2 (Fig. 4.5-right)	208	55 520	—	602	0.5 ms	15.53

Table 4.1: Simulation size and performance for the main examples presented in this thesis. The columns indicate, for each scene: the number of pure Lagrangian nodes (i.e., rod endings), the intra-fabric EoL nodes due to yarn-yarn contacts within a pattern, the maximum inter-fabric EoL nodes to satisfy implicit sliding contact between patches, and the maximum simultaneous EIL nodes to correctly handle discretization degeneracies. The last two columns show the default time step and the average simulation cost per time step.

For collision detection, we use a sphere packing approach for cloth-cloth collisions and self-collisions, and distance fields for external objects. For non-persistent contacts, we use stiff penalty potentials to resolve collisions.

To determine contacts that require EoL discretization, we combine two strategies. For intra-fabric contacts, we simply use the initial topology of the weave or knit pattern. For inter-fabric contacts, we select the contacts detected by the collision detection step. In our examples, we do this at initialization, as the various layers remain in a stacked configuration once initialized. We did not support dynamic addition of EoL contact nodes, as in the examples the cost of collision handling of dynamic contacts was negligible. We did support, however, removal of contact nodes. One obvious reason for removal is that the Eulerian coordinate of a node indicates that it has exit the length of the rod; another reason is that the normal force between two constrained EoL nodes pulls them together instead of pushing, as discussed in [Cirio et al., 2014].

Performance

Our simulation examples have been executed on an Intel Core i7-7700K 4-core 4.20 GHz PC with 32 GB of RAM and a Nvidia GeForce GTX 1080 Ti GPU with 11 GB of VRAM.

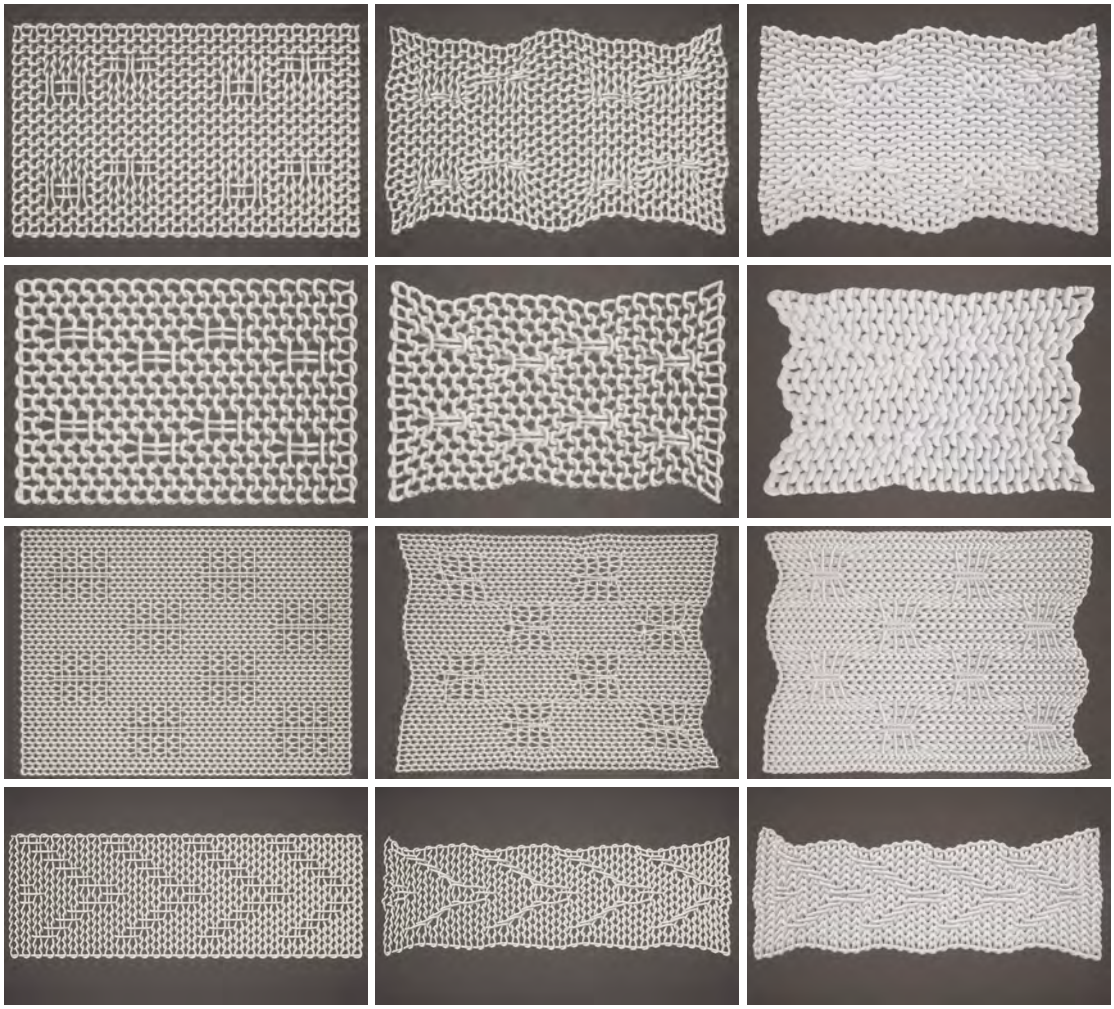

Figure 4.4: Four different knit patterns with slip-stitches, where yarn-yarn contacts slide over each other. These examples could not be handled by previous EoL yarn-level methods, and had to resort to purely Lagrangian methods with explicit contact handling. The left column shows the initial configuration for loose knit structures, the middle column the relaxed configuration after simulation of these loose knit structures, and the right column the relaxed configuration after simulation of tight knit structures. The three top-most examples are custom structures inspired by those of [Leaf et al., 2018], and the bottom-most example is a jacquard structure.

In Table 4.1 we show the simulation complexity of the examples shown in this thesis. We classify different types of nodes: fully Lagrangian nodes at rod endings, intra-fabric EoL nodes that represent persistent contacts in the topology of the pattern, maximum number of EoL nodes due to inter-fabric contact, and maximum number of simultaneous EIL nodes at any time in the simulation. All simulations run robustly de-

spite the large number of simultaneous EIL nodes, which is an indicator of the number of degenerate rod segments in the scene.

Table 4.1 also shows the simulation cost for each example, measured in seconds per time step. The default time step ranged from 0.5 ms to 2 ms. We have used adaptive time-stepping to reduce the time step if the Newton solver exhibits bad convergence. The examples occasionally reduce the time step, but they use the default value in the large majority of steps.

Complex Knits

Earlier yarn-level simulation methods assumed a fixed topology of the pattern mesh. This is sufficient for single-layer wovens or simple knits made of knit or purl stitches. However, in multi-layer wovens or complex knits with cables or slip stitches, sliding contacts often sandwich yarns and cross each other. Our rod simulation method enables robust handling of these structures through an efficient EoL approach. In particular, we have tested slip-stitch knit patterns where the slipped yarns can slide when the fabric gets deformed. In Fig. 4.4 we show the relaxation of four different patterns: three custom structures inspired by examples of [Leaf et al., 2018], and one jacquard structure. We have tested the four patterns under loose knitting, but also under tight knitting, which produces more complex contact configurations. Both settings are handled robustly.

We program the initial topology of knit patterns using a regular grid of instructions, and we tune the rest-length of slipped yarns to obtain relaxed patterns with different aesthetics. This approach is equivalent to the one followed by [Leaf et al., 2018]. for pattern design. However, with our EoL discretization, we also enable scalable draping of large-scale complex knits. In such case, purely Lagrangian yarn-level models can obviously not exploit patch periodicity, as done by [Leaf et al., 2018] Fig. 4.5 shows two large cloth patches draped on a sphere. These patches are stitched using two of the patterns in Fig. 4.4. The simulations consist of 55K and 75K nodes, with average inter-stitch distances of just 0.8 mm.

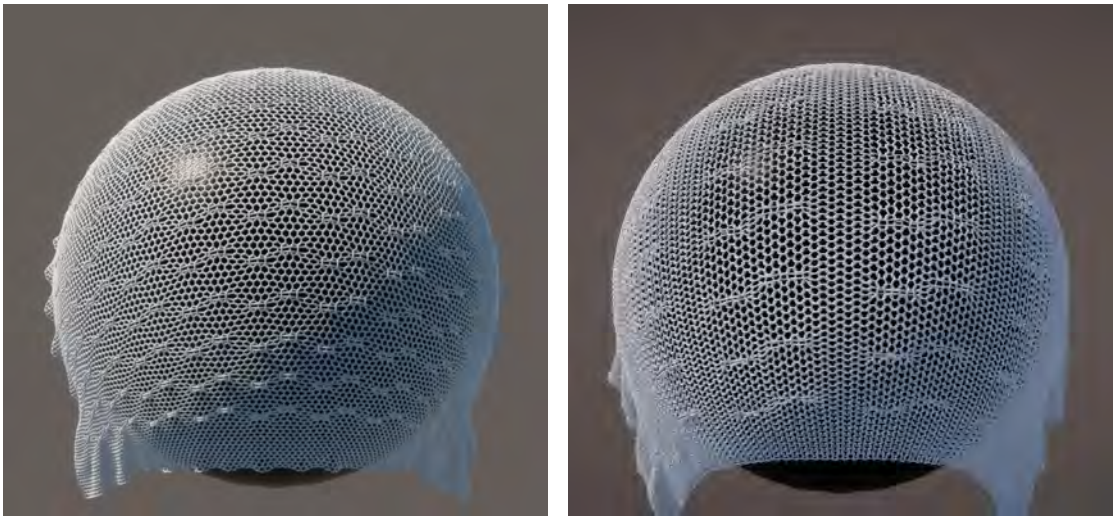

Figure 4.5: Two large knit patches draped on a sphere. The knit patterns are drawn from the examples in Fig. 4.4, and applied to larger patches. Thanks to our EoL formulation, the simulation of these complex knits scales to large sizes without compromising robustness.

Multiple Layers of Yarn-Level Cloth

Cloth often appears stacked in layers, either different garments on top of each other, or panels of the same garment stitched together. When contact between the layers persists over time, even if the layers slide relative to each other, the EoL approach offers an attractive way to simulate cloth deformation without explicit contact handling. We have evaluated the performance of our method when applied to the simulation of multiple layers of yarn-level cloth. The rods of the various layers pile up in complex contact arrangements, and require constant updates to the discretization to correctly handle the pervasive degeneracies.

Fig. 4.6 shows snapshots of a simulation of a jeans back pocket. The scene consists of two layers of twill denim fabric, stitched on the sides and at the bottom. The fabric is modeled at the yarn-level at a realistic resolution, with 44 yarns per inch. This yields a total of 645K nodes. We pull the pocket from the top and the bottom, inducing sliding of the two layers. When the tension grows, the lateral compression produces fine wrinkles that conform to the two layers of fabric.

Fig. 4.7 shows snapshots of a simulations of a shirt neck tag. The tag is stitched to the underlying shirt fabric on the sides. It is roughly 5 times stiffer than the shirt; therefore, when we pull from the fabric of the shirt, the deformation suffers a dis-

Figure 4.6: Snapshots of a simulation of a jeans back pocket. The scene consists of two layers of yarn-level twill denim fabric, stitched on the sides and at the bottom. We pull from the top and the bottom, inducing sliding of the two layers, as well as wrinkles influenced by the combined material. The full simulation is resolved with implicit contact handling in our EoL formulation, and it has over 645K nodes. When the layers slide, the two groups of sliding warp and weft yarns induce pervasive degeneracies in the discretization. The rightmost image shows the soup of nodes at the top of the pocket, with EIL nodes in red.

continuity at the boundary of the tag. The snapshots show horizontal stretch, vertical stretch, shear followed by vertical stretch in the middle, and vertical stretch in the middle followed by horizontal compression of the tag. Notice in the second and third snapshots visible sliding of the two layers, and in the first and third snapshots wrinkles next to the boundary of the tag due to the differences in material combined with sliding. The last snapshot also shows the tag separating as it buckles. In this last snapshot, the simulation begins by stretching the underlying cloth, and the EoL representation resolves the sliding motion of the two layers without the need for explicit contact handling. Then, we compress the tag, which buckles and produces sticking forces at EoL

contacts. We trigger automatically the removal of EoL contact constraints, allowing the tag to separate.

Fig. 4.1 and Fig. 4.8 show two simulations of stacked tablecloth layers with different friction properties. The tablecloths are modeled as thick-yarn plain weaves, with an inter-yarn separation of 5.6 mm, and yarn radius of 2.25 mm. In this scene, we also added EoL nodes at the edge of the table, to enable smooth sliding on sharp features. As described by [Weidner et al., 2018], the tablecloths suffer energy discontinuities or even get stuck if we do not do so. With three stacked layers, the number of simultaneous EIL nodes can be as high as 34% of the total nodes. The figures also show close-ups of the discretizations at particular instants in time. Despite continuous sliding and changes to the discretization, our simulation method handles contact and friction correctly. Note that friction is controlled simply through the Coulomb coeffi-

Figure 4.7: Snapshots of simulations of a shirt neck tag. The tag is roughly 5 times stiffer than the shirt, and is stitched on the sides. We apply different deformations to the underlying shirt fabric, from left to right: horizontal stretch, vertical stretch, shear followed by vertical stretch in the middle, and vertical stretch in the middle followed by horizontal compression of the tag. The difference in stiffness induces sliding of the layers, as well as wrinkling at the interface (see first and third snapshots). The last example shows the separation of the tag as it buckles. We trigger the separation of EoL contacts automatically by checking the sign of the normal force.

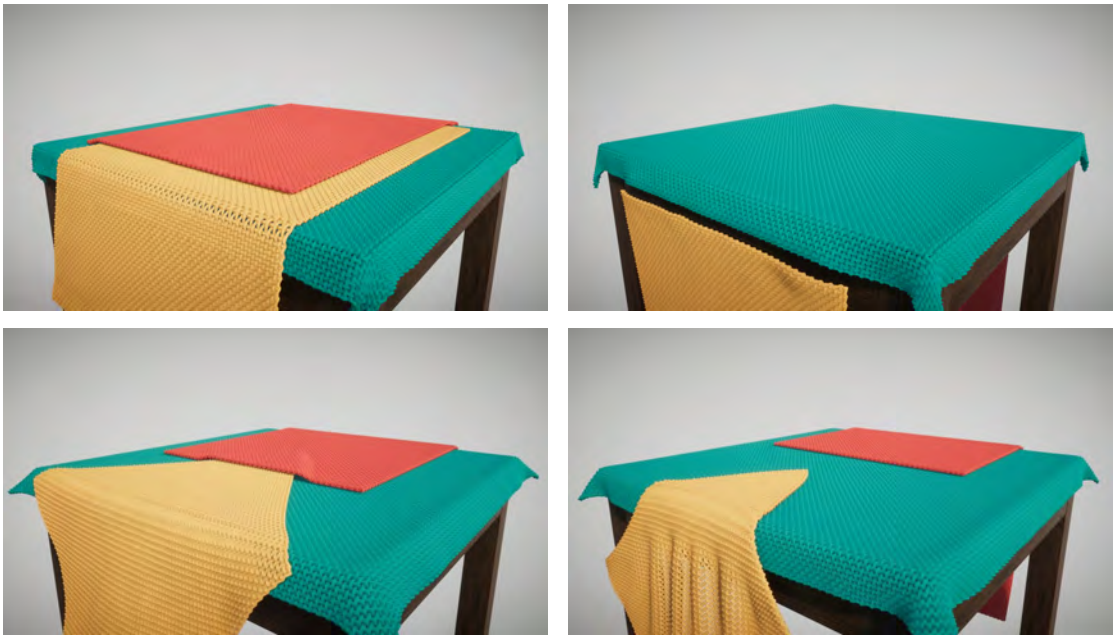

Figure 4.8: Similar scenes to the one in Fig. 4.1, but with no friction between the tablecloths, and in two different arrangements. Two left-most images: aligned tablecloths. Two right-most images: tablecloths at an angle. Despite continuous sliding and changes to the discretization, the green tablecloth remains perfectly on the table. Sliding is smooth and robust both when the tablecloths are aligned or at an angle. In the left scene, the number of simultaneous EIL nodes can be as high as 34% of the total nodes.

cient of the Eulerian anchor force (see Section 4.3.2 and [Cirio et al., 2014]). In the frictionless case shown in Fig. 4.8, the green tablecloth remains perfectly on the table.

4.5 Conclusions

In this work, we have extended EoL rod simulation to handle robustly complex contact arrangements with multiple stacked rods, and sliding and crossing contacts. As shown in our experiments, these conditions appear in diverse practical scenarios, including the simulation of complex knits, and contact between multiple layers of cloth. Our solution handles ubiquitous discretization degeneracies in a simple and elegant manner, and its implementation brings only small changes to previous methods.

In the development of our method and implementation, we have identified several limitations as well as opportunities for further investigation. As discussed in Sec-

tion 4.3.1, switching node assignments to and from EoL and EIL introduces discontinuities in energy and momentum. These discontinuities did not turn into artifacts in our examples, but perhaps they affected mildly the convergence of the Newton solve. Smoothing these discontinuities is possible, by locally optimizing the Lagrangian and Eulerian coordinates of switching nodes, or by making node transitions progressive.

In the examples, we did not implement dynamic addition of EoL nodes. It is not evident when this could turn beneficial or not. It would be necessary to design some metric that compares simulation accuracy and/or robustness with or without the addition of EoL nodes at contacts, and then use this metric to guide the addition of new EoL nodes.

The contact constraint of EoL and/or EIL nodes ignores the thickness of rods. However, this thickness should be accounted for in the computation of bending forces. We currently add the thickness as postprocessing for rendering, and the same procedure could be followed at runtime for force computation.

Our knit relaxation examples demonstrate the ability of EoL methods to support complex and tight knits with yarn sliding. However, some cases may be difficult to handle due dynamic creation of contacts. In such cases, one could use a purely Lagrangian method as in [Leaf et al., 2018] for the initial relaxation of the yarn structure, followed by our EoL method for dynamic simulation of larger patches or garments.

We have demonstrated our solution on patches of cloth simulated fully at yarn level. Such full yarn-level detail appears particularly relevant in our complex knit examples, to correctly capture sliding of slip-stitches. However, in other examples the simulation cost could be reduced drastically by considering yarn-level detail only when and where necessary.

To conclude, we think it is worth to explore the main ideas of our work beyond rods, for EoL formulations on other domains, such as thin-shell cloth [Weidner et al., 2018]. A key insight of our method is to avoid remeshing, and turn EoL nodes into EIL nodes when the discretization becomes degenerate. The extension of EIL nodes to other domains may be simple, but our node assignment algorithm is tied to the linear domain of rods.

Chapter 5
Conclusions

This chapter concludes the discussion of the presented works by providing general conclusions of the proposed ideas, potential applications and future strategies.

5.1 General Conclusions

This thesis aims to take further steps towards the realization of high-fidelity fabric simulation through the study of two fundamental aspects of cloth: the analysis of dissipative properties and their influence on the fabric's global behavior, and the efficient representation of complex knits and multiple fabrics in contact.

On one hand, we have found that dissipative properties are fundamental for characterizing high-fidelity textiles, yet the literature has usually overlooked this aspect. A major challenge in this regard lies in finding a simple and accurate model, capable of independently controlling the dissipative behavior of the different deformation modes of the fabric. We address this challenge in Chapter 3, where we provide the details of a framework for the design of damping forces using dissipation potentials. We analyze its application to different deformation models and demonstrate its advantages over traditional approaches. Even though the proposed framework does not directly address the subject of accuracy, it provides the basis for the definition of the concept of *good damping* and the means to design a dissipative model by analogy to elastic potentials while guaranteeing the controllability criterion we established.

On the other hand, we found an interesting research avenue in the management of contact between multiple layers of cloth, as it has been an open problem for many

years, fraught with technical challenges. Previous methods presented in the literature are often complex and computationally challenging, especially when considering the large amount of degrees of freedom necessary for the simulation of full-scale garments. The work we present in Chapter 4 addresses this challenge by introducing a highly efficient method for the simulation of complex rod assemblies and stacked layers of cloth. For this purpose, we take the fundamentals of persistent contact between yarns proposed by [Cirio et al., 2014] and modify the discretization as appropriate to enable sliding motion between different layers while avoiding instabilities caused by degenerate configurations.

The following sections will discuss the contributions of both techniques, highlighting the strengths of our methodology, their limitations, and potential paths for further research.

5.2 Strain Rate Dissipation for Elastic Deformations

The framework we presented enables the design of damping models by relying on the concept of dissipation potentials from classical mechanics. The proposed formulation, based on strain rate, achieves controllable damping for the different deformation modes, leaving other motions unaffected. Moreover, the analogy of the formulation with the design of elastic potentials, simplifies and generalizes our solution, reinforcing the concept of *good damping*. The proposed method has been successfully applied on two different deformation models, StVK hyperelasticity and yarn-level cloth with sliding persistent contacts. Furthermore, we demonstrate its advantages with respect to the classical Rayleigh model, concluding that the latter model does not satisfy our *good damping* criterion. However, it also suffers from some limitations:

Since strain rate is tightly coupled to the choice of strain, the designed damping model may inherit the same limitations of the elastic deformation model. Although constraining the damping forces to the direction of the strain gradient enables decoupling dissipative behavior across the different deformation modes, it also constitutes a limitation on itself. Our model needs to be complemented with other damping forces if modeling dissipation in the null-space of the strain gradient is required.

Our work also opens interesting avenues for future work. Damping models based on strain rate dissipation potentials set a solid framework for the design of dissipa-

tive behavior in the same way that energy-based elastic models set a solid framework for the design of elastic behavior. Moreover, the proposed model could be used as an integral building block of measurement-based damping estimation or artist-driven damping design.

Finally, posing dynamics as an optimization problem unlocks a wide range of high performance numerical solvers. However, formulating non-conservative effects such as damping into optimization form is challenging. Recent works [Brown et al., 2018] found success in the use of a specific form of dissipative potentials that is amenable to optimization-based integrators. Exploring the incorporation of the proposed framework into such schemes could be another interesting avenue for future work.

5.3 Robust Eulerian-On-Lagrangian Rods

We introduced a method to simulate complex rod assemblies and stacked layers of cloth with implicit contact handling using Eulerian-on-Lagrangian discretizations. Our method is simple, efficient and insensitive to degenerate elements without relying on the use of remeshing techniques. The mixed Eulerian-Lagrangian discretization we propose allows us to represent stacks of yarns sandwiched with nodes constantly sliding and crossing each other in the material domain.

Additionally, we provide the practical details essential to carry out an efficient implementation of the method. Along with the description of our EoL and EIL node selection strategy, we provide a simple and elegant algorithm for solving the resulting equations of motion based on a unified solver for dynamic and static equations.

We demonstrate the strengths of our approach through the simulation of multiple layers of cloth in contact sliding one over each other, as well as complex knit relaxations with tight knits that exhibit a large yarn sliding. Such scenarios are frequently encountered in high-performance clothing such as sportswear, where multiple layers of fabric are layered in tight configurations to imbue the garment with certain protection, comfort or thermal properties.

Nonetheless, during the development of our method, we have identified several limitations as well as opportunities for further research.

First, switching node assignments to and from EoL and EIL introduces discontinuities in energy and momentum. While they did not turn into artifacts in our ex-

periments, they have the potential of affecting the convergence of the Newton solve. Smoothing these discontinuities, either through the optimization of the switching degrees of freedom or through the introduction of progressive transitions, could alleviate this problem.

Moreover, our implementation does not support the dynamic addition of EoL nodes. This limitation makes it difficult to represent certain scenarios, such as separated fabric layers coming into contact and complex knit patterns whose relaxation could lead to the appearance of new contacts. The latter scenario could be handled by following a similar approach to [Leaf et al., 2018] by precomputing the relaxed configuration of a smaller portion of the fabric using a purely Lagrangian technique. The resulting configuration could then be used as a starting point for our EoL method for simulating the dynamics of the garment at full scale.

In cases when dynamic addition of EoL nodes is required, it is not evident when the generation of these new nodes could become beneficial. It would be necessary to design some metric that compares simulation accuracy and/or robustness with or without the addition of EoL nodes at contacts, and then use this metric to guide the addition of new EoL nodes. In any case, allowing the dynamic generation of EoL nodes requires the addition of an explicit collision detection algorithm, which may limit the computational efficiency advantages offered by our method. Exploring strategies to reduce detection costs, e.g. by adopting an algorithm similar to the Air Meshes method proposed by [Müller et al., 2015] for near-contact regions could, be an interesting line of future research.

A key insight of our method is to avoid remeshing, and turn EoL nodes into EIL nodes when the discretization becomes degenerate. We believe this strategy could find application in other domains beyond rods, such as thin-shell cloth [Weidner et al., 2018]. However, this scenario poses several challenges. To begin, our selection criteria for EIL nodes is tied to one-dimensional domains, such as rods. The transition to 2D manifolds significantly complicates the selection heuristic, and may even require the use of remeshing techniques. Furthermore, the regions shared across the different layers in material space must be treated with care to avoid locking artifacts while ensuring that optimal mesh properties are preserved.

5.4 Final remarks

Overall, we believe that the two approaches proposed in this thesis constitute a milestone towards building the foundations of high-fidelity textile simulation. Our contributions reach beyond academia, with some of the proposed solutions being adopted for production in the industry. An example of this is SEDDI, a young company that is widely regarded as a world-class leader in pioneering the digitalization of fashion. Recently, SEDDI adopted the dissipative model proposed in Chapter 3 for its internal simulation pipeline, recognizing its robustness and controllability as a qualitative jump over previously implemented solutions.

We acknowledge that there is still a long way to go to achieve the ambitious goal of high-fidelity approaches. However, the rapid evolution of the simulation methods, the ever-increasing computational prowess of current hardware platforms and the emergence of new technologies such as deep learning, that solve complex problems previously thought to be impossible; allow us to be optimistic about the future of digitalization in the fashion industry.

Bibliography

[Arribas and Alfaro, 2018] Arribas, V. and Alfaro, J. A. (2018). 3d technology in fashion: from concept to consumer. *Journal of Fashion Marketing and Management: An International Journal*. (Cited on page 1.)

[Baraff and Witkin, 1997] Baraff, D. and Witkin, A. (1997). Physically-based modeling, principles and practice, page course 34. *Course Notes of ACM SIGGRAPH*. (Cited on page 23.)

[Baraff and Witkin, 1998] Baraff, D. and Witkin, A. (1998). Large steps in cloth simulation. In *Proceedings of the 25th annual conference on Computer graphics and interactive techniques*, pages 43–54, New York, NY, USA. Association for Computing Machinery. (Cited on pages 13, 20, 24, 29, 32, 35, 40, and 93.)

[Barbič and James, 2005] Barbič, J. and James, D. L. (2005). Real-time subspace integration for st. venant-kirchhoff deformable models. *ACM transactions on graphics (TOG)*, 24(3):982–990. (Cited on pages 5 and 93.)

[Bender and Deul, 2013] Bender, J. and Deul, C. (2013). Adaptive cloth simulation using corotational finite elements. *Computers & Graphics*, 37:820–829. (Cited on pages 21 and 94.)

[Bergen, 1997] Bergen, G. v. d. (1997). Efficient collision detection of complex deformable models using aabb trees. *Journal of graphics tools*, 2(4):1–13. (Cited on page 23.)

[Bergou et al., 2010a] Bergou, M., Audoly, B., Vouga, E., Wardetzky, M., and Grinspun, E. (2010a). Discrete viscous threads. In *ACM Transactions on Graphics (TOG)*, volume 29, page 116. ACM. (Cited on page 15.)

[Bergou et al., 2010b] Bergou, M., Audoly, B., Vouga, E., Wardetzky, M., and Grinspun, E. (2010b). Discrete viscous threads. *ACM Trans. Graph.*, 29(4). (Cited on page 51.)

[Bergou et al., 2008] Bergou, M., Wardetzky, M., Robinson, S., Audoly, B., and Grinspun, E. (2008). Discrete elastic rods. *ACM Trans. Graph.*, 27(3):1–12. (Cited on pages xi, 15, 41, and 51.)

[Bertails et al., 2006] Bertails, F., Audoly, B., Cani, M.-P., Querleux, B., Leroy, F., and Lévundefinedque, J.-L. (2006). Super-helices for predicting the dynamics of natural hair. *ACM Trans. Graph.*, 25(3):1180–1187. (Cited on page 14.)

[Bhat et al., 2003] Bhat, K. S., Twigg, C. D., Hodgins, J. K., Khosla, P. K., Popović, Z., and Seitz, S. M. (2003). Estimating cloth simulation parameters from video. In *Proceedings of the 2003 ACM SIGGRAPH/Eurographics Symposium on Computer Animation*, pages 37–51. (Cited on page 29.)

[Bridson et al., 2002] Bridson, R., Fedkiw, R., and Anderson, J. (2002). Robust treatment of collisions, contact and friction for cloth animation. *ACM Trans. Graph.*, 21(3):594–603. (Cited on pages 12, 23, 24, and 94.)

[Bridson et al., 2003] Bridson, R., Marino, S., and Fedkiw, R. (2003). Simulation of clothing with folds and wrinkles. In *Proceedings of the 2003 ACM SIGGRAPH/Eurographics Symposium on Computer Animation*, pages 28–36. (Cited on pages 12, 13, 23, 24, 29, 32, 41, and 94.)

[Brown et al., 2018] Brown, G. E., Overby, M., Forootaninia, Z., and Narain, R. (2018). Accurate dissipative forces in optimization integrators. *ACM Transactions on Graphics (TOG)*, 37(6):1–14. (Cited on pages 75 and 99.)

[Carignan et al., 1992] Carignan, M., Yang, Y., Thalmann, N. M., and Thalmann, D. (1992). Dressing animated synthetic actors with complex deformable clothes. In *ACM Siggraph Computer Graphics*, volume 26, pages 99–104. ACM. (Cited on page 18.)

[Casafranca et al., 2020] Casafranca, J. J., Cirio, G., Rodríguez, A., Miguel, E., and Otaduy, M. A. (2020). Mixing yarns and triangles in cloth simulation. In *Computer Graphics Forum*, volume 39, pages 101–110. Wiley Online Library. (Cited on page 17.)

[Caughey and O'Kelly, 1965] Caughey, T. and O'Kelly, M. E. (1965). Classical normal modes in damped linear dynamic systems. (Cited on page 19.)

[Choe et al., 2005] Choe, B., Choi, M. G., and Ko, H.-S. (2005). Simulating complex hair with robust collision handling. In *Proceedings of the 2005 ACM SIGGRAPH/Eurographics symposium on Computer animation*, pages 153–160. (Cited on page 14.)

[Choi and Ko, 2005] Choi, K.-J. and Ko, H.-S. (2005). Stable but responsive cloth. In *ACM SIGGRAPH 2005 Courses*, page 1. ACM. (Cited on pages 13, 17, 21, and 24.)

[Cirio et al., 2014] Cirio, G., Lopez-Moreno, J., Miraut, D., and Otaduy, M. A. (2014). Yarn-level simulation of woven cloth. *ACM Transactions on Graphics (TOG)*, 33(6):207. (Cited on pages xi, 4, 5, 6, 7, 16, 19, 27, 31, 39, 41, 43, 53, 54, 55, 56, 60, 61, 62, 63, 64, 70, 74, 93, and 94.)

[Cirio et al., 2017] Cirio, G., Lopez-Moreno, J., and Otaduy, M. A. (2017). Yarn-level cloth simulation with sliding persistent contacts. *IEEE transactions on visualization and computer graphics*, 23(2):1152–1162. (Cited on pages xi, 2, 16, 39, 53, 56, 60, 61, and 96.)

[Curtis et al., 2008] Curtis, S., Tamstorf, R., and Manocha, D. (2008). Fast collision detection for deformable models using representative-triangles. In *Proceedings of the 2008 symposium on Interactive 3D graphics and games*, pages 61–69. (Cited on page 23.)

[Durville, 2009] Durville, D. (2009). Finite element simulation of textile materials at the fiber scale. *arXiv preprint arXiv:0912.1268*. (Cited on page 2.)

[Ericson, 2004] Ericson, C. (2004). *Real-time collision detection*. CRC Press. (Cited on page 23.)

[Fan et al., 2013] Fan, Y., Litven, J., Levin, D. I. W., and Pai, D. K. (2013). Eulerian-on-lagrangian simulation. *ACM Trans. Graph.*, 32(3). (Cited on pages 26 and 40.)

[Faure et al., 2007] Faure, F., Allard, J., and Nesme, M. (2007). *Eulerian contact for versatile collision processing*. PhD thesis, INRIA. (Cited on page 26.)

[Fedkiw et al., 2001] Fedkiw, R., Stam, J., and Jensen, H. W. (2001). Visual simulation of smoke. In *Proceedings of the 28th annual conference on Computer graphics and interactive techniques*, pages 15–22. (Cited on page 21.)

[Gast et al., 2015] Gast, T. F., Schroeder, C., Stomakhin, A., Jiang, C., and Teran, J. M. (2015). Optimization integrator for large time steps. *IEEE transactions on visualization and computer graphics*, 21(10):1103–1115. (Cited on pages 5, 19, 21, and 93.)

[Goldstein et al., 2002] Goldstein, H., Poole, C., and Safko, J. (2002). Classical mechanics. (Cited on pages 20 and 62.)

[Goldstein et al., 2014] Goldstein, H., Poole, C. P., and Safko, J. L. (2014). *Classical Mechanics: Pearson New International Edition*. Pearson Higher Ed. (Cited on pages 30 and 32.)

[Govindaraju et al., 2003] Govindaraju, N. K., Redon, S., Lin, M. C., and Manocha, D. (2003). Cullide: Interactive collision detection between complex models in large environments using graphics hardware. In *Proceedings of the ACM SIGGRAPH/EUROGRAPHICS conference on Graphics hardware*, pages 25–32. (Cited on page 23.)

[Grinspun et al., 2003] Grinspun, E., Hirani, A. N., Desbrun, M., and Schröder, P. (2003). Discrete shells. In *Proceedings of the 2003 ACM SIGGRAPH/Eurographics symposium on Computer animation*, pages 62–67. Eurographics Association. (Cited on pages 13, 19, and 93.)

[Guo et al., 2018] Guo, Q., Han, X., Fu, C., Gast, T., Tamstorf, R., and Teran, J. (2018). A material point method for thin shells with frictional contact. *ACM Trans. Graph.*, 37(4). (Cited on page 26.)

[Guo et al., 2020] Guo, R., Lin, J., Narayanan, V., and McCann, J. (2020). Representing crochet with stitch meshes. In *Symposium on Computational Fabrication*, pages 1–8. (Cited on page 17.)

[Hadap, 2006] Hadap, S. (2006). Oriented strands: dynamics of stiff multi-body system. In *Proceedings of the 2006 ACM SIGGRAPH/Eurographics symposium on Computer animation*, pages 91–100. (Cited on page 14.)

[Harmon et al., 2009] Harmon, D., Vouga, E., Smith, B., Tamstorf, R., and Grinspun, E. (2009). Asynchronous contact mechanics. In *ACM SIGGRAPH 2009 Papers*, SIGGRAPH '09, New York, NY, USA. Association for Computing Machinery. (Cited on page 24.)

[Hearle et al., 1969] Hearle, J. W., Grosberg, P., and Backer, S. (1969). Structural mechanics of fibers, yarns, and fabrics. (Cited on page 15.)

[Hernandez et al., 2013] Hernandez, F., Cirio, G., Perez, A., and Otaduy, M. (2013). Anisotropic strain limiting. In *Proc. of Congreso Español de Informática Gráfica*, volume 2. (Cited on page 12.)

[Iben et al., 2013] Iben, H., Meyer, M., Petrovic, L., Soares, O., Anderson, J., and Witkin, A. (2013). Artistic simulation of curly hair. In *Proceedings of the 12th ACM SIGGRAPH/Eurographics Symposium on Computer Animation*, pages 63–71, New York, NY, USA. Association for Computing Machinery. (Cited on page 14.)

[Jiang et al., 2017] Jiang, C., Gast, T., and Teran, J. (2017). Anisotropic elastoplasticity for cloth, knit and hair frictional contact. *ACM Trans. Graph.*, 36(4). (Cited on pages xi, 17, and 26.)

[Johnson and Cohen, 2001] Johnson, D. E. and Cohen, E. (2001). Spatialized normal come hierarchies. In *Proceedings of the 2001 symposium on Interactive 3D graphics*, pages 129–134. (Cited on page 23.)

[Kaldor et al., 2008] Kaldor, J. M., James, D. L., and Marschner, S. (2008). Simulating knitted cloth at the yarn level. *ACM Transactions on Graphics (TOG)*, 27(3). (Cited on pages 2, 4, 16, 17, 51, 53, and 93.)

[Kaldor et al., 2010] Kaldor, J. M., James, D. L., and Marschner, S. (2010). Efficient yarn-based cloth with adaptive contact linearization. *ACM Transactions on Graphics (TOG)*, 29(4). (Cited on page 16.)

[Karthik and Gopalakrishnan, 2014] Karthik, T. and Gopalakrishnan, D. (2014). Environmental analysis of textile value chain: an overview. *Roadmap to sustainable textiles and clothing*, pages 153–188. (Cited on page 1.)

[Kawabata et al., 1973] Kawabata, S., Niwa, M., and Kawai, H. (1973). 3—the finite-deformation theory of plain-weave fabrics part i: the biaxial-deformation theory. *Journal of the textile institute*, 64(1):21–46. (Cited on page 15.)

[Kharevych et al., 2006] Kharevych, L., Wei, W., Tong, Y., Kanso, E., Marsden, J. E., Schröder, P., and Desbrun, M. (2006). *Geometric, variational integrators for computer animation*. Eurographics Association. (Cited on page 21.)

[Leaf et al., 2018] Leaf, J., Wu, R., Schweickart, E., James, D. L., and Marschner, S. (2018). Interactive design of periodic yarn-level cloth patterns. *ACM Trans. Graph.*, 37(6). (Cited on pages 17, 53, 65, 66, 71, and 76.)

[Levin et al., 2011] Levin, D. I., Litven, J., Jones, G. L., Sueda, S., and Pai, D. K. (2011). Eulerian solid simulation with contact. *ACM Transactions on Graphics (TOG)*, 30(4):1–10. (Cited on page 25.)

[Li et al., 2013] Li, D., Sueda, S., Neog, D. R., and Pai, D. K. (2013). Thin skin elastodynamics. *ACM Transactions on Graphics (TOG)*, 32(4):1–10. (Cited on page 26.)

[Li et al., 2018] Li, J., Liu, T., and Kavan, L. (2018). Laplacian damping for projective dynamics. In *Proceedings of the 14th Workshop on Virtual Reality Interactions and Physical Simulations*, pages 29–36. (Cited on pages 20 and 93.)

[Long et al., 2011] Long, J., Burns, K., and Yang, J. J. (2011). Cloth modeling and simulation: a literature survey. In *International Conference on Digital Human Modeling*, pages 312–320. Springer. (Cited on page 2.)

[McAdams et al., 2009] McAdams, A., Selle, A., Ward, K., Sifakis, E., and Teran, J. (2009). Detail preserving continuum simulation of straight hair. *ACM Trans. Graph.*, 28(3). (Cited on page 26.)

[McGlockton et al., 2003] McGlockton, M., Cox, B., and McMeeking, R. (2003). A binary model of textile composites: Iii high failure strain and work of fracture in 3d weaves. *Journal of the Mechanics and Physics of Solids*, 51(8):1573–1600. (Cited on page 16.)

[Miguel et al., 2012] Miguel, E., Bradley, D., Thomaszewski, B., Bickel, B., Matusik, W., Otaduy, M. A., and Marschner, S. (2012). Data-driven estimation of cloth simulation models. In *Computer Graphics Forum*, volume 31, pages 519–528. Wiley Online Library. (Cited on page 14.)

[Miguel et al., 2016] Miguel, E., Miraut, D., and Otaduy, M. A. (2016). Modeling and Estimation of Energy-Based Hyperelastic Objects. *Computer Graphics Forum*, 35(2):385–396. (Cited on pages 14 and 30.)

[Mirtich and Canny, 1995] Mirtich, B. and Canny, J. (1995). Impulse-based simulation of rigid bodies. In *Proceedings of the 1995 symposium on Interactive 3D graphics*, pages 181–ff. (Cited on page 24.)

[Müller et al., 2015] Müller, M., Chentanez, N., Kim, T.-Y., and Macklin, M. (2015). Air meshes for robust collision handling. *ACM Trans. Graph.*, 34(4). (Cited on pages 25, 76, and 94.)

[Müller et al., 2002] Müller, M., Dorsey, J., McMillan, L., Jagnow, R., and Cutler, B. (2002). Stable real-time deformations. In *Proceedings of the 2002 ACM SIGGRAPH/Eurographics symposium on Computer animation*, pages 49–54. (Cited on page 13.)

[Müller et al., 2007] Müller, M., Heidelberger, B., Hennix, M., and Ratcliff, J. (2007). Position based dynamics. *Journal of Visual Communication and Image Representation*, 18(2):109–118. (Cited on page 15.)

[Nadler et al., 2006] Nadler, B., Papadopoulos, P., and Steigmann, D. J. (2006). Multiscale constitutive modeling and numerical simulation of fabric material. *International journal of solids and structures*, 43(2):206–221. (Cited on page 16.)

[Narain et al., 2012] Narain, R., Samii, A., and O'Brien, J. F. (2012). Adaptive anisotropic remeshing for cloth simulation. *ACM transactions on graphics (TOG)*, 31(6). (Cited on pages xi, 13, 14, 25, and 43.)

[Narayanan et al., 2019] Narayanan, V., Wu, K., Yuksel, C., and McCann, J. (2019). Visual knitting machine programming. *ACM Transactions on Graphics (TOG)*, 38(4):1–13. (Cited on page 17.)

[Oh et al., 2006] Oh, S., Ahn, J., and Wohn, K. (2006). Low damped cloth simulation. *The Visual Computer*, 22(2):70–79. (Cited on pages 21 and 94.)

[Otaduy et al., 2009] Otaduy, M. A., Tamstorf, R., Steinemann, D., and Gross, M. (2009). Implicit contact handling for deformable objects. In *Computer Graphics Forum*, volume 28, pages 559–568. Wiley Online Library. (Cited on page 24.)

[Pai, 2002] Pai, D. K. (2002). Strands: Interactive simulation of thin solids using cosserat models. *Computer Graphics Forum*, 21(3):347–352. (Cited on pages 14 and 51.)

[Pauly et al., 2004] Pauly, M., Pai, D. K., and Guibas, L. J. (2004). Quasi-rigid objects in contact. In *Proceedings of the 2004 ACM SIGGRAPH/Eurographics symposium on Computer animation*, pages 109–119. (Cited on page 24.)

[Peirce, 1937] Peirce, F. T. (1937). 5—the geometry of cloth structure. *Journal of the Textile Institute Transactions*, 28(3):T45–T96. (Cited on pages 2 and 15.)

[Penava et al., 2014] Penava, Ž., Šimić-Penava, D., and Knezic, Ž. (2014). Determination of the elastic constants of plain woven fabrics by a tensile test in various directions. *Fibres & Textiles in Eastern Europe*. (Cited on page 13.)

[Pizana et al., 2020] Pizana, J. M., Rodríguez, A., Cirio, G., and Otaduy, M. A. (2020). A bending model for nodal discretizations of yarn-level cloth. In *Computer Graphics Forum*, volume 39, pages 181–189. Wiley Online Library. (Cited on page 16.)

[Pons-Moll et al., 2015] Pons-Moll, G., Romero, J., Mahmood, N., and Black, M. J. (2015). Dyna: A model of dynamic human shape in motion. *ACM Transactions on Graphics (TOG)*, 34(4):1–14. (Cited on page 45.)

[Provot, 1997] Provot, X. (1997). Collision and self-collision handling in cloth model dedicated to design garments. In *Computer Animation and Simulation'97*, pages 177–189. Springer. (Cited on page 23.)

[Provot et al., 1995] Provot, X. et al. (1995). Deformation constraints in a mass-spring model to describe rigid cloth behaviour. In *Graphics interface*, pages 147–147. Canadian Information Processing Society. (Cited on page 12.)

[Rayleigh, 1896] Rayleigh, J. W. S. B. (1896). *The theory of sound*, volume 2. Macmillan. (Cited on pages 19, 29, 35, and 93.)

[Reese, 2003] Reese, S. (2003). Anisotropic elastoplastic material behavior in fabric structures. In *IUTAM Symposium on Computational Mechanics of Solid Materials at Large Strains*, pages 201–210. Springer. (Cited on page 16.)

[Rosenblum et al., 1991] Rosenblum, R. E., Carlson, W. E., and Tripp, E. R. (1991). Simulating the structure and dynamics of human hair: Modelling, rendering and animation. *Journal of Visualization and Computer Animation*, 2:141–148. (Cited on page 14.)

[Sachdeva et al., 2015] Sachdeva, P., Sueda, S., Bradley, S., Fain, M., and Pai, D. K. (2015). Biomechanical simulation and control of hands and tendinous systems. *ACM Transactions on Graphics (TOG)*, 34(4). (Cited on page 51.)

[Sánchez-Banderas and Otaduy, 2017] Sánchez-Banderas, R. M. and Otaduy, M. A. (2017). Dissipation potentials for yarn-level cloth. In *CEIG*, pages 11–18. (Cited on pages 8 and 98.)

[Sánchez-Banderas and Otaduy, 2018] Sánchez-Banderas, R. M. and Otaduy, M. A. (2018). Strain rate dissipation for elastic deformations. In *Computer Graphics Forum*, volume 37, pages 161–170. (Cited on pages 8 and 98.)

[Sánchez-Banderas et al., 2020] Sánchez-Banderas, R. M., Rodríguez, A., Barreiro, H., and Otaduy, M. A. (2020). Robust eulerian-on-lagrangian rods. *ACM Transactions on Graphics (TOG)*, 39(4):59–1. (Cited on pages 8 and 99.)

[Selle et al., 2008] Selle, A., Lentine, M., and Fedkiw, R. (2008). A mass spring model for hair simulation. *ACM Transactions on Graphics (TOG)*, 27(3). (Cited on pages 14 and 51.)

[Servin et al., 2010] Servin, M., Lacoursiere, C., Nordfelth, F., and Bodin, K. (2010). Hybrid, multiresolution wires with massless frictional contacts. *IEEE transactions on visualization and computer graphics*, 17(7):970–982. (Cited on page 51.)

[Sifakis and Barbic, 2012] Sifakis, E. and Barbic, J. (2012). Fem simulation of 3d deformable solids: A practitioner's guide to theory, discretization and model reduction. In *ACM SIGGRAPH 2012 Courses*, pages 20:1–20:50. (Cited on pages 31 and 39.)

[Sifakis et al., 2008] Sifakis, E., Marino, S., and Teran, J. (2008). Globally coupled collision handling using volume preserving impulses. In *Proceedings of the 2008 ACM SIGGRAPH/Eurographics Symposium on Computer Animation*, pages 147–153. (Cited on page 25.)

[Sifakis et al., 2007] Sifakis, E., Shinar, T., Irving, G., and Fedkiw, R. (2007). Hybrid simulation of deformable solids. In *Proceedings of the 2007 ACM SIGGRAPH/Eurographics Symposium on Computer Animation*, SCA '07, page 81–90. Eurographics Association. (Cited on page 61.)

[Simo and Fox, 1989] Simo, J. and Fox, D. (1989). On a stress resultant geometrically exact shell model. part i: Formulation and optimal parametrization. *Computer Methods in Applied Mechanics and Engineering*, 72(3):267–304. (Cited on page 13.)

[Sperl et al., 2020] Sperl, G., Narain, R., and Wojtan, C. (2020). Homogenized yarn-level cloth. *ACM Transactions on Graphics (TOG)*, 39(4):2. (Cited on page 17.)

[Spillmann and Teschner, 2007] Spillmann, J. and Teschner, M. (2007). C o r d e: Cosserat rod elements for the dynamic simulation of one-dimensional elastic objects. In *Proceedings of the 2007 ACM SIGGRAPH/Eurographics symposium on Computer animation*, pages 63–72. Eurographics Association. (Cited on page 15.)

[Spillmann and Teschner, 2008] Spillmann, J. and Teschner, M. (2008). An adaptive contact model for the robust simulation of knots. *Computer Graphics Forum*, 27(2):497–506. (Cited on page 15.)

[Su et al., 2013] Su, J., Sheth, R., and Fedkiw, R. (2013). Energy conservation for the simulation of deformable bodies. *IEEE Transactions on Visualization and Computer Graphics*, 19(2):189–200. (Cited on pages 21 and 29.)

[Sueda et al., 2011] Sueda, S., Jones, G. L., Levin, D. I., and Pai, D. K. (2011). Large-scale dynamic simulation of highly constrained strands. In *ACM Transactions on Graphics (TOG)*, volume 30, page 39. ACM. (Cited on pages 16, 27, 40, 51, 53, 54, 55, 56, 62, and 94.)

[Tang et al., 2012] Tang, M., Manocha, D., Otaduy, M. A., and Tong, R. (2012). Continuous penalty forces. *ACM Transactions on Graphics (TOG)*, 31(4):1–9. (Cited on pages 24 and 94.)

[Tang et al., 2013] Tang, X., Paluszny, A., and Zimmerman, R. (2013). Energy conservative property of impulse-based methods for collision resolution. *International journal for numerical methods in engineering*, 95(6):529–540. (Cited on page 24.)

[Terzopoulos et al., 1987] Terzopoulos, D., Platt, J., Barr, A., and Fleischer, K. (1987). Elastically deformable models. In *ACM Siggraph Computer Graphics*, volume 21, pages 205–214. ACM. (Cited on pages xi, 3, 4, 12, 18, and 24.)

[Teschner et al., 2003] Teschner, M., Heidelberger, B., Müller, M., Pomeranets, D., and Gross, M. (2003). Optimized spatial hashing for collision detection of deformable objects. *VMV'03: Proceedings of the Vision, Modeling, Visualization*, 3. (Cited on page 23.)

[Thomaszewski et al., 2009] Thomaszewski, B., Pabst, S., and Strasser, W. (2009). Continuum-based strain limiting. In *Computer Graphics Forum*, volume 28, pages 569–576. Wiley Online Library. (Cited on page 12.)

[Thomaszewski et al., 2005] Thomaszewski, B., Wacker, M., and Straßer, W. (2005). A consistent bending model for cloth simulation with corotational subdivision finite elements. (Cited on page 13.)

[Umetani et al., 2014] Umetani, N., Schmidt, R., and Stam, J. (2014). Position-based elastic rods. In *ACM SIGGRAPH 2014 Talks*, pages 1–1. (Cited on page 15.)

[Volino and Magnenat-Thalmann, 2000] Volino, P. and Magnenat-Thalmann, N. (2000). Implementing fast cloth simulation with collision response. In *Computer Graphics International*, volume 2000, pages 257–266. (Cited on pages 13 and 21.)

[Volino and Magnenat-Thalmann, 2001] Volino, P. and Magnenat-Thalmann, N. (2001). Comparing efficiency of integration methods for cloth simulation. In *Computer graphics international 2001. Proceedings*, pages 265–272. IEEE. (Cited on page 21.)

[Volino et al., 2009] Volino, P., Magnenat-Thalmann, N., and Faure, F. (2009). A simple approach to nonlinear tensile stiffness for accurate cloth simulation. *ACM Transactions on Graphics*, 28(4):Article–No. (Cited on page 13.)

[Wang, 2014] Wang, H. (2014). Defending continuous collision detection against errors. *ACM Transactions on Graphics (TOG)*, 33(4):1–10. (Cited on page 23.)

[Wang et al., 2011] Wang, H., O'Brien, J. F., and Ramamoorthi, R. (2011). Data-driven elastic models for cloth: modeling and measurement. *ACM transactions on graphics (TOG)*, 30(4):1–12. (Cited on page 14.)

[Weidner et al., 2018] Weidner, N. J., Piddington, K., Levin, D. I., and Sueda, S. (2018). Eulerian-on-lagrangian cloth simulation. *ACM Transactions on Graphics (TOG)*, 37(4). (Cited on pages 27, 53, 56, 69, 71, 76, and 94.)

[Weil, 1986] Weil, J. (1986). The synthesis of cloth objects. *ACM Siggraph Computer Graphics*, 20(4):49–54. (Cited on page 3.)

[Wu et al., 2019] Wu, K., Swan, H., and Yuksel, C. (2019). Knittable stitch meshes. *ACM Transactions on Graphics (TOG)*, 38(1):1–13. (Cited on page 17.)

[Xu and Barbič, 2017] Xu, H. and Barbič, J. (2017). Example-based damping design. *ACM Transactions on Graphics (TOG)*, 36(4):1–14. (Cited on pages xi, 20, and 93.)

[Xu and Barbič, 2017] Xu, H. and Barbič, J. (2017). Example-based damping design. *ACM Trans. Graph.*, 36(4):53:1–53:14. (Cited on page 29.)

[Xu et al., 2015] Xu, H., Sin, F., Zhu, Y., and Barbič, J. (2015). Nonlinear material design using principal stretches. *ACM Trans. Graph.*, 34(4):75:1–75:11. (Cited on page 30.)

[Yu et al., 2000] Yu, W., Kang, T., and Chung, K. (2000). Drape simulation of woven fabrics by using explicit dynamic analysis. *Journal of the Textile Institute*, 91(2):285–301. (Cited on page 17.)

[Yuksel et al., 2012] Yuksel, C., Kaldor, J. M., James, D. L., and Marschner, S. (2012). Stitch meshes for modeling knitted clothing with yarn-level detail. *ACM Transactions on Graphics (TOG)*, 31(4). (Cited on pages 2 and 17.)

Appendix A

Resumen

Los textiles están siempre presentes en nuestra vida diaria, siendo la industria textil y de la moda uno de los principales motores de la economía mundial. No obstante, a pesar de los avances tecnológicos, esta industria se resiste a la irrupción de los procesos de diseño digital. La razón radica en que los modelos computacionales existentes desarrollados en el ámbito de la ingeniería, aunque precisos, no satisfacen los requisitos de rendimiento compatibles con los procesos industriales.

Recientemente, los avances en los métodos de simulación para la informática gráfica han dado lugar al desarrollo de soluciones de alto rendimiento para simular tejidos a nivel de hilo que reducen la brecha de precisión con los enfoques de ingeniería. Aunque las tendencias actuales apuntan a la aparición en un futuro próximo de modelos de alta fidelidad que satisfagan los requisitos para la creación de prototipos digitales predictivos, hoy en día siguen existiendo retos abiertos que limitan la consecución de este objetivo.

En esta tesis abordamos algunos de estos retos y contribuimos hacia la creación de modelos de simulación de alta fidelidad. Para ello, nos enfocamos en dos aspectos relevantes para la caracterización y el comportamiento de la tela. El modelado del comportamiento disipativo y la simulación de prendas multicapa (Fig. A.1).

En este capítulo proporcionamos un resumen del desarrollo de esta tesis a lo largo de las diferentes secciones: antecedentes, objetivos, metodología, resultados y conclusiones.

Figure A.1: En esta tesis nos enfocamos en dos aspectos relevantes para la caracterización y el comportamiento de la tela: el modelado del comportamiento disipativo y la simulación de prendas multicapa.

A.1 Antecedentes

La creación de modelos de alta fidelidad capaces de reproducir las complejas propiedades mecánicas de los tejidos, sigue siendo el pilar fundamental de la simulación de telas. Sin embargo, las aplicaciones gráficas requieren un delicado equilibrio entre el coste computacional y la precisión para que estos enfoques sean prácticos.

Simulación de Telas

Los numerosos y complejos retos que surgen en la simulación de telas hacen que sea un reto difícil. Por un lado, la representación mecánica de la tela debe ser lo suficientemente precisa como para capturar las no linealidades y las grandes deformaciones inherentes a la misma. Por otro lado, las interacciones entre las telas y los materiales rígidos y deformables, así como las autocolisiones, deben tratarse con eficacia y precisión para evitar la aparición de artefactos en la simulación.

Durante décadas, la aproximación más destacada ha sido el uso de modelos de estructura laminar (thin-shell). Sin embargo, estos modelos tienen dificultades para captar los efectos macroscópicos que surgen de las sutiles interacciones que se producen a nivel del hilo (por debajo de la escala milimétrica) y que son fundamentales para una caracterización de alta fidelidad.

[Kaldor et al., 2008] fue pionero en la simulación de grandes piezas de tela a nivel de hilo para la informática gráfica. En su trabajo, la mecánica de cada hilo individual es capturada a través de un modelo de varilla inextensible (*inextensible rod*) utilizando un sistema de gestión de contactos explícito. No obstante, la gran cantidad de hilos presentes en una prenda real hace que su coste computacional sea poco abarcable. Pocos años después, [Cirio et al., 2014], mejoró su eficiencia considerando el contacto entre hilos como persistente, consiguiendo una sustancial mejora computacional a costa de limitar el rango de posibles estructuras que es capaz de representar.

Ambos trabajos suponen un hito en el desarrollo de la simulación de telas de alta fidelidad. No obstante, y a pesar de estos notables avances, estos métodos todavía están lejos de los niveles de precisión y eficiencia requeridos para ser considerados de alta fidelidad, quedando todavía muchos retos por resolver.

Fenómenos Disipativos

Entre los diferentes retos, se encuentra el modelado de las propiedades disipativas de los tejidos, que, por desgracia, ha sido uno de los aspectos más desatendidos en la literatura. La amortiguación de la energía de un sistema puede producirse por diversos motivos: por contacto, fricción o por la propia resistencia de la materia. Sin embargo, a pesar de la gran cantidad de literatura sobre el tema, todavía no se conocen bien ni los mecanismos ni las variables de estado relevantes que lo originan. Por ello, muchos trabajos en el área de la informática gráfica se limitan a recurrir a modelos de amortiguación lineales o se centran en mitigar la disipación inducida por la integración numérica [Barbič and James, 2005, Gast et al., 2015, Cirio et al., 2014].

Entre los trabajos que emplean modelos de amortiguación lineales, el modelo de amortiguamiento de [Rayleigh, 1896] es probablemente el más antiguo, pero sigue siendo el más utilizado. Si bien este modelo destaca por su simplicidad y facilidad de implementación, las fuerzas disipativas que produce afectan indiscriminadamente a la dinámica global del objeto, dando lugar a una amortiguación excesiva del sistema. Por desgracia, su simplicidad ha hecho que muchos trabajos en gráficos implementen este modelo [Grinspun et al., 2003, Cirio et al., 2014, Gast et al., 2015, Xu and Barbič, 2017, Li et al., 2018]. Como alternativa, [Baraff and Witkin, 1998] describió un método para la amortiguación que evita la disipación innecesaria en la energía cinética total del sistema. Si bien este trabajo ha inspirado a trabajos posteriores [Bender and

Deul, 2013, Oh et al., 2006], su derivación no se rige por fundamentos de mecánica del continuo, lo que dificulta su aplicación a formulaciones más generales.

Prendas Multicapa

Muchas prendas cotidianas suelen estar compuestas por varias capas de tela en contacto: volantes, bolsillos, bordados, etc. Las propiedades visuales y mecánicas que presentan, las hacen muy distintivas y deseables para una gran variedad de aplicaciones, desde la moda hasta la creación de prendas y tejidos funcionales.

No obstante, el tratamiento de los contactos sigue siendo otro de los grandes retos sin resolver. Si bien los algoritmos de detección y resolución de colisiones han evolucionado hasta ofrecer soluciones robustas a las intrincadas configuraciones que suelen aparecer en las telas [Bridson et al., 2002, Bridson et al., 2003, Tang et al., 2012, Müller et al., 2015], éstos suponen todavía un gran reto computacional. Algunos trabajos como los de [Sueda et al., 2011], [Cirio et al., 2014] y [Weidner et al., 2018] identifican soluciones parciales de mayor eficiencia computacional a costa de limitar su alcance a problemas más específicos. Sin embargo, no existen modelos que proporcionen una gestión eficiente de los contactos entre múltiples capas que además permitan la posibilidad de que deslicen entre sí.

A.2 Objetivos

El objetivo general de esta tesis es el estudio y diseño de soluciones eficaces que permitan superar algunos de los actuales límites del estado del arte, acercando así el objetivo final de la creación de modelos de simulación de tejido de alta fidelidad.

Para ello, nos centramos en dos retos de gran interés y que tienen un impacto directo en la consecución de dicho objetivo: el modelado del comportamiento disipativo de la tela, y la gestión de contacto multicapa.

Modelado del Comportamiento Disipativo

Lograr una simulación precisa de la tela requiere encontrar modelos que permitan describir de forma controlable el comportamiento disipativo de los diferentes modos

de deformación. La solución alcanzada debe garantizar el desacoplamiento entre modos y reducir lo máximo posible la disipación indiscriminada de la energía cinética. Además de esto, el método debe ser versátil y robusto, permitiendo una correcta aplicación a diferentes formulaciones.

Gestión de Contacto Multicapa

La gestión de lo contactos supone uno de los principales cuellos de botella en los métodos de simulación de tela. El método propuesto deberá conseguir reducir de forma efectiva el coste computacional asociado a la resolución de contactos entre múltiples capas. Además de esto, se deberá hacer especial enfásis en su robustez, manteniendo la estabilidad de la simulación incluso ante la presencia de grandes deslizamientos entre las diferentes capas.

A.3 Metodología

Para la realización de esta tesis, hemos seguido la siguiente metodología:

Revisión Bibliográfica

En el Capítulo 2 de esta tesis se recoge un exhaustivo análisis del estado del arte en simulación de telas, en concreto de aquellos trabajos que están más relacionados con los objetivos que abordamos en esta tesis. Comenzamos con la identificación de los diferentes retos y oportunidades, realizando un estudio general de las diferentes vertientes que atañen a la simulación de telas. Tras esto, nos centramos en estudiar detalladamente los trabajos previos que han abordado el modelado disipativo, analizando sus ventajas e inconvenientes, así como aquellos trabajos que proponen modelos para la gestión de contactos entre múltiples capas de tejido.

Estudio y Diseño de un Modelo Disipativo Controlable

Tras el análisis del estado del arte, pasamos a abordar el primero de los retos identificados: el modelado del comportamiento disipativo de la tela. En el Capítulo 3

Figure A.2: Ejemplo de aplicación de nuestro método de disipación al modelo hiperelástico de Saint Venant-Knirchhoff (StVK)

proponemos un marco para el diseño de fuerzas de amortiguación basado en potenciales de disipación formulados como funciones de la tasa de deformación. Para su desarrollo estudiamos los fundamentos relacionados de la mecánica clásica, derivando así la formulación que finalmente daría lugar a nuestro trabajo. Tras esto, estudiamos su posible aplicación a modelos de deformación continua y discreta, sus implicaciones prácticas y sus ventajas sobre los modelos de disipación comúnmente adoptados. Estos estudios se materializaron en la aplicación de nuestro método a dos modelos de deformación muy diferentes, la hiperelasticidad de Saint Venant-Kirchhoff (StVK) (Fig. A.2) y las telas a nivel de hilo con contactos persistentes deslizantes.

Estudio y Diseño de un Modelo de Simulación Multicapa

Asimismo, en el Capítulo 4 abordamos el reto de la representación de tejidos multicapa, introduciendo un método robusto para la simulación de ensamblajes complejos de varillas y capas deslizantes apiladas con gestión implícita de los contactos. Para su desarrollo partimos del trabajo de [Cirio et al., 2017], el cual no es capaz de manejar de forma robusta estas situaciones debido a la aparición de degeneraciones intrínsecas (Fig. A.3). Para solventar este problema, formulamos y prototipamos diferentes variantes de la discretización y de la formulación energética empleada en el trabajo de

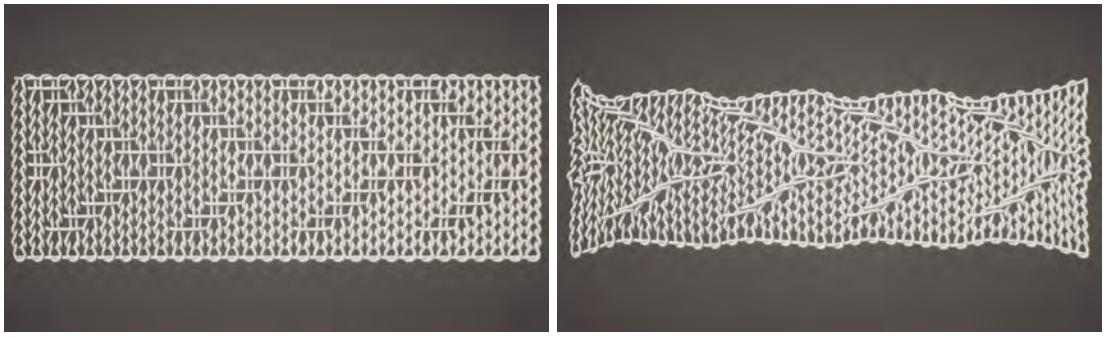

Figure A.3: Ejemplo de aplicación de nuestro método para la simulación de tejidos de punto de gran complejidad. En este caso aplicado a una estructura de tipo *jacquard*. La imagen de la izquierda muestra la configuración inicial, mientras que la imagen de la derecha muestra el estado relajado. Durante el proceso de relajación, los hilos han deslizado dando lugar a diversas configuraciones degeneradas que nuestro modelo es capaz de resolver de manera robusta.

Cirio et al., analizando su efectividad y robustez sobre casos de ejemplo. La solución que alcanzamos es sencilla y elegante, produciendo simulaciones robustas incluso en escenarios a gran escala con degeneraciones generalizadas. Tras esto, estudiamos sus implicaciones prácticas, llevando a cabo una implementación capaz de simular telas de alta resolución de forma eficiente con el fin de poder demostrar el rango de aplicaciones del modelo.

A.4 Resultados

Las contribuciones principales de esta tesis pueden ser resumidas de la siguiente forma:

- En el Capítulo 3 introducimos un marco para el diseño de modelos de amortiguación basado en potenciales de disipación formulados como funciones de la tasa de deformación. Nuestro modelo de amortiguación se basa en el concepto de potenciales de disipación de la mecánica clásica. Este enfoque es paralelo al diseño de los modelos de deformación elástica basados en formulaciones energéticas y simplifica la aplicación de lo que denominamos condiciones de *amortiguación correcta*. Este marco también nos ayuda a demostrar por qué el clásico modelo de amortiguamiento de Rayleigh falla para los modelos de deformación no lineales.

- En el Capítulo 3 también analizamos en detalle la aplicación de potenciales de disipación a dos modelos de deformación muy diferentes: El modelo de hiperelasticidad de Saint-Venant Kirchhoff (StVK) y el modelo de simulación de tela a nivel de hilo con contactos persistentes deslizantes. Estos modelos de deformación representan el rango de aplicabilidad de nuestro modelo de amortiguación.

- En el Capítulo 4 introducimos un método para simular configuraciones complejas de varillas y capas apiladas de tela haciendo una gestión implícita de los contactos mediante discretizaciones *Eulerian-on-Lagrangian* (EoL). Los métodos EoL anteriores no son capaces de manejar estas configuraciones complejas, debido a la aparición de degeneraciones ubicuas e intrínsecas en la geometría de los contactos que impiden el uso de técnicas de remallado y hacen que las simulaciones se tornen inestables. Proponemos una nueva discretización mixta que permite modelar el contacto de forma tan precisa y eficiente como en los métodos EoL, pero que además es transparente a las fuerzas internas de las varillas, y por tanto insensible a las degeneraciones.

- En el Capítulo 4 combinamos nuestra discretización novedosa con la discretización estándar EoL según convenga, derivando ecuaciones de movimiento mixtas estático-dinámicas que pueden resolverse de forma unificada con métodos de resolución estándar. Nuestra solución es sencilla y elegante en la práctica, produciendo simulaciones robustas en escenarios a gran escala con disposiciones complejas y degeneraciones generalizadas. En nuestros resultados, mostramos la aplicación de nuestra solución a simulaciones desafiantes de telas a nivel de hilo. Ampliamos la potencia de los métodos EoL a las capas apiladas de tejidos, gestionando de forma implícita los contactos intra e inter tejido.

Los resultados de las contribuciones de esta tesis se encuentran compilados en los siguientes trabajos

- Capítulo 3: "Dissipation Potentials for Yarn-Level Cloth" - Rosa M. Sánchez-Banderas and Miguel A. Otaduy - *CEIG, 11-18* [Sánchez-Banderas and Otaduy, 2017].

- Capítulo 3: "Strain Rate Dissipation for Elastic Deformations" - Rosa M. Sánchez-Banderas and Miguel A. Otaduy - *Computer Graphics Forum 37 (8), 161-170.* [Sánchez-Banderas and Otaduy, 2018].

- Capítulo 4: "Robust eulerian-on-lagrangian rods" - Rosa M. Sánchez-Banderas, Alejandro Rodríguez, Héctor Barreiro and Miguel A. Otaduy - *ACM Transactions on Graphics (TOG) 39 (4), 59: 1-59: 10.* [Sánchez-Banderas et al., 2020].

A.5 Conclusiones

En el Capítulo 5 presentamos las distintas conclusiones alcanzadas de los resultados obtenidos en cada uno de los modelos propuestos en esta tesis, así como sus limitaciones y posibles líneas de investigación futuras.

Por un lado, proporcionamos los detalles de un marco para el diseño de las fuerzas de amortiguación utilizando potenciales de disipación. Analizamos su aplicación a diferentes modelos de deformación y demostramos sus ventajas sobre los enfoques tradicionales. Aunque el marco propuesto no aborda directamente el tema de la precisión, proporciona los medios para diseñar un modelo disipativo garantizando el criterio de controlabilidad que establecimos. No obstante, nuestro modelo requiere ser complementado con otras fuerzas de amortiguación si se requiere modelar disipación en el espacio nulo del gradiente de deformación. Además de esto, nuestro trabajo también abre interesantes vías para trabajos futuros. El modelo propuesto podría utilizarse como un bloque de construcción integral de la estimación de la amortiguación basada en la medición o en criterios arísticos. Además, de forma similar a trabajos recientes [Brown et al., 2018], el uso de potenciales disipativos podría permitir su integración en esquemas de integración basados en optimización.

Por otro lado, introducimos un método para simular configuraciones complejas de varillas y capas apiladas de tela con gestión implícita de los contactos. Nuestro método es simple, eficiente e insensible a los elementos degenerados sin depender del uso de técnicas de remallado. Proporcionamos los detalles prácticos esenciales para llevar a cabo una implementación eficiente del método y demostramos sus fortalezas a través de la simulación de casos complejos. No obstante, durante su desarrollo hemos identificado varias limitaciones, así como oportunidades de investigación futura. La transición entre discretizaciones introduce discontinuidades en la energía y el momento, que pese a no haberse manifestado como artefactos en nuestros experimentos, tienen el potencial de afectar a la convergencia de la simulación. La introducción de métodos para suavizar estas discontinuidades podría aliviar este problema. Por otro lado, nuestra implementación no admite la adición dinámica de nodos EoL, lo que di-

ficulta la representación de determinados casos en los que aparecen nuevos contactos. En estos casos, no es evidente cuándo la generación de nuevos nodos podría resultar beneficiosa. Además de ésto, la inclusión de un algoritmo explícito de detección de colisiones podría limitar las ventajas de eficiencia computacional que ofrece nuestro método. Explorar estrategias que reduzcan su impacto podría ser una interesante línea de investigación futura.

En general, creemos que los dos enfoques propuestos en esta tesis constituyen un hito hacia la construcción de las bases de la simulación textil de alta fidelidad. Nuestras contribuciones van más allá del ámbito académico, ya que algunas de las soluciones propuestas se están adoptando en la industria para su uso en producción. Ejemplo de ello es la empresa SEDDI, la cual adoptó el modelo disipativo propuesto en en el Capítulo 3 para su uso interno, reconociendo su robustez y controlabilidad como un salto cualitativo sobre las soluciones implementadas anteriormente.